F. profunda in sapropel S5 is in line with maximum rates of $\delta^{18}O$ Asian speleothems and with the CH_4 overshoot in EDC;

F. profunda DCM development in glacials, due to sea-level lowering that reduced water-mass transport through straits;

Holococcolith enhanced preservation during cold spells, in response to AMOC slowdown and weakened monsoon activity;

Middle-Late Pleistocene Eastern Mediterranean nutricline depth and coccolith preservation linked to Monsoon activity and Atlantic Meridional Overturning Circulation

Alessandro Incarbona[1*], Gianluca Marino[2,3], Enrico Di Stefano[1], Michael Grelaud[4], Nicola Pelosi[5], Laura Rodríguez-Sanz[3], Eelco J. Rohling[3,6]

[1]Università degli Studi di Palermo, Dipartimento di Scienze della Terra e del Mare, Via Archirafi 22, 90134 Palermo, Italy.

[2]Centro de Investigación Mariña, Universidade de Vigo, GEOMA, Palaeoclimatology Lab, Vigo, 36310, Spain.

[3]Research School of Earth Sciences, The Australian National University, Canberra, Australian Capital Territory 2601, Australia

[4]Universitat Autònoma de Barcelona (UAB), Institute of Environmental Science and Technology (ICTA), Edifici Z, Carrer de les Columnes, Campus de la UAB, 08193 Bellaterra (Cerdanyola del Vallès), Barcelona, Spain

[5]Consiglio Nazionale delle Ricerche, Istituto di Scienze del Patrimonio Culturale, Via Cardinale Guglielmo Sanfelice 8, 80134 Naples, Italy.

[6] Ocean and Earth Science, University of Southampton, Southampton SO14 3ZH, UK

* Corresponding Author: e-mail, alessandro.incarbona@unipa.it; telephone, +39 091 23864648.

Abstract

The eastern Mediterranean Sea lies under the influence of high- and low-latitude climatic systems. The northern part of the basin is affected by Atlantic depressions and continental and polar air masses that promote intermediate and deep-water formation. The southern part is influenced by subtropical conditions and monsoon activity. Monsoon intensification results in enhanced freshwater discharge from the

Nile River and other (now dry) systems along the North African margin. This freshwater influx into the Mediterranean Sea reduces surface water buoyancy loss. Disentangling the influences of these diverse climatic forcings is hindered by inherent proxy data limitations and by interactions between the climatic forcings. Here we use a wealth of published and new paleoclimate records across Termination II to understand the impacts of the higher latitude and subtropical/monsoon climate influences on coccolithophore ecology and holococcolith preservation in Aegean Sea sediment core LC21. We then use these findings to interpret coccolith assemblage variations at Ocean Drilling Program Site 967 (located nearby LC21, at the Eratosthenes Seamount) during multiple glacial-interglacial cycles across the Middle Pleistocene (marine isotopic stages 14-9). The LC21 analysis suggests that holococcolith preservation was enhanced during Heinrich Stadial 11 (~ 133 ka) and cold spell C26 (~ 119 ka). These two events have been previously linked to cold conditions in the North Atlantic and Atlantic Meridional Overturning Circulation weakening. We propose that associated atmospheric perturbations over the Mediterranean Sea promoted deep-water formation, and thus holococcolith preservation. Similarly, in the Middle Pleistocene (MIS 14-9) of Site 967, we observe temporal coincidence between ten episodes of enhanced holococcolith preservation and episodes of Atlantic Meridional Overturning Circulation slowdown. In Site 967, we also identified repeated fluctuations in placoliths and in *Florisphaera profunda*, which indicate nutricline depth variations. The development of a deep chlorophyll maximum is associated with the North Africa and wet phases, as recently observed using elemental proxy records at Site 967, during the deposition of sapropel layers. A further deep chlorophyll maximum development is identified during MISs 12 and 10, as a result of pycnocline and nutricline shoaling within the lower part of the photic zone due to glacial sea-level lowering and water mass transport reduction at both the Gibraltar and Sicily Straits. Finally, enhanced holococcolith preservation during cold/dry events is clearly correlated to weakened monsoon activity in both Africa and Asia.

1 – Introduction

Paleoclimate reconstructions document the competing influence of southern *versus* northern climate systems on the hydrography and hydrology of the eastern Mediterranean Sea and its borderlands over a range of timescales (Emeis et al., 2000b; Grant et al., 2017, 2016; Lourens, 2004; Rohling et al., 2002b). During precession minima (Northern Hemisphere insolation maxima), the African monsoon intensified and shifted northward, with attendant enhancement of the freshwater release into the Mediterranean basin via large North African river systems and/or currently inactive wadis (Amies et al., 2019; Marino et al., 2009; Osborne et al., 2008; Rohling et al., 2002a; Rohling et al., 2015; van der Meer et al., 2007). This impacted the basin's hydrography and weakened or even shut down dense water formation, leading to oxygen starvation at depth and deposition of layers (sapropels) with elevated organic carbon concentrations (De Lange et al., 2008; Rohling et al., 2015; Rossignol-Strick et al., 1982). Millennial-scale climatic variations have been less well documented and appear to be associated with variations in the strength of the Atlantic Meridional Overturning Circulation (AMOC) (Grant et al., 2017, 2016; Stockhecke et al., 2016).

Coccolithophores are marine unicellular phytoplankton organisms living in the upper part of the water column. The ecology of coccolithophore species shows a strong sensitivity to modern gradients within the Mediterranean Sea and different species thrive in different areas, mainly in response to West-East temperature and nutrient gradients, water column dynamics, and meso-scale oceanographic features (Bonomo et al., 2012; D'Amario et al., 2017; Knappertsbusch, 1993; Oviedo et al., 2015). In the sedimentary archive, calcite coccolithophore remains (coccoliths) have been used successfully to infer orbital and suborbital variations in climate, productivity, and nutricline depth in oceans and marginal seas (Beaufort et al., 1997; Flores et al., 1997; Incarbona et al., 2013, 2010a; Marino et al., 2008; Molfino and McIntyre,

1990a; Rogalla and Andruleit, 2005). In the eastern Mediterranean Sea, coccolith-based paleoenvironmental reconstructions have been mostly aimed at assessing the shallow *versus* deep position of the nutricline within the photic layer and its relationship with the basin's freshwater budget, water mass circulation, and deep-sea ventilation during sapropel deposition (e.g., Grelaud et al., 2012). These studies attest to the development of a deep chlorophyll maximum (DCM) while organic carbon-rich layers were accumulating on the oxygen-starved eastern Mediterranean seafloor (Castradori, 1993; Giunta et al., 2003; Grelaud et al., 2012; Incarbona et al., 2019, 2011; Incarbona and Di Stefano, 2019; Maiorano et al., 2013; Negri et al., 1999; Principato et al., 2006; Triantaphyllou et al., 2009b, 2009a), corroborating findings based on other marine planktonic groups (Kemp et al., 1999; Meier et al., 2004; Rohling and Gieskes, 1989).

Here we present new data that complement a previous dataset of coccolith assemblages from south-eastern Aegean Sea core LC21 (Grelaud et al., 2012), across the penultimate glacial termination (termination II, T-II) and the last interglacial period, with a precise, radiometrically constrained chronology (Grant et al., 2012). This allows comparison of LC21 "coccolith proxies" with time series of palaeoclimate variability in the monsoon and the North Atlantic region (Cheng et al., 2009; Hodell et al., 2013), as well as atmospheric methane (CH_4) concentrations. Our combined dataset is probabilistically evaluated to decipher the amplitude and timing of change by quantitatively assessing the impact of chronological, analytical, and proxy uncertainties. We use this analysis as a proof of concept for new, highly resolved coccolith data from Ocean Drilling Program (ODP) Site 967 from the Eratosthenes Seamount, South of Cyprus, within the Nile Delta Basin province (Emeis et al., 1996). The new ODP 967 time series spans, at centennial-scale resolution, three glacial/interglacial cycles of the Middle Pleistocene, from glacial Marine Isotope Stage (MIS) 14 to interglacial MIS 9. Collectively, our new data and analyses provide insights into climate variability at orbital and sub-orbital timescales

during both glacial and interglacial periods, complementing a wealth of existing knowledge of the intervals of sapropel deposition. Specifically, we explore modifications in nutrient dynamics and holococcolith preservation during the Middle Pleistocene. These changes are compared with recently acquired variations in elemental abundances, elemental ratios, and climate indices for ODP Site 967 (Section 6.3) that portray the alternation of wet and dry North Africa periods at both orbital and sub-orbital timescales (Grant et al., 2017). Finally, we centre on the correlation between holococcolith preservation, AMOC, and boreal monsoon activity (both in Africa and in a wider Asian context) to assess: (*i*) the atmospheric impact of continental/polar air outbreaks on the eastern Mediterranean deep-sea ventilation and seafloor calcite preservation during cold stadials; and (*ii*) impact of millennial-scale atmospheric perturbations on the eastern Mediterranean Sea.

2 – Environmental Setting

A negative hydrological balance maintains a robust antiestuarine thermohaline circulation pattern in the Mediterranean Sea (Robinson and Golnaraghi, 1994). Surface Atlantic water (Modified Atlantic Water – MAW) enters the Mediterranean Sea and occupies the uppermost 100-200 m depth (Millot, 1999; POEM group, 1992). MAW spread out into the eastern Mediterranean Sea *via* the Mid-Mediterranean Jet and reaches the Eratosthenes Seamount where a quasi-permanent anticyclonic summer circulation exists, that is known as the Shikmona Gyre (Malanotte-Rizzoli et al., 2014; Pinardi and Masetti, 2000; POEM group, 1992). Levantine Intermediate Water (LIW) formation takes place close to the Eratosthenes Seamount (Ovchinnikov I.M., 1984; POEM group, 1992). Eastern Mediterranean Deep Water (EMDW) forms in the Adriatic and Aegean Sea (Fig. 1) due to winter heat loss under the influence of intense Bora and Vardar winds (Malanotte-Rizzoli et al., 2014; POEM group, 1992).

Today, the eastern Mediterranean Sea is one of the most oligotrophic areas globally. Primary productivity is more than three times lower than in the western basin, in accordance with a similar nutrient depletion trend (Krom et al., 2010, 1991). Primary production is also seasonally controlled: higher productivity occurs in winter, after winter convection, while severe oligotrophy occurs in summer due to deepening of the thermocline and nutricline (Allen et al., 2002; Klein and Coste, 1984). The Eratosthenes region is classified as a no-bloom area by satellite-based chlorophyll analyses. The severe late spring-summer oligotrophy is followed by relatively higher chlorophyll values in winter (D'Ortenzio and Ribera d'Alcalà, 2009).

High- and low-latitude climate systems impact on the eastern Mediterranean Sea. In summer, subtropical high-pressure conditions cause stable dry and warm conditions throughout the Mediterranean area (Lionello, 2012). In winter, the North African subtropical high pressure is shifted southward, and cold and dry polar/continental air outbreaks occur into the eastern Mediterranean from the north (Lionello, 2012; Rohling et al., 2019, 2015). Expansion of the Siberian High is an important driver for advection of cold air toward the eastern Mediterranean. Intensification of the Siberian High during Holocene rapid climatic changes is thought to be an important driver of surface water cooling and atmospheric perturbations in the central-eastern Mediterranean Sea (Incarbona et al., 2008; Rohling et al., 2002b; Rohling et al., 2019). Prolonged and strengthened polar/continental air outbreaks promote sea surface heat loss and deep-water formation (Josey et al., 2011; Rohling et al., 2019; Velaoras et al., 2017).

3 – Material and Methods

3.1 - Sediment cores

ODP Site 967 (34°04.098'N, 32°43.523'E, 2,553 m water depth) is located at the base of the northern slope of the Eratosthenes Seamount, a structure that emerges from the Nile Delta Cone (Fig. 1). Sediments are dominated by horizontal and sub-

horizontal brown and light gray, bioturbated nannofossil ooze and nannofossil clay, intercalated with sapropels and turbidites (Emeis et al., 1996). Specifically, there are five sapropel layers that show signs of moderate bioturbation (S13, S12, S11, b and S10) in the studied interval (Emeis et al., 1996), while no turbidites and/or other sedimentary disturbances were identified (Konijnendijk et al., 2014).

Sediment core LC21 (35°40'N, 26°35'E; 1,522 m water depth) was recovered in 1995 by *RV* Marion Dufresne in the southeastern Aegean Sea (Fig. 1). Lithology consists of hemipelagic sediments, with visible sapropels (S1, S3, S4, and S5) and tephra layers (Grant et al., 2016; Satow et al., 2015).

3.2 - Coccolith data

We carried out coccolith analyses at ODP Site 967 at 1 cm resolution between 14.80 and 21.49 m composite depth (mcd) (Emeis et al., 1996), for a total of 668 samples, which were analysed with a polarized microscope at ~ 1000× magnification. Rippled smear slides were prepared following standard procedures (Bown and Young, 1998). On average 350 specimens were identified following the taxonomic concepts for living coccolithophores of Young et al. (2003) and Jordan et al. (2004). Taxa were grouped as 'placoliths', 'miscellaneous group', 'upper photic zone (UPZ) group', 'lower photic zone (LPZ) group' and 'holococcoliths' (Di Stefano and Incarbona, 2004; Incarbona et al., 2010). Placoliths include small placoliths, small *Gephyrocapsa*, *Gephyrocapsa muellerae*, and *Gephyrocapsa oceanica*. The miscellaneous group includes *Helicosphaera* spp., *Coccolithus pelagicus*, *Syracosphaera histrica*, *Pontosphaera* spp., *Calcidiscus leptoporus*, *Coronosphaera* spp., *Braarudosphaera* spp., *Oolithotus fragilis*, *Calciosolenia* spp., and specimens of all the other species. UPZ group includes *Syracosphaera pulchra*, *Umbellosphaera* spp., *Discosphaera tubifera*, *Rhabdosphaera* spp., *Umbilicosphaera* spp., and *Ceratolithus* spp.. LPZ group comprises *F. profunda*, which dominates the group, with negligible amounts of *Gladiolithus flabellatus* in a few samples. Holococcoliths

include all the coccoliths produced during the haploid life-cycle stage (Incarbona et al., 2019).

The holococcolith analysis at Aegean Sea core LC21 was carried out by observation with a polarized microscope at about 1000× magnification, following the standard procedure for rippled smear slides (Bown and Young, 1998). Holococcolith percentage values were evaluated on 102 samples *versus* heterococcoliths specimens, examining about 500 coccoliths. *Florisphaera profunda* percentage values at LC21 Aegean Sea core were presented before (Grelaud et al., 2012), following the same procedure adopted in this study, and that earlier dataset is available at https://doi.pangaea.de/10.1594/PANGAEA.805357.

3.3 - Statistical analysis of the time series

We use a Monte Carlo approach based on MATLAB coding (Marino et al., 2015; Thirumalai et al., 2016) to: (*i*) stack the $\delta^{18}O$ time series for different stalagmites (SB11, SB23, and SB25) from Sanbao Cave, China, that cover T-II and the last interglacial period (Cheng et al., 2009); (*ii*) calculate rates of $\delta^{18}O$ change in the Sanbao Cave stalagmites; (*iii*) probabilistically evaluate the chronological (Bazin et al., 2013; Veres et al., 2013) and measurement uncertainties associated with the time series of atmospheric methane (CH_4) concentrations from EPICA Dome C (EDC) (Loulergue et al., 2008); and (*iv*) probabilistically evaluate chronological and counting uncertainties associated with the *F. profunda* (Grelaud et al., 2012) and new holococcolith records for core LC21.

Speleothem $\delta^{18}O$ time series from Sanbao Cave have been probabilistically evaluated and stacked across the 140-110 ka interval. Input data for the Monte Carlo routine are sample ages with 1σ uncertainties, and speleothem $\delta^{18}O$ with 1σ uncertainties (Cheng et al., 2009). For each stalagmite (SB11, SB23, and SB25), individual data points are then separately and randomly sampled 10,000 times within their chronological and

$\delta^{18}O$ uncertainties. The chronological uncertainties are evaluated using a random walk Monte Carlo routine that employs a Metropolis–Hastings approach to reject steps in the random walk that will result in age reversals (Rodríguez-Sanz et al., 2017). That is, we imposed a stratigraphic constraint (monotonic increase of age with depth, analogous to Rohling et al., 2014) to the data that are measured in a stratigraphically coherent manner along individual stalagmites. All realizations are then linearly interpolated on an equally spaced time scale and stacked to produce 10,000 speleothem $\delta^{18}O$ stacks with and without a correction that probabilistically quantifies the impacts of the global ^{18}O enrichment/depletion (Schrag et al., 2002) associated with ice-volume changes (Grant et al., 2012). Next, we calculated the 1st time derivative, to obtain rates of speleothem $\delta^{18}O$ change for each of the 10,000 ice-volume corrected 'stacks'. This is done by smoothing each realization using 0.75 kyr Gaussian window to remove sample-to-sample noise, which would result in spurious jumps in the estimated rates of change, and by then differentiating the smoothed realizations. Monte Carlo analysis of the EDC methane record and of the eastern Mediterranean coccolith time series are performed using the same approach. Finally, the 10,000 iterations of each of these time series are linearly interpolated and the probability distribution assessed at each time step, thereby determining the 68% (16^{th}–84^{th} percentile) and 95% (2.5^{th}–97.5^{th} percentile) probability intervals and the probability maximum (PMAX, modal value) of the data.

4 – Coccolith taxon ecology

Placoliths are so-called 'r-strategist taxa' that rapidly exploit nutrients in the photic zone (Baumann et al., 2005; Young, 1994). In the eastern Mediterranean Sea, placoliths bloom in winter, after nutrient fertilization (Di Stefano et al., 2011; Knappertsbusch, 1993; Triantaphyllou et al., 2004; Ziveri et al., 2000). *Florisphaera profunda* is a deep photic zone species that indicates the occurrence of a deep nutricline (McIntyre and Molfino, 1996; Molfino and McIntyre, 1990a). In low- and middle-latitude open ocean regions, the relative abundance of this species is

anticorrelated with primary productivity (Beaufort et al., 2001, 1997; Hernández-Almeida et al., 2019).

In the Mediterranean Sea, except for a limited area in the central part of the basin, there is no apparent relationship between *F. profunda* abundance and satellite-observed (surface) primary productivity levels (Hernández-Almeida et al., 2019; Incarbona et al., 2008). However, *F. profunda* has been generally used to decipher water column stratification and development of a deep nutricline due to monsoon-fuelled freshwater discharge in the eastern Mediterranean and entrainment of nutrients into the lower photic zone from below (Castradori, 1993; Grelaud et al., 2012; Incarbona et al., 2019; Negri et al., 1999; Triantaphyllou et al., 2009b). This occurs through the develoment of a distinct DCM in the eastern Mediterranean during sapropel deposition. DCM development resulted from nutrient entrainment into the photic zone from relatively buoyant intermediate waters that likely originated from the Adriatic Sea, while the volume of MAW inflow through the Sicily Strait was reduced (Myers et al., 1998; Rohling, 1991b; Rohling and Gieskes, 1989). Accordingly, relative abundances of placoliths and *F. profunda*, or their ratio, provide a robust indication of the depth of the nutricline in the eastern Mediterranean Sea. Specifically, presence (absence) of placoliths (*F. profunda*) in the coccolith assemblage reflects a shallow (deep) nutricline (Di Stefano et al., 2015; Flores et al., 2000; Molfino and McIntyre, 1990b).

The UPZ group consistes of so-called ‘K-strategist taxa’, specialized to exploit a minimum uptake of nutrients in surface water (Bazzicalupo et al., 2020; Di Stefano and Incarbona, 2004; Young, 1994). Miscellaneous taxa reflect the lack of either an apparent distinctive ecological preference or of an undertanding of their ecological preferences, with a potential weak K-strategy (Incarbona et al., 2010; Young, 1994). Holococcoliths prefer dwelling in warm, oligotrophic surface water and are abundant in the eastern Mediterranean Sea (D’Amario et al., 2017; Kleijne, 1991;

Knappertsbusch, 1993; Dimiza et al., 2015; Oviedo et al., 2015; Skampa et al., 2019). Poor preservation of holococcoliths in sapropel S1 sediments was firstly recognised by Crudeli et al. (2006) and was later confirmed across the whole eastern Mediterranean, included the Eratosthenes Seamount (Incarbona et al., 2019; Incarbona and Di Stefano, 2019) and Pliocene sapropel layers in sedimentary sequences on Cyprus (Athanasiou et al., 2015). Importantly, potential preservation of tiny holococcolith crystals improves when dense water renewal ensures vigorous ventilation/oxygenation of the seafloor, even during short reventilation episodes that "interrupt" sapropel deposition (Incarbona et al., 2019).

5 –Chronology

The original shipboard age model by Sakamoto et al. (1998) at ODP Site 967 has since been revised, because of some inconsistent tuning to orbital insolation (Konijnendijk et al., 2014; Lourens et al., 2001). More recently, Grant et al. (2017) developed a monsoon runoff (sapropel) proxy from the principal component analysis of sedimentary elemental data in ODP Site 967 that they tuned to precession minima. They use a zero phase lag, which relies upon the assumption that little or no lag exists when monsoon maxima did not immediately follow a high-amplitude glacial termination (Grant et al., 2016; Lourens et al., 2001). In this study, we adopt the chronology by Grant et al. (2017) for the coccolith data. Sedimentation rates between MIS 14 and MIS 9 range from 1.4 cm kyr^{-1} to 3.9 cm kyr^{-1}, implying that the mean sampling resolution of our coccolith time series is about 340 years.

The LC21 chronology follows Grant et al. (2012) (see section 6.1). The mean sedimentation rate is about 4.4 cm kyr^{-1}, with a mean sampling resolution of about 225 years.

6 – Results and Discussion

6.1 – Coccolith assemblages in Aegean Sea core LC21

318 *Florisphaera profunda* (Grelaud et al., 2012) and holococcoliths across T-II and the
319 last interglacial in south-eastern Aegean core LC21 are used to evaluate their
320 relationship with water column stratification and deep-sea ventilation, respectively.
321 Several features make this core and the timespan that we target ideal to provide a
322 'proof of concept' for the interpretation of the new records from ODP Site 967 that
323 spans multiple glacial-interglacial cycles. First, core LC21 has a radiometrically
324 constrained chronology across T-II and the last interglacial period (Grant et al.,
325 2012). This has been corroborated through comparison with western Mediterranean
326 sediment cores and speleothem records, and it is consistent with the latest ice core
327 chronology across the study interval (Marino et al., 2015). Second, prominent
328 episodes of climate change punctuated T-II, including a multi-millennial Heinrich
329 stadial associated with major freshwater discharge into the North Atlantic and AMOC
330 slowdown (Deaney et al., 2017; Marino et al., 2015). Third, during the last
331 interglacial period, an organic rich layer (sapropel S5) was deposited in the eastern
332 Mediterranean under persistently anoxic or even euxinic conditions (Marino et al.,
333 2007; Rohling et al., 2015, 2006). Sapropel S5 conditions developed in response to
334 extensive monsoon-fuelled freshwater discharge along the North African Margin
335 (Amies et al., 2019; Osborne et al., 2008; Rohling et al., 2002a; Rohling et al., 2004)
336 that reduced surface salinity (van der Meer et al., 2007) and produced strong water
337 column stratification (Amies et al., 2019; Grelaud et al., 2012; Marino et al., 2007;
338 Rohling et al., 2006).
339
340 In Figure 2a-c we show *F. profunda* relative abundances from core LC21 (Grelaud et
341 al., 2012) with upper mixed layer depth fluctuations reconstructed for the same core
342 (Amies et al., 2019), and with the contemporaneous EDC time series of atmospheric
343 CH_4 concentrations and the Sanbao Cave $\delta^{18}O$ stack, which are thought to reflect
344 fluctuations in boreal monsoon intensity and attendant changes in the spatial coverage
345 of tropical wetlands (Cheng et al., 2016, 2009, 2006; Möller et al., 2013; Petrenko et
346 al., 2009). We present the *F. profunda* time series (Grelaud et al., 2012) on the

radiometrically constrained chronology of Grant et al. (2012), as natural logarithm of the original data. Within uncertainties of the various records, we note a strong similarity between the LC21 *F. profunda* record and variations of both Sanbao Cave speleothem $\delta^{18}O$ (Fig. 2a) and EDC CH_4 (Fig. 2b). Notably, a distinct *F. profunda* peak at ~129 ka appears contemporaneous with upper mixed layer thinning, with a maximum in the rates of Sanbao Cave $\delta^{18}O$ change and with the CH_4 overshoot in EDC. This suggests: (*i*) synchronous intensification of the African and Asian monsoons at the onset of the last interglacial period, in line with what has been documented for the early Holocene (Fleitmann et al., 2003; Marino et al., 2009; Nicholson et al., 2020; Tierney et al., 2008); and (*ii*) a rapid increase in freshwater discharge into the eastern Mediterranean at the onset of the last interglacial monsoon maximum, quantified as up to ~8.8 times the modern pre- Aswan Nile discharge and responsible for the most intense thinning of the upper summer mixed layer (Amies et al., 2019). Observation (*ii*) is particularly relevant because it alludes to the influence of the rates of monsoon intensification on stratification in the eastern Mediterranean. When large amounts of monsoon-fuelled freshwater are rapidly added to the basin, the strong evaporative climate of the Levant cannot keep up with sea-surface dilution (Rohling et al., 1991b) and the water column becomes strongly stratified (Rohling and Gieskes, 1989; Rohling et al., 2006; Marino et al., 2007; Athanasiou et al., 2015, 2017; Amies et al., 2019), causing shoaling of the pycnocline, the nutricline to be positioned at the base of the photic layer and the attendant development of a pronounced DCM.

In Figure 2d-f, LC21 holococcolith data are compared with North Atlantic and western Mediterranean Sea records. It is evident that there is no or poor preservation of holococcoliths during sapropel S5 (Fig. 2e). Peaks of holococcoliths below S5 correlate with low alkenone-derived SSTs in the Alboran Sea (Martrat et al., 2014) (Fig. 2d) and with variations in AMOC strength proxies (Figs. 2e,f) from the Iberian Margin. Specifically, log (Ca/Ti), benthic foraminiferal $\delta^{13}C$, and $C_{26}OH$ ratios

(Hodell et al., 2015; Martrat et al., 2007) unequivocally indicate that AMOC had collapsed during Heinrich event HS11 (Böhm et al., 2015); we find that, at the same time, holococcolith preservation was enhanced. A similar relationship is evident above sapropel S5, especially with C_{26}OH ratio data (Fig. 2f), and may be correlated with North Atlantic cold event C26 (Oppo et al., 2006, 2001; Tzedakis et al., 2018). Coupled ocean-atmosphere hindcasts suggest that the AMOC slowdown/shutdown may have propagated through the Mediterranean Sea in the form of major cooling and intense atmospheric perturbations (Manabe and Stouffer, 1997; Vellinga and Wood, 2002). Both cooling and atmospheric perturbations are major prerequisites for surface water buoyancy loss and deep-water formation, explaining enhanced Mediterranean bottom water ventilation during Heinrich and Stadial events in the last glacial, based on benthic foraminifera $\delta^{13}C$ and alcohol index records (Cacho et al., 2000; Sprovieri et al., 2012; Toucanne et al., 2012). Our new results from the Aegean Sea explicitly link holococcolith preservation to Heinrich and Stadial events in response to deep-water formation and seafloor ventilation increases in the Mediterranean Sea during those events.

6.2 – Coccolith assemblages at ODP Site 967

At ODP Site 967, coccolith distribution patterns are compared (Figure 3) with: (*i*) June 21st insolation at 65°N (Laskar et al., 2004); (*ii*) the benthic $\delta^{18}O$ composite record from ODP Sites 967 and 968 (Konijnendijk et al., 2015); and (*iii*) the LR04 benthic $\delta^{18}O$ stack (Lisiecki and Raymo, 2005). Overall, coccolith assemblages are dominated by placoliths, with percentages between 25 and 98% (average = 70%, Fig. 3D). The deep photic zone species *F. profunda* features high-amplitude fluctuations between intervals in which it is barely occurring (1%) and intervals in which it becomes the dominant (up to 74%)~~, and an average of 26%~~ (Fig. 3E). Placoliths' peak (low) abundances occur when *F. profunda* percentages are at a minimum (maximum), as highlighted by the pronounced anticorrelation (R^2= 0.95, n = 668) displayed in Figure 4.

The observed alternating dominance of the placoliths and *F. profunda* (see above) at ODP Site 967 suggests that between MIS 14 and MIS 9 the upper water column in the easternmost Mediterranean Sea repeatedly switched between dominant winter-induced fertilization (placoliths' peaks, shallow nutricline), similar to today's winter conditions (Knappertsbusch, 1993), and a predominantly DCM-focused productivity (*F. profunda*'s peaks, deep nutricline) during both glacial and interglacial periods. Shoaling of the pycnocline, which promoted a deep nutricline (DCM), in association with intensifications of the North African monsoon and sea-level lowering (Rohling and Gieskes, 1989; Rohling, 1991a, 1991b) is the most plausible explanation for the peak abundance of *F. profunda* at ODP Site 967 during sapropels and glacial periods, respectively. Accordingly, *F. profunda* would be particularly sensitive to nutrient (re)distribution within the photic zone, with intervals of positive shifts in the basins freshwater budget (monsoon maxima, Rohling, 1991b) and reduced water exchange at straits (glacial lowstands, Rohling, 1991a) both leading to enhanced stratification in the upper water column, shoaling of the pycnocline, and development of a nutricline at the based of the photic layer. This conceptual framework indicated by box-model calculations (Rohling, 1991a,b) provides an explanation for the *F. profunda* peaks both in sapropel layers (e.g., S12, S11, b, S10) and during MIS 12 and MIS 10 glacial periods (see also Section 6.3).

The remaining three coccolith groups at Site 967 are largely subordinate. Low abundance of UPZ taxa (0.0-5.4%, 1.4% on average, Fig. 3F) and Miscellaneous taxa (0.0-11.1%, 1.2% on average, Fig. 3G) is unexpected in the severe oligotrophy of the eastern Mediterranean Sea, especially for UPZ taxa that include dominant coccolithophore species in summer/autumn (Knappertsbusch, 1993; Malinverno et al., 2009; Oviedo et al., 2015). However, living coccolithophore surveys show that winter production (placolith blooming) is about an order of magnitude higher than summer production, thereby explaining the apparent ecological contradiction in taxa proportions (Knappertsbusch, 1993).

Holococcolith percentage values range between 0.0 and 20.8%, 1.9% on average (Fig. 3H). As was the case in late Quaternary sapropels, tiny holococcoliths are again not preserved in sapropel layers, but we also note that that poor preservation extends far beyond sapropel layers.

6.3 – Comparison between coccoliths, element ratios and climatic indices at ODP Site 967

Florisphaera profunda and holococcolith distribution patterns at ODP Site 967 (Figs. 5A-B) are compared with sedimentary elemental ratios and climatic indices from the same sedimentary sequence (Grant et al., 2017). A principal component analysis carried out on elemental proxies by these authors highlighted that principal components PC1 (not shown) and PC2 (Fig. 5D) account for 79% of variance and reflect terrigenous input and sapropel deposition (enhanced monsoon runoff), respectively. Moreover, aeolian dust fluxes (Fig. 5E) and a North Africa humidity/aridity index (Fig. 5F) were calculated and are also compared with coccolith abundance fluctuations.

Intensification of East African monsoon precipitation coincided with northward displacement of the Intertropical Convergence Zone (ITCZ) and subsequent intensification of precipitation over the catchment basins of the Nile and other rivers, which fuelled enhanced freshwater discharge along the wider North African margin into the eastern Mediterranean (Ehrmann et al., 2016; Rohling et al., 2002a; Rohling et al., 2015). *Florisphaera profunda* proliferates because it benefits from the nutricline positioned in deep photic zone and the establishment of a DCM (Castradori, 1993; Girone et al., 2013; Grelaud et al., 2012; Incarbona et al., 2011; Negri et al., 1999), following the rationale outlined above (Myers et al., 1998; Rohling, 1991a; Rohling and Gieskes, 1989). This scenario has been described for eastern Mediterranean sapropels and is further supported by the coupling of the *F. profunda* signal and enhanced humidity in North Africa that leads to enhanced

463 monsoon runoff into the eastern Mediterranean, especially during S12, S11, b and
464 S10 (Fig. 5). Also evident is decoupling between *F. profunda* and the
465 humidity/aridity index, for instance during glacial sapropel S13 and during sapropel
466 layer b. This suggests that the climatic indices at ODP Site 967 reflect increased
467 rainfall over North Africa and Sahara, without sufficient northward monsoon
468 penetration that determines the intensity of monsoon-related runoff into the eastern
469 Mediterranean Sea (Grant et al., 2017). Also, different nutrient dynamics may have
470 developed during the glacial sapropel S13, with surface fertilization that supports
471 placolith-bearing species competition.
472
473 However, the coccolith record at Site 967 suggests that *F. profunda* increases are a
474 recurring feature of the record that is not necessarily associated with the deposition of
475 organic-rich layers deposition on the eastern Mediterranean seafloor, especially in
476 glacial episodes (Fig. 5A). The Ba/Al signal indicates that many sapropel layers have
477 been partially oxidized (Fig. 5G), so that their currently visible extents do not
478 represent the original thickness of anoxic sediments. Yet, we argue that *F. profunda*
479 peaks are not exclusively linked to the environmental changes associated with
480 sapropel formation. Positive *Florisphaera profunda* peaks without a corresponding
481 sapropel layer (be it visible, or oxidized) are evident in all eastern Mediterranean
482 records that span sufficiently long time intervals (Castradori, 1993; Giunta et al.,
483 2003; Maiorano et al., 2013; Negri et al., 1999; Triantaphyllou et al., 2010). The
484 occurrence of *F. profunda* during glacial periods identifies a second mode of DCM
485 development in the eastern Mediterranean, as proposed on the basis of planktonic
486 foraminiferal assemblages (Rohling and Gieskes, 1989) and modeling (Myers et al.,
487 1998; Rohling, 1991a). Again, the DCM development would be driven by the
488 pycnocline and nutricline shoaling within the lower part of the photic zone. But, for
489 glacials, the eustatic sea-level drop (Fig. 5C) would have been the main trigger
490 mechanism, after reducing water mass transport at both Gibraltar and Sicily Straits
491 and ultimately shoaling the pycnocline and nutricline depth up to ~ 80 m (Myers et

al., 1998; Rohling, 1991a). However, the scattered *F. profunda* abundance signal in MISs 12 and 10 suggests that other factors may operate in conjunction with sea-level fall, for reducing water transport across the Gibraltar and Sicily Straits. Among these, less frequent and intense northern outbreaks in deep water production sites and the inflow of low-density meltwater from the Atlantic Ocean may have weakened the Mediterranean thermohaline circulation and may have caused transient reductions in the water transport at straits, like during last glacial cold spells (Sierro et al., 2005; Sprovieri et al., 2012; Toucanne et al., 2012; Azibeiro et al., 2021).

Holococcoliths are made of small calcite rhombohedra, arranged in different patterns. They are the most vulnerable coccoliths to selective dissolution (Roth and Coulbourn, 1982). Comparison between the new ODP 967 holococcolith record and the humidity/aridity index (Figs. 5B, F) shows strong similarities throughout the time span studied, which clearly point to the dissolution of haploid-life calcite remains at the Erathostenes seamount during humid phases. This agrees with the notion that surface buoyancy gain by freshwater river discharge negatively impacted deep-water formation in the eastern Mediterranean Sea, which enhanced organic carbon preservation (De Lange et al., 2008; Myers et al., 1998; Rohling et al., 2015) and, thus, worsened holococcolith preservation, like during sapropel S1 (Crudeli et al., 2006; Incarbona et al., 2019; Incarbona and Di Stefano, 2019) and sapropel S5 (Fig. 2, this study).

It is worth noting that the three major aeolian dust peaks during MIS 13-12 (Fig. 5E) did not match with increasing holococcolith preservation but fall within 'no preservation' intervals. Aeolian dust peaks are associated with weakened monsoon activity and North Africa dry periods, as seen from the Ti/Al ratio (Konijnendijk et al., 2015; Lourens et al., 2001; Wehausen and Brumsack, 2000; Ziegler et al., 2010), and would imply a lower freshwater input into the eastern Mediterranean Sea. Ideally, these conditions would enhance deep water formation, reduce organic matter

preservation on the seafloor and increase preservation of holococcolith calcite. However, dust accumulation in marine cores depends on wind strength and direction (Moulin et al., 1997; Zabel et al., 1999). Thus, aeolian dust peaks are not necessarily tied to cooling and atmospheric perturbations that, for instance during the latest Quaternary, led to enhanced Mediterranean bottom water ventilation in coincidence of glacials and stadials (Cacho et al., 1999; 2000; Sprovieri et al., 2012; Toucanne et al., 2012).

6.4 – AMOC slowdown, holococcolith preservation and monsoon weakening

In Figure 6, North Atlantic geochemical records (Fig. 6A-B), Mediterranean holococcolith data (Fig. 6C), and oxygen isotopes of China speleothems (Fig. 6D) are plotted using their own original age models (Cheng et al., 2016; Grant et al., 2017; Hodell et al., 2015; Martrat et al., 2007). The grey boxes used for correlation are drawn and link correlative events in these various Northern Hemisphere records. Records shown in Figure 6 help with outlining a concept of atmosphere/ocean interactions that resulted in the correlation between Northern Hemisphere climate variability and surface water ecosystem modifications and seafloor diagenesis in the eastern Mediterranean.

The correlation boxes in Figure 6 are drawn assuming that AMOC slowdown/shutdown caused an atmospheric perturbation that impacted a vast area of the northern Hemisphere, including the eastern Mediterranean Sea, East African and Asian monsoon sites (Vellinga and Wood, 2002). The log (Ca/Ti) record from the Iberian Margin (Fig. 6B) is a proxy for millennial-scale variability (Hodell et al., 2015): minima indicate stadial/Heinrich phases during which the AMOC was severely weakened or collapsed (McManus et al., 2004, 1999). Previous studies based on $\delta^{13}C$, alcohol index and sortable silt records support the hypothesis that Mediterranean bottom water ventilation at least in the western sub-basin was more intense during glacial periods and stadial events (Cacho et al., 2000, 1999; Frigola et

al., 2008; Sprovieri et al., 2012; Toucanne et al., 2012) and strengthened Mediterranean outflow into the Gulf of Cadiz and in the Iberian Margin (Sierro et al., 2020). Simultaneous enhancement of EMDW ventilation would have enhanced holococcolith preservation, as observed below and above sapropel S1 (Incarbona et al., 2019; Incarbona and Di Stefano, 2019) and during HS11 and C26 in the Aegean Sea (this study, Fig. 2). The physico-chemical processes in the seafloor microsystem by which tiny holococcolith calcite rhombohedra are preferentially preserved under oxic conditions is not clear yet. Incarbona et al. (2019b) hypothesized a possible detrimental action of organic acid produced by bacteria under a dysoxic/anoxic state on the water/sediment interface, in analogy with results from modern surveys in the Gulf of California (Ziveri and Thunell, 2000). However, specific studies are needed to better understand the processes involved.

The link between AMOC slowdown/shutdown and East African, Indian, and Asian monsoon weakening is well-established (Deplazes et al., 2014; Porter and Zhisheng, 1995; Rohling et al., 2002; Rohling et al., 2006; Schulz et al., 1998; Sirocko et al., 1993; Tjallingii et al., 2008), and may involve severe drought development due to southward ITCZ displacement (Krebs and Timmermann, 2007; Vellinga and Wood, 2002; Zhang and Delworth, 2006). Yet, an ITCZ shift and associated Hadley cell changes likely explain only part of the impacts on monsoon circulation, which also depends on regional and local processes (Donohoe et al., 2013; Geen et al., 2020). For example, recent modeling shows that Northern Hemisphere glacial cooling, increased ice-sheet albedo, and sea-level lowering produce an anomalous thermal gradient between the Arabian Peninsula and the Arabian Sea that results in a weakened Walker circulation in the Indian Ocean and drought in the monsoon systems of the Indo-Pacific region (DiNezio et al., 2018). As mentioned before for the HS 11 and C26 cold spells (section 6.1), AMOC slowdown/shutdown also produces cooling and intense atmospheric perturbations in the Mediterranean region (Manabe and Stouffer, 1997; Vellinga and Wood, 2002), facilitating deep-water

formation and bottom water ventilation (Cacho et al., 2000; Sprovieri et al., 2012; Toucanne et al., 2012). Thus, AMOC slowdown/shutdown may have both strengthened cold and dry polar/continental air outbreaks and reduced Indian-African monsoon activity, with both processes conducive to enhanced EMDW production (the prerequisite for holococcolith preservation).

In Fig. 6, grey correlation boxes indicate a link between AMOC slowdown/shutdown phases (Fig. 6B) and both the heaviest oxygen isotopic values in Chinese Sanbao Cave speleothems (Fig. 6D) and enhanced holococcolith preservation in the Mediterranean (Fig. 6C).

The atmospheric CH_4 record from Antarctica ice cores (Fig. 6E) reflects emissions from boreal and monsoonal wetlands (Guo et al., 2012; Landais et al., 2010). The signal has been be separated into three principal components, a glacial-interglacial forced component, a bi-hemispheric insolation driven component, and a millennial-scale oscillatory component, which respectively explain 80%, 15% and 5% of the variance (Guo et al., 2012). Glacial-interglacial cycles force globally synchronous monsoonal variations in methane emission. The other two forcings are hemispheric in nature, because of the two hemispheres' anti-phasing for low-latitude summer insolation changes in ITCZ oscillations and for millennial-scale bipolar see-saw (strengthening/weakening) AMOC circulation (Guo et al., 2012). The limited number of grey correlation boxes between the Antarctic CH_4 signal and of Asian monsoon activity (Fig. 6D-E) suggests that the activity of Southern Hemisphere monsoon systems (South America, South Africa, Australia) have been a major driver of methane emission between 550 and 300 ka However, we note the occurrence of three different peaks of Antarctic CH_4 during MIS 13, a signal which is also visible in Mediterranean holococcoliths and the China speleothem record (Fig. 6). This feature supports reduced emission from southern hemisphere methane sources during MIS 13 and an increased and synchronous emission from northern monsoons and boreal wetlands (Guo et al., 2012).

608 7 – Conclusions

609 The chronology and age uncertainties of SE Aegean Sea core LC21 coccolith data,
610 Iberian Margin geochemical records, $\delta^{18}O$ in the Sanbao Cave stalagmites, and
611 atmospheric methane concentrations from EDC have been probabilistically assessed
612 for the last interglacial and TII. The *F. profunda* peak at the base of sapropel S5 layer
613 is contemporaneous with a maximum in the rates of $\delta^{18}O$ change in Sanbao Cave and
614 with the CH_4 overshoot in EDC, which suggests an African and Asian monsoon
615 intensification at the onset of the last interglacial and the raising of the summer upper
616 mixed layer depth. Holococcolith preservation was enhanced during Heinrich event
617 HS11 and the C26 cold spell, when AMOC was severely weakened or collapsed.
618 Cooling and atmospheric perturbations promoted surface-water buoyancy loss and
619 deep-water formation, and thus increased Mediterranean bottom water ventilation
620 rates. These results for LC21 explicitly link holococcolith preservation to episodes of
621 enhanced deep-water formation and seafloor ventilation in the eastern Mediterraenan
622 Sea during Heinrich and Stadial events.

623

624 We also analysed 668 samples from ODP Site 967 to reconstruct variations in
625 coccolithophore ecology in the region of the Eratosthenes Seamount (eastern
626 Mediterranean Sea) between about 550 and 300 ka (Middle Pleistocene, MIS 14-9).
627 Placoliths and *F. profunda* abundance fluctuations are strongly anticorrelated (R^2 =
628 0.95, n = 668) and together dominate the coccolith assemblages at Site 967, which
629 suggests that the surface water environment repeatedly switched between
630 predominant winter-induced fertilization (shallow nutricline) and predominant
631 monsoon-induced deep nutricline conditions (and Deep Chlorophyll Maximum
632 development) associated with a shoaling of the pycnocline to a position within the
633 lower photic zone. In analogy with results for core LC21, Middle Pleistocene phases
634 of enhanced monsoon runoff into the eastern Mediterranean appear to have caused
635 shoaling of the pycnocline into the lower photic layer, which provides a deep
636 nutricline that fosters *F. profunda* proliferation. A second mode of *F. profunda*

proliferation and DCM development is seen in glacials, when the nutricline shoaled into the lower photic zone due to sea-level lowering that reduced water-mass transport through the main Mediterranean straits. Thus, our coccolithophore assemblage analyses corroborate earlier suggestions of such a phenomenon based on planktonic foraminiferal analyses (Rohling and Gieskes, 1989) and modeling (Myers et al., 1998; Rohling, 1991a).

Scattered but statistically significant peaks of holococcoliths (up to ~ 20%) mark increased carbonate preservation on the seafloor due to enhanced production of EMDW, which match changes in recently proposed North Africa aridity indices (Grant et al., 2017). Finally, holococcolith enhanced preservation during cold spells is linked to increased deep-water formation in the Mediterranean Sea, in response to Atlantic Meridional Overturning Circulation slowdown and weakened monsoon activity during Northern Hemisphere cold events.

Acknowledgments

We are grateful to an anonymous reviewer and to Fabienne Marret-Davies for their comments and suggestions. FFR2021 grant to A.I. is acknowledged. G.M. acknowledges support from the Universidade de Vigo's programme to attract excellent research talent (RR04092017), a Beatriz Galindo Fellowship (2020), and a generous start-up package. M.G. acknowledges support from the CALMED project (CTM2016-79547-R) and the Generalitat de Catalunya (MERS, 2014 SGR – 1356).

Bibliographic references

Allen, J.I., Somerfield, P.J., Siddorn, J., 2002. Primary and bacterial production in the Mediterranean Sea: A modelling study. J. Mar. Syst. 33–34, 473–495. doi:10.1016/S0924-7963(02)00072-6

Amies, J.D., Rohling, E.J., Grant, K.M., Rodríguez-Sanz, L., Marino, G., 2019. Quantification of African Monsoon Runoff During Last Interglacial Sapropel S5.

Paleoceanogr. Paleoclimatology 34, 1487–1516. doi:10.1029/2019PA003652
Athanasiou, M., Boloubassi, I., Gogou, A., Klein, V., Dimiza, M.D., Parinos, C., Skampa, E., Triantaphyllou, M.V., 2017. Sea surface temperatures and environmental conditions during the 'warm Pliocene' interval (4.1-3.2 Ma) in the Eastern Mediterranean (Cyprus). Global Planetary Change 150, 46-57.
Athanasiou, M., Triantaphyllou, M.V., Dimiza, M.D., Gogou, A., Theodorou, G., 2015. Zanclean/Piacenzian transition on Cyprus (SE Mediterranean): calcareous nannofossil evidence of sapropel formation. Geo-Marine Letters 35, 367-385.
Azibeiro, L. A., Sierro, F. J., Capotondi, L., Lirer, F., Andersen, N., González-Lanchas, A., Alonso-Garcia, M., Flores, J.-A., Cortina, A., Grimalt, J. O., Martrat, B., Cacho, I., 2021. Meltwater flux from northern ice-sheets to the mediterranean during MIS 12. Quaternary Science Reviews, 268, 107108. https://doi.org/https://doi.org/10.1016/j.quascirev.2021.107108
Baumann, K.-H., Andruleit, H., Böckel, B., Geisen, M., Kinkel, H., 2005. The significance of extant coccolithophores as indicators of ocean water masses, surface water temperature, and paleoproductivity: a review. Pal{ä}ontologische Zeitschrift 79, 93–112. doi:10.1007/bf03021756
Bazin, L., Landais, A., Lemieux-Dudon, B., Toyé Mahamadou Kele, H., Veres, D., Parrenin, F., Martinerie, P., Ritz, C., Capron, E., Lipenkov, V., Loutre, M.-F., Raynaud, D., Vinther, B., Svensson, A., Rasmussen, S.O., Severi, M., Blunier, T., Leuenberger, M., Fischer, H., Masson-Delmotte, V., Chappellaz, J., Wolff, E., 2013. An optimized multi-proxy, multi-site Antarctic ice and gas orbital chronology (AICC2012): 120–800 ka. Clim. Past 9, 1715–1731. doi:10.5194/cp-9-1715-2013
Bazzicalupo, P., Maiorano, P., Girone, A., Marino, M., Combourieu-Nebout, N., Pelosi, N., Salgueiro, E., Incarbona, A., 2020. Holocene climate variability of the Western Mediterranean: Surface water dynamics inferred from calcareous plankton assemblages. The Holocene. doi:10.1177/0959683619895580
Beaufort, L., de Garidel-Thoron, T., Mix, A.C., Pisias, N.G., 2001. ENSO-like

695 forcing on oceanic primary production during the Late Pleistocene. Science 293,
696 2440–2444. doi:10.1126/science.293.5539.2440
697 Beaufort, L., Lancelot, Y., Camberlin, P., Cayre, O., Vincent, E., Bassinot, F.,
698 Labeyrie, L., 1997. Insolation Cycles as a Major Control of Equatorial Indian
699 Ocean Primary Production. Science 278, 1451–1454.
700 Böhm, E., Lippold, J., Gutjahr, M., Frank, M., Blaser, P., Antz, B., Fohlmeister, J.,
701 Frank, N., Andersen, M.B., Deininger, M., 2015. Strong and deep Atlantic
702 meridional overturning circulation during the last glacial cycle. Nature 517, 73–
703 76. doi:10.1038/nature14059
704 Bonomo, S., Grelaud, M., Incarbona, A., Malinverno, E., Placenti, F., Bonanno, A.,
705 Stefano, E.D., Patti, B., Sprovieri, M., Genovese, S., Rumolo, P., Mazzola, S.,
706 Zgozi, S., Ziveri, P., 2012. Living Coccolithophores from the Gulf of Sirte
707 (Southern Mediterranean Sea) during the summer of 2008. Micropaleontology
708 58, 487–503.
709 Bown, Paul R., Young, J.R., 1998. Techniques, in: Bown, P.R. (Ed.), Calcareous
710 Nannofossil Biostratigraphy. Chapman and Kluwer Academic, London, pp. 16–
711 28.
712 Cacho, I., Grimalt, J.O., Pelejero, C., Canals, M., Sierro, F.J., Flores, J.A.,
713 Shackleton, N., 1999. Dansgaard-Oeschger and Heinrich event imprints in
714 Alboran Sea paleotemperatures. Paleoceanography 14, 698–705.
715 doi:10.1029/1999PA900044
716 Cacho, I., Grimalt, J.O., Sierro, F.J., Shackleton, N., Canals, M., 2000. Evidence for
717 enhanced Mediterranean thermohaline circulation during rapid climatic coolings.
718 Earth Planet. Sci. Lett. 183, 417–429. doi:10.1016/S0012-821X(00)00296-X
719 Castradori, D., 1993. Calcareous nannofossils and the origin of Eastern
720 Mediterranean sapropel. Paleoceanography 8, 459–471.
721 Cheng, H., Edwards, R.L., Broecker, W.S., Denton, G.H., Kong, X., Wang, Y.,
722 Zhang, R., Wang, X., 2009. Ice Age Terminations. Science (80-.). 326, 248–252.
723 doi:10.1126/science.1177840

724 Cheng, H., Edwards, R.L., Sinha, A., Spötl, C., Yi, L., Chen, S., Kelly, M., Kathayat,
725 G., Wang, X., Li, X., Kong, X., Wang, Y., Ning, Y., Zhang, H., 2016. The Asian
726 monsoon over the past 640,000 years and ice age terminations. Nature 534, 640–
727 646. doi:10.1038/nature18591
728 Cheng, H., Edwards, R.L., Wang, Y., Kong, X., Ming, Y., Kelly, M.J., Wang, X.,
729 Gallup, C.D., Liu, W., 2006. A penultimate glacial monsoon record from Hulu
730 Cave and two-phase glacial terminations. Geology 34, 217–220.
731 doi:10.1130/G22289.1
732 Crudeli, D., Young, J.R., Erba, E., Geisen, M., Ziveri, P., de Lange, G.J., Slomp,
733 C.P., 2006. Fossil record of holococcoliths and selected hetero-holococcolith
734 associations from the Mediterranean (Holocene-late Pleistocene): Evaluation of
735 carbonate diagenesis and palaeoecological-palaeocenographic implications.
736 Palaeogeogr. Palaeoclimatol. Palaeoecol. 237, 191–212.
737 doi:10.1016/j.palaeo.2005.11.022
738 D'Amario, B., Ziveri, P., Grelaud, M., Oviedo, A., Kralj, M., 2017. Coccolithophore
739 haploid and diploid distribution patterns in the Mediterranean Sea: Can a haplo-
740 diploid life cycle be advantageous under climate change? J. Plankton Res. 39,
741 781–794. doi:10.1093/plankt/fbx044
742 Dimiza, M.D., Triantaphyllou, M.V., Malinverno, E., Psarra, S., Karatsolis, B., Mara,
743 P., lagaria, A., Gogou, A., 2015. The composition and distribution of living
744 coccolithophores in the Aegean sea (NE Mediterranean). Micropaleontology 61,
745 521-540.
746 D'Ortenzio, F., Ribera d'Alcalà, M., 2009. On the trophic regimes of the
747 Mediterranean Sea: a satellite analysis. Biogeosciences 6, 139–148.
748 doi:10.5194/bg-6-139-2009
749 De Lange, G.J., Thomson, J., Reitz, A., Slomp, C.P., Principato, M.S., Erba, E.,
750 Corselli, C., 2008. Synchronous basin-wide formation and redox-controlled
751 preservation of a Mediterranean sapropel. Nat. Geosci. 1, 606–610.
752 doi:10.1038/ngeo283

753 Deaney, E.L., Barker, S., van de Flierdt, T., 2017. Timing and nature of AMOC
754 recovery across Termination 2 and magnitude of deglacial CO2 change. Nat.
755 Commun. 8, 14595. doi:10.1038/ncomms14595
756 Deplazes, G., Lückge, A., Stuut, J.-B.W., Pätzold, J., Kuhlmann, H., Husson, D.,
757 Fant, M., Haug, G.H., 2014. Weakening and strengthening of the Indian
758 monsoon during Heinrich events and Dansgaard-Oeschger oscillations.
759 Paleoceanography 29, 99–114. doi:10.1002/2013PA002509
760 Di Stefano, A., Foresi, L.M., Incarbona, A., Sprovieri, M., Vallefuoco, M., Iorio, M.,
761 Pelosi, N., Di Stefano, E., Sangiorgi, P., Budillon, F., 2015. Mediterranean
762 coccolith ecobiostratigraphy since the penultimate Glacial (the last 145,000years)
763 and ecobioevent traceability. Mar. Micropaleontol. 115.
764 doi:10.1016/j.marmicro.2014.12.002
765 Di Stefano, E., Incarbona, A., 2004. High-resolution palaeoenvironmental
766 reconstruction of ODP Hole 963D (Sicily Channel) during the last deglaciation
767 based on calcareous nannofossils. Mar. Micropaleontol. 52.
768 doi:10.1016/j.marmicro.2004.04.009
769 Di Stefano, E., Incarbona, A., Bonomo, S., Pelosi, N., 2011. Coccolithophores in
770 water samplesand fossil assemblages in sedimentary archives of the
771 Mediterranean Sea: A review, New Oceanography Research Developments:
772 Marine Chemistry, Ocean Floor Analyses and Marine Phytoplankton.
773 DiNezio, P.N., Tierney, J.E., Otto-Bliesner, B.L., Timmermann, A., Bhattacharya, T.,
774 Rosenbloom, N., Brady, E., 2018. Glacial changes in tropical climate amplified
775 by the Indian Ocean. Sci. Adv. 4, eaat9658. doi:10.1126/sciadv.aat9658
776 Donohoe, A., Marshall, J., Ferreira, D., Mcgee, D., 2013. The Relationship between
777 ITCZ Location and Cross-Equatorial Atmospheric Heat Transport: From the
778 Seasonal Cycle to the Last Glacial Maximum. J. Clim. 26, 3597–3618.
779 doi:10.1175/JCLI-D-12-00467.1
780 Ehrmann, W., Schmiedl, G., Seidel, M., Krüger, S., Schulz, H., 2016. A distal
781 140\,kyr sediment record of Nile discharge\hack{\newline} and East African

782 monsoon variability. Clim. Past 12, 713–727. doi:10.5194/cp-12-713-2016
783 Emeis, K.-C., Robertson, A.H.F., Richter, C., Party, S., 1996. Site 967. In:
784 Proceedings of the Ocean Drilling Program, Initial Reports, Leg 160 (Emeis, K.-
785 C., Robertson, A.H.F. and Richter, C. Eds). pp. 215–287.
786 Emeis, K.C., Sakamoto, T., Wehausen, R., Brumsack, H.J., 2000a. The sapropel
787 record of the eastern Mediterranean Sea - Results of Ocean Drilling Program Leg
788 160. Palaeogeogr. Palaeoclimatol. Palaeoecol. 158, 371–395. doi:10.1016/S0031-
789 0182(00)00059-6
790 Emeis, K.C., Struck, U., Schulz, H.M., Rosenberg, R., Bernasconi, S., Erlenkeuser,
791 H., Sakamoto, T., Martinez-Ruiz, F., 2000b. Temperature and salinity variations
792 of Mediterranean Sea surface waters over the last 16,000 years from records of
793 planktonic stable oxygen isotopes and alkenone unsaturation ratios. Palaeogeogr.
794 Palaeoclimatol. Palaeoecol. 158, 259–280. doi:10.1016/S0031-0182(00)00053-5
795 Fleitmann, D., Burns, S.J., Mudelsee, M., Neff, U., Kramers, J., Mangini, A., Matter,
796 A., 2003. Holocene Forcing of the Indian Monsoon Recorded in a Stalagmite
797 from Southern Oman. Science (80-.). 300, 1737–1739.
798 doi:10.1126/science.1083130
799 Flores, J.A., Bárcena, M.A., Sierro, F.J., 2000. Ocean-surface and wind dynamics in
800 the Atlantic Ocean off Northwest Africa during the last 140 000 years.
801 Palaeogeogr. Palaeoclimatol. Palaeoecol. 161, 459–478. doi:10.1016/S0031-
802 0182(00)00099-7
803 Flores, J.A., Sierro, F.J., Francés, G., Vazquez, A., Zamarreno, I., 1997. The last
804 100,000 years in the western Mediterranean: sea surface water and frontal
805 dynamics as revealed by coccolithophores. Mar. Micropaleontol. 29, 351–366.
806 Frigola, J., Moreno, A., Cacho, I., Canals, M., Sierro, F.J., Flores, J.A., Grimalt, J.O.,
807 2008. Evidence of abrupt changes in Western Mediterranean Deep Water
808 circulation during the last 50 kyr: A high-resolution marine record from the
809 Balearic Sea. Quat. Int. 181, 88–104. doi:10.1016/j.quaint.2007.06.016
810 Geen, R., Bordoni, S., Battisti, D.S., Hui, K., 2020. Monsoons, ITCZs, and the

811 Concept of the Global Monsoon. Rev. Geophys. 58, e2020RG000700.
812 doi:https://doi.org/10.1029/2020RG000700
813 Girone, A., Capotondi, L., Ciaranfi, N., Di Leo, P., Lirer, F., Maiorano, P., Marino,
814 M., Pelosi, N., Pulice, I., 2013. Paleoenvironmental changes at the lower
815 Pleistocene Montalbano Jonico section (southern Italy): Global versus regional
816 signals. Palaeogeogr. Palaeoclimatol. Palaeoecol. 371, 62–79.
817 doi:10.1016/j.palaeo.2012.12.017
818 Giunta, S., Negri, a., Morigi, C., Capotondi, L., Combourieu-Nebout, N., Emeis,
819 K.C., Sangiorgi, F., Vigliotti, L., 2003. Coccolithophorid ecostratigraphy and
820 multi-proxy paleoceanographic reconstruction in the Southern Adriatic Sea
821 during the last deglacial time (Core AD91-17). Palaeogeogr. Palaeoclimatol.
822 Palaeoecol. 190, 39–59. doi:10.1016/S0031-0182(02)00598-9
823 Grant, K.M., Grimm, R., Mikolajewicz, U., Marino, G., Ziegler, M., Rohling, E.J.,
824 2016. The timing of Mediterranean sapropel deposition relative to insolation,
825 sea-level and African monsoon changes. Quat. Sci. Rev. 140, 125–141.
826 doi:10.1016/j.quascirev.2016.03.026
827 Grant, K.M., Rohling, E.J., Bar-Matthews, M., Ayalon, A., Medina-Elizalde, M.,
828 Ramsey, C.B., Satow, C., Roberts, A.P., 2012. Rapid coupling between ice
829 volume and polar temperature over the past 50,000 years. Nature 491, 744–747.
830 doi:10.1038/nature11593
831 Grant, K.M., Rohling, E.J., Westerhold, T., Zabel, M., Heslop, D., Konijnendijk, T.,
832 Lourens, L., 2017. A 3 million year index for North African humidity/aridity and
833 the implication of potential pan-African Humid periods. Quat. Sci. Rev. 171,
834 100–118. doi:https://doi.org/10.1016/j.quascirev.2017.07.005
835 Grelaud, M., Marino, G., Ziveri, P., Rohling, E.J., 2012. Abrupt shoaling of the
836 nutricline in response to massive freshwater flooding at the onset of the last
837 interglacial sapropel event. Paleoceanography 27. doi:10.1029/2012PA002288
838 Guo, Z., Zhou, X., Wu, H., 2012. Glacial-interglacial water cycle, global monsoon
839 and atmospheric methane changes. Clim. Dyn. 39, 1073–1092.

840 doi:10.1007/s00382-011-1147-5
841 Hernández-Almeida, I., Ausín, B., Saavedra-Pellitero, M., Baumann, K.-H., Stoll,
842 H.M., 2019. Quantitative reconstruction of primary productivity in low latitudes
843 during the last glacial maximum and the mid-to-late Holocene from a global
844 Florisphaera profunda calibration dataset. Quat. Sci. Rev. 205, 166–181.
845 doi:https://doi.org/10.1016/j.quascirev.2018.12.016
846 Hodell, D., Crowhurst, S., Skinner, L., Tzedakis, P.C., Margari, V., Channell, J.E.T.,
847 Kamenov, G., MacLachlan, S., Rothwell, G., 2013. Response of Iberian Margin
848 sediments to orbital and suborbital forcing over the past 420 ka.
849 Paleoceanography 28, 185–199. doi:10.1002/palo.20017
850 Hodell, D., Lourens, L., Crowhurst, S., Konijnendijk, T., Tjallingii, R., Jiménez-
851 Espejo, F., Skinner, L., Tzedakis, P.C., Abrantes, F., Acton, G.D., Alvarez
852 Zarikian, C.A., Bahr, A., Balestra, B., Barranco, E.L., Carrara, G., Ducassou, E.,
853 Flood, R.D., Flores, J.-A., Furota, S., Grimalt, J., Grunert, P., Hernández-Molina,
854 J., Kim, J.K., Krissek, L.A., Kuroda, J., Li, B., Lofi, J., Margari, V., Martrat, B.,
855 Miller, M.D., Nanayama, F., Nishida, N., Richter, C., Rodrigues, T., Rodríguez-
856 Tovar, F.J., Roque, A.C.F., Sanchez Goñi, M.F., Sierro Sánchez, F.J., Singh,
857 A.D., Sloss, C.R., Stow, D.A.V., Takashimizu, Y., Tzanova, A., Voelker, A.,
858 Xuan, C., Williams, T., 2015. A reference time scale for Site U1385 (Shackleton
859 Site) on the SW Iberian Margin. Glob. Planet. Change 133, 49–64.
860 doi:10.1016/j.gloplacha.2015.07.002
861 Incarbona, A., Abu-Zied, R.H., Rohling, E.J., Ziveri, P., 2019. Reventilation
862 Episodes During the Sapropel S1 Deposition in the Eastern Mediterranean Based
863 on Holococcolith Preservation. Paleoceanogr. Paleoclimatology 34, 1597–1609.
864 doi:10.1029/2019PA003626
865 Incarbona, A., Di Stefano, E., 2019. Calcareous nannofossil palaeoenvironmental
866 reconstruction and preservation in sapropel S1 at the Eratosthenes Seamount
867 (Eastern Mediterranean). Deep Sea Res. Part II Top. Stud. Oceanogr. 164, 206–
868 215. doi:https://doi.org/10.1016/j.dsr2.2018.10.004

869 Incarbona, A., Di Stefano, E., Parti, B., Pelosi, N., Bonomo, S., Mazzola, S.,
870 Sprovieri, R., Tranchida, G., Zgozi, S., Bonanno, A., 2008. Holocene millennial-
871 scale productivity variations in the Sicily Channel (Mediterranean Sea).
872 Paleoceanography 23, 1–18. doi:10.1029/2007PA001581
873 Incarbona, A., Martrat, B., Di Stefano, E., Grimalt, J.O., Pelosi, N., Patti, B.,
874 Tranchida, G., 2010a. Primary productivity variability on the Atlantic Iberian
875 Margin over the last 70,000 years: Evidence from coccolithophores and fossil
876 organic compounds. Paleoceanography 25, 1–15. doi:10.1029/2008PA001709
877 Incarbona, A., Sprovieri, M., Di Stefano, A., Di Stefano, E., Salvagio Manta, D.,
878 Pelosi, N., Ribera d'Alcalà, M., Sprovieri, R., Ziveri, P., 2013. Productivity
879 modes in the mediterranean sea during dansgaard-oeschger (20,000-70,000yr
880 ago) oscillations. Palaeogeogr. Palaeoclimatol. Palaeoecol. 392.
881 doi:10.1016/j.palaeo.2013.09.023
882 Incarbona, A., Ziveri, P., Di Stefano, E., Lirer, F., Mortyn, G., Patti, B., Pelosi, N.,
883 Sprovieri, M., Tranchida, G., Vallefuoco, M., Albertazzi, S., Bellucci, L.G.,
884 Bonanno, A., Bonomo, S., Censi, P., Ferraro, L., Giuliani, S., Mazzola, S.,
885 Sprovieri, R., 2010b. The Impact of the Little Ice Age on Coccolithophores in the
886 Central Mediterranea Sea. Clim. Past 6, 795–805. doi:10.5194/cp-6-795-2010
887 Incarbona, A., Ziveri, P., Sabatino, N., Manta, D.S., Sprovieri, M., 2011. Conflicting
888 coccolithophore and geochemical evidence for productivity levels in the Eastern
889 Mediterranean sapropel S1. Mar. Micropaleontol. 81, 131–143.
890 doi:10.1016/j.marmicro.2011.09.003
891 Jordan, R.W., Cros, L., Young, J.R., 2004. A revised classification scheme for living
892 haptophytes. Micropaleontology 50, 55–79. doi:10.2113/50.Suppl_1.55
893 Josey, S.A., Somot, S., Tsimplis, M., 2011. Impacts of atmospheric modes of
894 variability on Mediterranean Sea surface heat exchange. J. Geophys. Res. Ocean.
895 116, 1–15. doi:10.1029/2010JC006685
896 Kemp, A.E.S., Pearce, R.B., Koizumi, I., Pike, J., Rance, S.J., 1999. The role of mat-
897 forming diatoms in the formation of Mediterranean sapropels. Nature 398, 57.

898 Kleijne, A., 1991. Holococcolithophorids from the Indian-Ocean, Red-Sea,
899 Mediterranean-Sea and North-Atlantic Ocean. Mar. Micropaleontol. 17, 1–76.
900 doi:Doi 10.1016/0377-8398(91)90023-Y
901 Klein, P., Coste, B., 1984. Effects of wind-stress variability on nutrient transport into
902 the mixed layer. Deep Sea Res. Part A. Oceanogr. Res. Pap. 31, 21–37.
903 doi:10.1016/0198-0149(84)90070-0
904 Knappertsbusch, M., 1993. Geographic distribution of living and Holocene
905 coccolithophores in the Mediterranean Sea. Mar. Micropaleontol.
906 doi:10.1016/0377-8398(93)90016-Q
907 Konijnendijk, T.Y.M., Ziegler, M., Lourens, L., 2014. Chronological constraints on
908 Pleistocene sapropel depositions from high-resolution geochemical records of
909 ODP Sites 967 and 968, Newsletters on Stratigraphy. doi:10.1127/0078-
910 0421/2014/0047
911 Konijnendijk, T.Y.M., Ziegler, M., Lourens, L.J., 2015. On the timing and forcing
912 mechanisms of late Pleistocene glacial terminations: Insights from a new high-
913 resolution benthic stable oxygen isotope record of the eastern Mediterranean.
914 Quat. Sci. Rev. 129, 308–320. doi:10.1016/j.quascirev.2015.10.005
915 Krebs, U., Timmermann, A., 2007. Tropical Air–Sea Interactions Accelerate the
916 Recovery of the Atlantic Meridional Overturning Circulation after a Major
917 Shutdown. J. Clim. 20, 4940–4956. doi:10.1175/JCLI4296.1
918 Krom, M.D., Emeis, K.C., Van Cappellen, P., 2010. Why is the Eastern
919 Mediterranean phosphorus limited? Prog. Oceanogr. 85, 236–244.
920 doi:10.1016/j.pocean.2010.03.003
921 Krom, M.D., Kress, N., Brenner, S., Gordon, L.I., 1991. Phosphorus Limitation of
922 Primary Productivity in the Eastern Mediterranean-Sea. Limnol. Oceanogr. 36,
923 424–432.
924 Landais, A., Dreyfus, G., Capron, E., Masson-Delmotte, V., Sanchez-Goñi, M.F.,
925 Desprat, S., Hoffmann, G., Jouzel, J., Leuenberger, M., Johnsen, S., 2010. What
926 drives the millennial and orbital variations of δ18Oatm? Quat. Sci. Rev. 29, 235–

246. doi:https://doi.org/10.1016/j.quascirev.2009.07.005
Larrasoaña, J.C., Roberts, A.P., Rohling, E.J., Winklhofer, M., Wehausen, R., 2003. Three million years of monsoon variability over the northern Sahara. Clim. Dyn. 21, 689–698. doi:10.1007/s00382-003-0355-z
Laskar, J., Robutel, P., Joutel, F., Gastineau, M., Correia, a C.M., Levrard, B., 2004. Astrophysics A long-term numerical solution for the insolation. Astronomy 285, 261–285. doi:10.1051/0004-6361
Lionello, P., 2012. The Climate of the Mediterranean Region: From the Past to the Future, 1st ed. Elsevier Inc. doi:10.1016/B978-0-12-416042-2.00009-4
Lisiecki, L.E., Raymo, M.E., 2005. A Pliocene-Pleistocene stack of 57 globally distributed benthic ?? 18O records. Paleoceanography 20, 1–17. doi:10.1029/2004PA001071
Loulergue, L., Schilt, A., Spahni, R., Masson-Delmotte, V., Blunier, T., Lemieux, B., Barnola, J.-M., Raynaud, D., Stocker, T.F., Chappellaz, J., 2008. Orbital and millennial-scale features of atmospheric CH4 over the past 800,000 years. Nature 453, 383–386. doi:10.1038/nature06950
Lourens, L.J., 2004. Revised tuning of Ocean Drilling Program Site 964 and KC01B (Mediterranean) and implications for the $δ$18O, tephra, calcareous nannofossil, and geomagnetic reversal chronologies of the past 1.1 Myr. Paleoceanography 19, 1–20. doi:10.1029/2003PA000997
Lourens, L.J., Wehausen, R., Brumsack, H.J., 2001. Geological constraints on tidal dissipation and dynamical ellipticity of the Earth over the past three million years. Nature 409, 1029.
Maiorano, P., Tarantino, F., Marino, M., De Lange, G.J., 2013. Paleoenvironmental conditions at Core KC01B (Ionian Sea) through MIS 13-9: Evidence from calcareous nannofossil assemblages. Quat. Int. 288, 97–111. doi:10.1016/j.quaint.2011.12.007
Malanotte-Rizzoli, P., Artale, V., Borzelli-Eusebi, G.L., Brenner, S., Crise, A., Gacic, M., Kress, N., Marullo, S., Ribera D'Alcalà, M., Sofianos, S., Tanhua, T.,

956 Theocharis, A., Alvarez, M., Ashkenazy, Y., Bergamasco, A., Cardin, V.,
957 Carniel, S., Civitarese, G., D'Ortenzio, F., Font, J., Garcia-Ladona, E., Garcia-
958 Lafuente, J.M., Gogou, A., Gregoire, M., Hainbucher, D., Kontoyannis, H.,
959 Kovacevic, V., Kraskapoulou, E., Kroskos, G., Incarbona, A., Mazzocchi, M.G.,
960 Orlic, M., Ozsoy, E., Pascual, A., Poulain, P.M., Roether, W., Rubino, A.,
961 Schroeder, K., Siokou-Frangou, J., Souvermezoglou, E., Sprovieri, M., Tintoré,
962 J., Triantafyllou, G., 2014. Physical forcing and physical/biochemical variability
963 of the Mediterranean Sea: A review of unresolved issues and directions for future
964 research. Ocean Sci. 10, 281–322. doi:10.5194/os-10-281-2014
965 Malinverno, E., Triantaphyllou, M. V, Stavrakakis, S., Ziveri, P., Lykousis, V., 2009.
966 Seasonal and spatial variability of coccolithophore export production at the
967 South-Western margin of Crete (Eastern Mediterranean). Mar. Micropaleontol.
968 71, 131–147. doi:10.1016/j.marmicro.2009.02.002
969 Manabe, S., Stouffer, R.J., 1997. Coupled ocean-atmosphere model response to
970 freshwater input: Comparison to Younger Dryas Event. Paleoceanography 12,
971 321–336. doi:10.1029/96PA03932
972 Marino, G., Rohling, E.J., Rijpstra, W.I.C., Sangiorgi, F., Schouten, S., Sinninghe
973 Damsté, J.S., 2007. Aegean sea as driver of hydrographic and ecological changes
974 in the eastern Mediterranean. Geology 35, 675–678. doi:10.1130/G23831A.1
975 Marino, G., Rohling, E.J., Rodríguez-Sanz, L., Grant, K.M., Heslop, D., Roberts,
976 A.P., Stanford, J.D., Yu, J., 2015. Bipolar seesaw control on last interglacial sea
977 level. Nature 522, 197–201. doi:10.1038/nature14499
978 Marino, G., Rohling, E.J., Sangiorgi, F., Hayes, A., Casford, J.L., Lotter, A.F.,
979 Kucera, M., Brinkhuis, H., 2009. Early and middle Holocene in the Aegean Sea:
980 interplay between high and low latitude climate variability. Quat. Sci. Rev. 28,
981 3246–3262. doi:10.1016/j.quascirev.2009.08.011
982 Marino, M., Maiorano, P., Lirer, F., 2008. Changes in calcareous nannofossil
983 assemblages during the Mid-Pleistocene Revolution. Mar. Micropaleontol. 69,
984 70–90. doi:10.1016/j.marmicro.2007.11.010

985 Martrat, B., Grimalt, J.O., Shackleton, N.J., de Abreu, L., Hutterli, M. a, Stocker,
986 T.F., 2007. Four climate cycles of recurring deep and surface water
987 destabilizations on the Iberian margin. Science 317, 502–507.
988 doi:10.1126/science.1139994
989 Martrat, B., Jimenez-Amat, P., Zahn, R., Grimalt, J.O., 2014. Similarities and
990 dissimilarities between the last two deglaciations and interglaciations in the
991 North Atlantic region. Quat. Sci. Rev. 99, 122–134.
992 doi:10.1016/j.quascirev.2014.06.016
993 McIntyre, A., Molfino, B., 1996. Forcing of Atlantic Equatorial and Subpolar
994 Millennial Cycles by Precession. Science. doi:10.1126/science.274.5294.1867
995 McManus, J.F., Francois, R., Gherardi, J.-M., Keigwin, L.D., Brown-Leger, S., 2004.
996 Collapse and rapid resumption of Atlantic meridional circulation linked to
997 deglacial climate changes. Nature 428, 834–837. doi:10.1038/nature02494
998 McManus, J.F., Oppo, D.W., Cullen, J.L., 1999. A 0.5-Million-Year Record of
999 Millennial-Scale Climate Variability in the North Atlantic. Science 283.
1000 Meier, K.J.S., Zonneveld, K.A.F., Kasten, S., Willems, H., 2004. Different nutrient
1001 sources forcing increased productivity during eastern Mediterranean S1 sapropel
1002 formation as reflected by calcareous dinoflagellate cysts. Paleoceanography 19,
1003 1–12. doi:10.1029/2003PA000895
1004 Millot, C., 1999. Circulation in the Western Mediterranean Sea. J. Mar. Syst. 20,
1005 423–442. doi:10.1016/S0924-7963(98)00078-5
1006 Molfino, B., McIntyre, A., 1990a. Precessional forcing of nutricline dynamics in the
1007 equatorial atlantic. Science 249, 766–769. doi:10.1126/science.249.4970.766
1008 Molfino, B., McIntyre, A., 1990b. Nutricline variation in the equatorial Atlantic
1009 coincident with the Younger Dryas. Paleoceanography.
1010 doi:10.1029/PA005i006p00997
1011 Möller, L., Sowers, T., Bock, M., Spahni, R., Behrens, M., Schmitt, J., Miller, H.,
1012 Fischer, H., 2013. Independent variations of CH4 emissions and isotopic
1013 composition over the past 160,000 years. Nat. Geosci. 6, 885–890.

doi:10.1038/ngeo1922
Myers, P.G., Haines, K., Rohling, E.J., 1998. Modeling the paleocirculation of the Mediterranean: The last glacial maximum and the Holocene with emphasis on the formation of sapropel S1. Paleoceanography 13, 586–606.
Negri, a., Capotondi, L., Keller, J., 1999. Calcareous nannofossils, planktonic foraminifera and oxygen isotopes in the late Quaternary sapropels of the Ionian Sea. Mar. Geol. 157, 89–103. doi:10.1016/S0025-3227(98)00135-2
Nicholson, S.L., Pike, A.W.G., Hosfield, R., Roberts, N., Sahy, D., Woodhead, J., Cheng, H., Edwards, R.L., Affolter, S., Leuenberger, M., Burns, S.J., Matter, A., Fleitmann, D., 2020. Pluvial periods in Southern Arabia over the last 1.1 million-years. Quat. Sci. Rev. 229, 106112. doi:https://doi.org/10.1016/j.quascirev.2019.106112
Oppo, D.W., Keigwin, L.D., McManus, J.F., 2001. Persistent suborbital climate variability in marine isotope stage 5 and Termination II. Paleoceanography 16, 280–292.
Oppo, D.W., McManus, J.F., Cullen, J.L., 2006. Evolution and demise of the Last Interglacial warmth in the subpolar North Atlantic. Quat. Sci. Rev. 25, 3268–3277. doi:10.1016/j.quascirev.2006.07.006
Osborne, A.H., Vance, D., Rohling, E.J., Barton, N., Rogerson, M., Fello, N., 2008. A humid corridor across the Sahara for the migration of early modern humans out of Africa 120,000 years ago. Proc. Natl. Acad. Sci. U. S. A. 105, 16444–16447. doi:10.1073/pnas.0804472105
Ovchinnikov I.M., 1984. The formation of Intermediate Water in the Mediterranean. Oceanology 24, 168–173.
Oviedo, A., Ziveri, P., Álvarez, M., Tanhua, T., 2015. Is coccolithophore distribution in the Mediterranean Sea related to seawater carbonate chemistry? Ocean Sci 11, 13–32. doi:10.5194/os-11-13-2015
Petrenko, V. V, Smith, A.M., Brook, E.J., Lowe, D., Riedel, K., Brailsford, G., Hua, Q., Schaefer, H., Reeh, N., Weiss, R.F., Etheridge, D., Severinghaus, J.P., 2009.

1043 ¹⁴CH₄ Measurements in
1044 Greenland Ice: Investigating Last Glacial Termination
1045 CH₄ Sources. Science (80-.). 324, 506 LP – 508.
1046 doi:10.1126/science.1168909
1047 Pinardi, N., Masetti, E., 2000. Variability of the large scale general circulation of the
1048 Mediterranean Sea from observations and modelling: A review. Palaeogeogr.
1049 Palaeoclimatol. Palaeoecol. 158, 153–174. doi:10.1016/S0031-0182(00)00048-1
1050 POEM group, 1992. General-Circulation of the Eastern Mediterranean. Earth-Science
1051 Rev. 32, 285–309.
1052 Porter, S.C., Zhisheng, A., 1995. Correlation between climate events in the North
1053 Atlantic and China during the last glaciation. Nature 375, 305–308.
1054 doi:10.1038/375305a0
1055 Principato, M.S., Crudeli, D., Ziveri, P., Slomp, C.P., Corselli, C., Erba, E., de Lange,
1056 G.J., 2006. Phyto- and zooplankton paleofluxes during the deposition of sapropel
1057 S1 (eastern Mediterranean): Biogenic carbonate preservation and paleoecological
1058 implications. Palaeogeogr. Palaeoclimatol. Palaeoecol. 235, 8–27.
1059 doi:10.1016/j.palaeo.2005.09.021
1060 Robinson, A.R., Golnaraghi, M., 1994. The physical and dynamical oceanography of
1061 the Mediterranean Sea, in: Ocean Processes in Climate Dynamics: Global and
1062 Mediterranean Examples. pp. 255–306. doi:10.1007/978-94-011-0870-6_12
1063 Rodríguez-Sanz, L., Bernasconi, S.M., Marino, G., Heslop, D., Müller, I.A.,
1064 Fernandez, A., Grant, K.M., Rohling, E.J., 2017. Penultimate deglacial warming
1065 across the Mediterranean Sea revealed by clumped isotopes in foraminifera. Sci.
1066 Rep. 7, 16572. doi:10.1038/s41598-017-16528-6
1067 Rogalla, U., Andruleit, H., 2005. Precessional forcing of coccolithophore
1068 assemblages in the northern Arabian Sea: Implications for monsoonal dynamics
1069 during the last 200,000 years. Mar. Geol. 217, 31–48.
1070 doi:10.1016/j.margeo.2005.02.028
1071 Rohling, E.J., 1991a. Shoaling of the Eastern Mediterranean Pycnocline due to

1072 reduction of excess evaporation: Implications for sapropel formation.
1073 Paleoceanography 6, 747–753. doi:https://doi.org/10.1029/91PA02455
1074 Rohling, E.J., 1991b. A Simple Two-Layered Model for Shoaling of the Eastern
1075 Mediterranean Pycnocline Due to Glacio-Eustatic Sea Level Lowering.
1076 Paleoceanography 6, 537–541. doi:https://doi.org/10.1029/91PA01328
1077 Rohling, E J, Cane, T.R., Cooke, S., Sprovieri, M., Bouloubassi, I., Emeis, K.C.,
1078 Schiebel, R., Kroon, D., Jorissen, F.J., Lorre, A., Kemp, A.E.S., 2002a. African
1079 monsoon variability during the previous interglacial maximum. Earth Planet. Sci.
1080 Lett. 202, 61–75. doi:https://doi.org/10.1016/S0012-821X(02)00775-6
1081 Rohling, E.J., Foster, G.L., Grant, K.M., Marino, G., Roberts, A.P., Tamisiea, M.E.,
1082 Williams, F., 2014. Sea-level and deep-sea-temperature variability over the past
1083 5.3 million years. Nature 508, 477–482. doi:10.1038/nature13230
1084 Rohling, E.J., Gieskes, W.W., 1989. Late Quaternary changes in Mediterranean
1085 intermediate water density and formaton rate. Paleoceanography 4, 531–545.
1086 Rohling, E.J., Hopmans, E.C., Damsté, J.S.S., 2006. Water column dynamics during
1087 the last interglacial anoxic event in the Mediterranean (sapropel S5).
1088 Paleoceanography 21, 1–8. doi:10.1029/2005PA001237
1089 Rohling, Eelco J., Kemp, A.E.S., Cooke, S., Pearce, R.B., 2002. High-resolution
1090 stratigraphic framework for Mediterranean sapropel S5: Defining temporal
1091 relationships between records of Eemian climate variability. Palaeogeogr.
1092 Palaeoclimatol. Palaeoecol. 183, 87–101. doi:10.1016/S0031-0182(01)00461-8
1093 Rohling, E.J., Marino, G., Grant, K.M., 2015. Mediterranean climate and
1094 oceanography, and the periodic development of anoxic events (sapropels). Earth-
1095 Science Rev. 143, 62–97. doi:10.1016/j.earscirev.2015.01.008
1096 Rohling, E.J., Marino, G., Grant, K.M., Mayewski, P.A., Weninger, B., 2019. A
1097 model for archaeologically relevant Holocene climate impacts in the Aegean-
1098 Levantine region (easternmost Mediterranean). Quat. Sci. Rev. 208, 38–53.
1099 doi:https://doi.org/10.1016/j.quascirev.2019.02.009
1100 Rohling, E J, Mayewski, P., Abu-Zied, R., Casford, J., Hayes, A., 2002b. Holocene

1101 atmosphere-ocean interactions: Records from Greenland and the Aegean sea.
1102 Clim. Dyn. 18, 587–594. doi:10.1007/s00382-001-0194-8
1103 Rohling, E.J., Sprovieri, M., Cane, T., Casford, J.S.L., Cooke, S., Bouloubassi, I.,
1104 Emeis, K.C., Schiebel, R., Rogerson, M., Hayes, a., Jorissen, F.J., Kroon, D.,
1105 2004. Reconstructing past planktic foraminiferal habitats using stable isotope
1106 data: A case history for Mediterranean sapropel S5. Mar. Micropaleontol. 50, 89–
1107 123. doi:10.1016/S0377-8398(03)00068-9
1108 Rossignol-Strick, M., Nesteroff, W., Olive, P., Vergnaud-Grazzini, C., 1982. After
1109 the deluge: Mediterranean stagnation and sapropel formation. Nature 295, 105.
1110 Roth, P.H., Coulbourn, W.T., 1982. Floral and solution patterns of coccoliths in
1111 surface sediments of the North Pacific. Mar. Micropaleontol. 7, 1–52.
1112 doi:10.1016/0377-8398(82)90014-7
1113 Sakamoto, T., Janecek, T., Emeis, K., 1998. 4 . Continuous Sedimentary Sequences
1114 From the Eastern Mediterranean Sea : Composite Depth Sections 1 160, 37–59.
1115 Satow, C., Tomlinson, E.L., Grant, K.M., Albert, P.G., Smith, V.C., Manning, C.J.,
1116 Ottolini, L., Wulf, S., Rohling, E.J., Lowe, J.J., Blockley, S.P.E., Menzies, M.A.,
1117 2015. A new contribution to the Late Quaternary tephrostratigraphy of the
1118 Mediterranean: Aegean Sea core LC21. Quat. Sci. Rev. 117, 96–112.
1119 doi:https://doi.org/10.1016/j.quascirev.2015.04.005
1120 Schrag, D.P., Adkins, J.F., McIntyre, K., Alexander, J.L., Hodell, D.A., Charles,
1121 C.D., McManus, J.F., 2002. The oxygen isotopic composition of seawater during
1122 the Last Glacial Maximum. Quat. Sci. Rev. 21, 331–342.
1123 Schulz, H., Rad, U., Erlenkeuser, H., 1998. Correlations between Arabian Sea and
1124 Greenland climate oscillations of the past 110,00 years. Nature 393, 54–57.
1125 Sierro, F.J., Hodell, D. a., Curtis, J.H., Flores, J. a., Reguera, I., Colmenero-Hidalgo,
1126 E., Bárcena, M. a., Grimalt, J.O., Cacho, I., Frigola, J., Canals, M., 2005. Impact
1127 of iceberg melting on Mediterranean thermohaline circulation during Heinrich
1128 events. Paleoceanography 20, 1–13. doi:10.1029/2004PA001051
1129 Sierro, F.J., Hodell, D.A., Andersen, N., Azibeiro, L.A., Jimenez-Espejo, F.J., Bahr,

A., Flores, J.A., Ausin, B., Rogerson, M., Lozano-Luz, R., Lebreiro, S.M., Hernandez-Molina, F.J., 2020. Mediterranean Overflow Over the Last 250 kyr: Freshwater Forcing From the Tropics to the Ice Sheets. Paleoceanogr. Paleoclimatology 35, e2020PA003931. doi:https://doi.org/10.1029/2020PA003931

Sirocko, F., Sarnthein, M., Erlenkeuser, H., Lange, H., Arnold, M., Duplessy, J.C., 1993. Century-scale events in monsoonal climate over the past 24,000 years. Nature 364, 322–324. doi:10.1038/364322a0

Skampa, E., Triantaphyllou, M.V., Dimiza, M.D., Gogou, A., Malinverno, E., Stavrakakis, S., Panagiotopoulos, I.P., Parinos, C., Baumann, K.-H., 2019. Coupling plankton - sediment trap - surface sediment coccolithophore regime in the North Aegean Sea (NE Mediterranean). Marine Micropaleontology 152, 101729.

Spratt, R.M., Lisiecki, L.E., 2016. A Late Pleistocene sea level stack. Clim. Past 12, 1079–1092. doi:10.5194/cp-12-1079-2016

Sprovieri, M., Di Stefano, E., Incarbona, A., Salvagio Manta, D., Pelosi, N., Ribera d'Alcalà, M., Sprovieri, R., 2012. Centennial- to millennial-scale climate oscillations in the Central-Eastern Mediterranean Sea between 20,000 and 70,000 years ago: evidence from a high-resolution geochemical and micropaleontological record. Quat. Sci. Rev. 46, 126–135. doi:https://doi.org/10.1016/j.quascirev.2012.05.005

Stockhecke, M., Timmermann, A., Kipfer, R., Haug, G.H., Kwiecien, O., Friedrich, T., Menviel, L., Litt, T., Pickarski, N., Anselmetti, F.S., 2016. Millennial to orbital-scale variations of drought intensity in the Eastern Mediterranean. Quat. Sci. Rev. 133, 77–95. doi:10.1016/j.quascirev.2015.12.016

Thirumalai, K., Quinn, T.M., Marino, G., 2016. Constraining past seawater δ18O and temperature records developed from foraminiferal geochemistry. Paleoceanography 31, 1409–1422. doi:10.1002/2016PA002970

Tierney, J.E., Russell, J.M., Huang, Y., Damsté, J.S.S., Hopmans, E.C., Cohen, A.S.,

2008. Northern Hemisphere Controls on Tropical Southeast African Climate During the Past 60,000 Years. Science (80-.). 322, 252 LP – 255. doi:10.1126/science.1160485

Tjallingii, R., Claussen, M., Stuut, J.B.W., Fohlmeister, J., Jahn, A., Bickert, T., Lamy, F., Röhl, U., 2008. Coherent high- and low-latitude control of the northwest African hydrological balance. Nat. Geosci. 1, 670–675. doi:10.1038/ngeo289

Toucanne, S., Jouet, G., Ducassou, E., Bassetti, M.A., Dennielou, B., Angue Minto'o, C.M., Lahmi, M., Touyet, N., Charlier, K., Lericolais, G., Mulder, T., 2012. A 130,000-year record of Levantine Intermediate Water flow variability in the Corsica Trough, western Mediterranean Sea. Quat. Sci. Rev. 33, 55–73. doi:10.1016/j.quascirev.2011.11.020

Triantaphyllou, M. V, Antonarakou, A., Dimiza, M.D., Anagnostou, C., 2010. Calcareous nannofossil and planktonic foraminiferal distributional patterns during deposition of sapropels S6, S5 and S1 in the Libyan Sea (Eastern Mediterranean). Geo-Marine Lett. 30, 1–13. doi:10.1007/s00367-009-0145-7

Triantaphyllou, M. V, Antonarakou, A., Kouli, K., Dimiza, M.D., Kontakiotis, G., Papanikolaou, M.D., Ziveri, P., Mortyn, P.G., Lianou, V., Lykousis, V., Dermitzakis, M.D., 2009a. Late Glacial-Holocene ecostratigraphy of the south-eastern Aegean Sea, based on plankton and pollen assemblages. Geo-Marine Lett. 29, 249–267. doi:10.1007/s00367-009-0139-5

Triantaphyllou, M. V, Ziveri, P., Gogou, A., Marino, G., Lykousis, V., Bouloubassi, I., Emeis, K.C., Kouli, K., Dimiza, M.D., Rosell-Melé, A., Papanikolaou, M., Katsouras, G., Nunez, N., 2009b. Late Glacial-Holocene climate variability at the south-eastern margin of the Aegean Sea. Mar. Geol. 266, 182–197. doi:10.1016/j.margeo.2009.08.005

Triantaphyllou, M. V, Ziveri, P., Tselepides, A., 2004. Coccolithophore export production and response to seasonal surface water variability in the oligotrophic Cretan Sea (NE Mediterranean). Micropaleontology 50, 127–144.

1188 Tzedakis, P.C., Drysdale, R.N., Margari, V., Skinner, L.C., Menviel, L., Rhodes,
1189 R.H., Taschetto, A.S., Hodell, D.A., Crowhurst, S.J., Hellstrom, J.C., Fallick,
1190 A.E., Grimalt, J.O., McManus, J.F., Martrat, B., Mokeddem, Z., Parrenin, F.,
1191 Regattieri, E., Roe, K., Zanchetta, G., 2018. Enhanced climate instability in the
1192 North Atlantic and southern Europe during the Last Interglacial. Nat. Commun.
1193 9, 4235. doi:10.1038/s41467-018-06683-3
1194 van der Meer, M.T.J., Baas, M., Rijpstra, W.I.C., Marino, G., Rohling, E.J.,
1195 Sinninghe Damsté, J.S., Schouten, S., 2007. Hydrogen isotopic compositions of
1196 long-chain alkenones record freshwater flooding of the Eastern Mediterranean at
1197 the onset of sapropel deposition. Earth Planet. Sci. Lett. 262, 594–600.
1198 doi:10.1016/j.epsl.2007.08.014
1199 Velaoras, D., Papadopoulos, V.P., Kontoyiannis, H., Papageorgiou, D.K., Pavlidou,
1200 A., 2017. The Response of the Aegean Sea (Eastern Mediterranean) to the
1201 Extreme 2016–2017 Winter. Geophys. Res. Lett. 44, 9416–9423.
1202 doi:10.1002/2017GL074761
1203 Vellinga, M., Wood, R.A., 2002. Global Climatic Impacts of a Collapse of the
1204 Atlantic Thermohaline Circulation. Clim. Change 54, 251–267.
1205 doi:10.1023/A:1016168827653
1206 Veres, D., Bazin, L., Landais, A., Toyé Mahamadou Kele, H., Lemieux-Dudon, B.,
1207 Parrenin, F., Martinerie, P., Blayo, E., Blunier, T., Capron, E., Chappellaz, J.,
1208 Rasmussen, S.O., Severi, M., Svensson, A., Vinther, B., Wolff, E.W., 2013. The
1209 Antarctic ice core chronology (AICC2012): an optimized multi-parameter and
1210 multi-site dating approach for the last 120 thousand years. Clim. Past 9, 1733–
1211 1748. doi:10.5194/cp-9-1733-2013
1212 Wehausen, R., Brumsack, H., 2000. Chemical cycles in Pliocene sapropel-bearing
1213 and sapropel-barren eastern Mediterranean sediments. Palaeogeogr.
1214 Palaeoclimatol. Palaeoecol. 158, 325–352.
1215 Young, J.R., 1994. Functions of coccoliths, in: Winter, A., Siesser, W.G. (Eds.),
1216 Coccolithophores. Cambridge Univ. Press, Cambridge, pp. 63–82.

1217 Young, J.R., Geisen, M., Cros, L., Kleijne, A., Sprengel, C., Probert, I., Østergaard,
1218 J., 2003. A guide to extant coccolithophore taxonomy. J. Nannoplankt. Res. 125.
1219 Zhang, R., Delworth, T.L., 2006. Impact of Atlantic multidecadal oscillations on
1220 India/Sahel rainfall and Atlantic hurricanes. Geophys. Res. Lett. 33.
1221 doi:10.1029/2006GL026267
1222 Ziegler, M., Lourens, L.J., Tuenter, E., Hilgen, F., Reichart, G.-J., Weber, N., 2010.
1223 Precession phasing offset between Indian summer monsoon and Arabian Sea
1224 productivity linked to changes in Atlantic overturning circulation.
1225 Paleoceanography 25, 1–16. doi:10.1029/2009PA001884
1226 Ziveri, P., Broerse, A.T.C., van Hinte, J.E., Westbroek, P., Honjo, S., 2000. The fate
1227 of coccoliths at 48°N 21°W, Northeastern Atlantic. Deep Sea Res. Part II Top.
1228 Stud. Oceanogr. 47, 1853–1875. doi:10.1016/S0967-0645(00)00009-6
1229 Ziveri, P., Thunell, R. C., 2000. Coccolithophore export production in Guaymas
1230 Basin, Gulf of California: response to climate forcing. Deep-Sea Research Part
1231 II, 47, 2073–2100. https://doi.org/http://dx.doi.org/10.1016/S0967-
1232 0645(00)00017-5
1233
1234
1235 Captions
1236 Fig. 1: location of ODP Site 967 and of records used for correlation. A) Red arrows
1237 indicate the location of International Ocean Discovery program (IODP) Site U1385 in
1238 the Iberian Margin, ODP Site 967 in the eastern Mediterranean, Core LC21 in the
1239 Aegean Sea, Sanbao Cave in China and EPICA Dome C in Antarctica. B) Inset map
1240 of the red box in A). The blue and red circles respectively indicate the location of
1241 core LC21 and ODP Site 967. The dashed line shows the Nile cone province. Black
1242 arrows point out the path of Eastern Mediterranean Deep-water from Adriatic and
1243 Aegean Sea.
1244

Fig. 2: plot of coccolith data in the Aegean Sea core LC21 and comparison with selected records. a) *Florisphaera profunda* percentage values (blue circles), expressed as natural logarithm (Grelaud et al., 2012). The 1st derivative of Sanbao Cave speleothem $\delta^{18}O$ (orange line) for each of the 10,000 ice-volume corrected 'stacks', following the chronology by Cheng et al. (2009) and after ice-volume correction. b) *Florisphaera profunda* percentage values (blue line), expressed as natural logarithm (Grelaud et al., 2012). Epica Dome C CH_4 (grey circles and grey line), following the Antarctic Ice Core chronology AICC2012 (Bazin et al., 2013) c) *Florisphaera profunda* percentage values (blue line), expressed as natural logarithm (Grelaud et al., 2012). Upper Summer Mixed Layer depth in the three different experiments by Amies et al. (2019) (respectively pink, orange and red lines for experiments A, B and C). d) Alkenone-derived SST (red circles) from the Alboran Sea (Martrat et al., 2014). e) Holococcoliths percentage values (blue circles, this study) and superimposed $\delta^{13}C$ values of the benthic foraminifera species *Cibicidoides wuellestorfi* from the Iberian Margin (green circles) (Martrat et al., 2007). f) Ca/Ti ratio, expressed as logarithm (green line), in sediments from the Iberian Margin (Hodell et al., 2015), superimposed to the $C_{26}OH$ ratio from the same area (red circles) (Martrat et al., 2007). Thick lines represent the 3-pt running average and coloured shadows indicate the 95% confidence level. The sapropel S5 and HS11 extent is also shown.

Fig. 3: plot of coccolith data at ODP Site 967 and comparison with selected records. A) June 21st insolation curve at 65°N (Laskar et al., 2004). B) Benthic $\delta^{18}O$ composite record from ODP Sites 967 and 968 (Konijnendijk et al., 2015). C) LR04 benthic $\delta^{18}O$ stack (Lisiecki and Raymo, 2005). D) Downcore percentage variations of Placoliths. E) Downcore percentage variations of *F. profunda*. F) Downcore percentage variations of UPZ taxa. G) Downcore percentage variations of Miscellaneous taxa. H) Downcore percentage variations of holococcoliths. Black horizontal bars show the error associated to countings for a 95% confidence level.

Red filling indicates values higher than the total average percentage. Horizontal thick black lines indicate MIS boundaries from Lisiecki and Raymo (2005). Horizontal yellow boxes show visible sapropel layers in the ODP 967 composite section (Emeis et al., 2000a).

Fig. 4: scatter plot of placoliths and *F. profunda* percentage values at ODP Site 967. The black line shows the linear fit. The equation of the linear fit, R^2 correlation index and number of samples are also reported.

Fig. 5: coccolith, element ratios, indices and principal component scores at ODP Site 967. A) *Florisphaera profunda* percentage values (black circles, the black line is the 3-pt running average, this study). B) Holococcolith percentage values (blue circles, the blue line is the 3-pt running average, this study). C) Relative sea-level (Spratt and Lisiecki, 2016). D) PC2 of elemental proxies that reflects sapropel/monsoon runoff layers (Grant et al., 2017). E) The Aeolian residual by Larrasoaña et al. (2003) plotted by the Grant et al. (2017) chronology. F) The North Africa humidity/aridity index (Grant et al., 2017). G) The Ba/Al ratio (Grant et al., 2017). Horizontal thick black lines indicate MIS boundaries from Lisiecki and Raymo (2005). Horizontal yellow boxes show visible sapropel layers in the ODP 967 composite section (Emeis et al., 2000a).

Fig. 6: correlation among Mediterranean, North Atlantic, Asian and Antarctica records. A) Alkenone-based SSTs (°C) at Site MD01-2444, Iberian Margin (Martrat et al., 2007). B) Log (Ca/Ti) at IODP Site U1385, Iberian Margin (Hodell et al., 2015). Note the reversed axis. C) 3-pt running average of holococcolith percentage values at ODP Site 967, eastern Mediterranean Sea (present study). Note the reversed axis. D) $\delta^{18}O$ speleothem data at Sanbao Cave, China (Cheng et al., 2016). Note the reversed axis. E) Epica Dome C CH_4, Antarctica (Bazin et al., 2013).

Grey boxes indicate correlations among different records: cooling and AMOC weakening/shutdown in the Iberian Margin (A, B), holococcolith preservation in the eastern Mediterranean seafloor (C), monsoon activity weakening in China (D) and EDC methane concentration decrease in Antarctica (see Section 6 for further explanation).

Middle-Late Pleistocene Eastern Mediterranean nutricline depth and coccolith preservation linked to Monsoon activity and Atlantic Meridional Overturning Circulation

Alessandro Incarbona[1*], Gianluca Marino[2,3], Enrico Di Stefano[1], Michael Grelaud[4], Nicola Pelosi[5], Laura Rodríguez-Sanz[3], Eelco J. Rohling[3,6]

[1]Università degli Studi di Palermo, Dipartimento di Scienze della Terra e del Mare, Via Archirafi 22, 90134 Palermo, Italy.

[2]Centro de Investigación Mariña, Universidade de Vigo, GEOMA, Palaeoclimatology Lab, Vigo, 36310, Spain.

[3]Research School of Earth Sciences, The Australian National University, Canberra, Australian Capital Territory 2601, Australia

[4]Universitat Autònoma de Barcelona (UAB), Institute of Environmental Science and Technology (ICTA), Edifici Z, Carrer de les Columnes, Campus de la UAB, 08193 Bellaterra (Cerdanyola del Vallès), Barcelona, Spain

[5]Consiglio Nazionale delle Ricerche, Istituto di Scienze del Patrimonio Culturale, Via Cardinale Guglielmo Sanfelice 8, 80134 Naples, Italy.

[6] Ocean and Earth Science, University of Southampton, Southampton SO14 3ZH, UK

* Corresponding Author: e-mail, alessandro.incarbona@unipa.it; telephone, +39 091 23864648.

Abstract

The eastern Mediterranean Sea lies under the influence of high- and low-latitude climatic systems. The northern part of the basin is affected by Atlantic depressions and continental and polar air masses that promote intermediate and deep-water formation. The southern part is influenced by subtropical conditions and monsoon activity. Monsoon intensification results in enhanced freshwater discharge from the

Nile River and other (now dry) systems along the North African margin. This freshwater influx into the Mediterranean Sea reduces surface water buoyancy loss. Disentangling the influences of these diverse climatic forcings is hindered by inherent proxy data limitations and by interactions between the climatic forcings. Here we use a wealth of published and new paleoclimate records across Termination II to understand the impacts of the higher latitude and subtropical/monsoon climate influences on coccolithophore ecology and holococcolith preservation in Aegean Sea sediment core LC21. We then use these findings to interpret coccolith assemblage variations at Ocean Drilling Program Site 967 (located nearby LC21, at the Eratosthenes Seamount) during multiple glacial-interglacial cycles across the Middle Pleistocene (marine isotopic stages 14-9). The LC21 analysis suggests that holococcolith preservation was enhanced during Heinrich Stadial 11 (~ 133 ka) and cold spell C26 (~ 119 ka). These two events have been previously linked to cold conditions in the North Atlantic and Atlantic Meridional Overturning Circulation weakening. We propose that associated atmospheric perturbations over the Mediterranean Sea promoted deep-water formation, and thus holococcolith preservation. Similarly, in the Middle Pleistocene (MIS 14-9) of Site 967, we observe temporal coincidence between ten episodes of enhanced holococcolith preservation and episodes of Atlantic Meridional Overturning Circulation slowdown. In Site 967, we also identified repeated fluctuations in placoliths and in *Florisphaera profunda*, which indicate nutricline depth variations. The development of a deep chlorophyll maximum is associated with the North Africa and wet phases, as recently observed using elemental proxy records at Site 967, during the deposition of sapropel layers. A further deep chlorophyll maximum development is identified during MISs 12 and 10, as a result of pycnocline and nutricline shoaling within the lower part of the photic zone due to glacial sea-level lowering and water mass transport reduction at both the Gibraltar and Sicily Straits. Finally, enhanced holococcolith preservation during cold/dry events is clearly correlated to weakened ~~Asian~~ monsoon activity in both

Africa and Asia~~, establishing a vast Northern Hemisphere link for stadial perturbations~~.

1 – Introduction

Paleoclimate reconstructions document the competing influence of southern *versus* northern climate systems on the hydrography and hydrology of the eastern Mediterranean Sea and its borderlands over a range of timescales (Emeis et al., 2000b; Grant et al., 2017, 2016; Lourens, 2004; Rohling et al., 2002b). During precession minima (Northern Hemisphere insolation maxima), the African monsoon intensified and shifted northward, with attendant enhancement of the freshwater release into the Mediterranean basin via large North African river systems and/or currently inactive wadis (Amies et al., 2019; Marino et al., 2009; Osborne et al., 2008; Rohling et al., 2002a; Rohling et al., 2015; van der Meer et al., 2007). This impacted the basin's hydrography and weakened or even shut down dense water formation, leading to oxygen starvation at depth and deposition of layers (sapropels) with elevated organic carbon concentrations (De Lange et al., 2008; Rohling et al., 2015; Rossignol-Strick et al., 1982). ~~Superimposed upon these orbital-scale changes in basin hydrography, circulation, and biogeochemistry are regional m~~Millennial-scale climatic variations~~ that~~ have been less well documented and appear to be associated with variations in the strength of the Atlantic Meridional Overturning Circulation (AMOC) (Grant et al., 2017, 2016; Stockhecke et al., 2016).

Coccolithophores are marine unicellular phytoplankton organisms living in the upper part of the water column. The ecology of c~~C~~occolithophore species~~' ecology is~~ shows a strong sensitivity~~very sensitive~~ to modern gradients within the Mediterranean Sea and different species thrive in different areas, mainly in response to West-East temperature and nutrient gradients, water column dynamics, and meso-scale oceanographic features (Bonomo et al., 2012; D'Amario et al., 2017; Knappertsbusch, 1993; Oviedo et al., 2015). In the sedimentary archive, calcite

coccolithophore remains (coccoliths) have been used successfully to infer orbital and suborbital variations in climate, productivity, and nutricline depth in oceans and marginal seas (Beaufort et al., 1997; Flores et al., 1997; Incarbona et al., 2013, 2010a; Marino et al., 2008; Molfino and McIntyre, 1990a; Rogalla and Andruleit, 2005). In the eastern Mediterranean Sea, coccolith-based paleoenvironmental reconstructions ~~were~~ have been mostly aimed at assessing the shallow *versus* deep position of the nutricline within the photic layer and its relationship with the basin's freshwater budget, water mass circulation, and deep-sea ventilation during sapropel deposition (e.g., Grelaud et al., 2012). These studies attest to the development of a deep chlorophyll maximum (DCM) while organic carbon-rich layers were accumulating on the oxygen-starved eastern Mediterranean seafloor (Castradori, 1993; Giunta et al., 2003; Grelaud et al., 2012; Incarbona et al., 2019, 2011; Incarbona and Di Stefano, 2019; Maiorano et al., 2013; Negri et al., 1999; Principato et al., 2006; Triantaphyllou et al., 2009b, 2009a), corroborating findings based on other marine planktonic groups (Kemp et al., 1999; Meier et al., 2004; Rohling and Gieskes, 1989).

Here we present new data that complement a previous dataset of coccolith assemblages from south-eastern Aegean Sea core LC21 (Grelaud et al., 2012), across the penultimate glacial termination (termination II, T-II) and the last interglacial period, with a precise, radiometrically constrained chronology (Grant et al., 2012). This allows comparison of LC21 "coccolith proxies" with time series of palaeoclimate variability in the monsoon and the North Atlantic region (Cheng et al., 2009; Hodell et al., 2013), as well as atmospheric methane (CH_4) concentrations. Our combined dataset is probabilistically evaluated to decipher the amplitude and timing of change by quantitatively assessing the impact of chronological, analytical, and proxy uncertainties. We use this analysis as a proof of concept for new, highly resolved coccolith data from Ocean Drilling Program (ODP) Site 967 from the Eratosthenes Seamount, South of Cyprus, within the Nile Delta Basin province (Emeis et al., 1996). The new ODP 967 time series spans, at centennial-scale

resolution, three glacial/interglacial cycles of the Middle Pleistocene, from glacial Marine Isotope Stage (MIS) 14 to interglacial MIS 9. Collectively, our new data and analyses provide insights into climate variability at orbital and sub-orbital timescales ~~both~~ during both glacial and interglacial periods, complementing ~~the~~ a wealth of existing knowledge of the intervals of sapropel deposition. Specifically, we explore modifications in nutrient dynamics and holococcolith preservation during the Middle Pleistocene. These changes are compared with recently acquired variations in elemental abundances, elemental ratios, and climate ind~~ex variation~~ices ~~recently acquired at~~for ODP Site 967 (Section 6.3) that portray the alternation of wet and dry North Africa periods at both orbital and sub-orbital timescales (Grant et al., 2017). Finally, we centre on the correlation between holococcolith preservation, AMOC, ~~Asian~~ and boreal monsoon activity (both in Africa and in a wider Asian context) ~~activity~~ to assess: (*i*) the atmospheric impact of continental/polar air outbreaks on the eastern Mediterranean deep-sea ventilation and seafloor calcite preservation during cold stadials; and (*ii*) impact of millennial-scale atmospheric perturbations on the eastern Mediterranean Sea.

2 – Environmental Setting

A negative hydrological balance maintains a robust antiestuarine thermohaline circulation pattern in the Mediterranean Sea (Robinson and Golnaraghi, 1994). Surface Atlantic water (Modified Atlantic Water – MAW) enters the Mediterranean Sea and occupies the uppermost 100-200 m depth (Millot, 1999; POEM group, 1992). MAW spread out into the eastern Mediterranean Sea *via* the Mid-Mediterranean Jet and reaches the Eratosthenes Seamount where a quasi-permanent anticyclonic summer circulation exists, that is known as the Shikmona Gyre (Malanotte-Rizzoli et al., 2014; Pinardi and Masetti, 2000; POEM group, 1992). Levantine Intermediate Water (LIW) formation takes place close to the Eratosthenes Seamount (Ovchinnikov I.M., 1984; POEM group, 1992). Eastern Mediterranean Deep Water (EMDW) forms in the Adriatic and Aegean Sea (Fig. 1) due to winter

heat loss~~, when~~ under the influence of intense Bora and Vardar winds ~~blow~~ (Malanotte-Rizzoli et al., 2014; POEM group, 1992).

Today, the eastern Mediterranean Sea is one of the most oligotrophic areas globally. Primary productivity is more than three times lower than in the western basin, in accordance with a similar nutrient depletion trend (Krom et al., 2010, 1991). Primary production is also seasonally controlled: higher productivity occurs in winter, after winter convection, while severe oligotrophy occurs in summer due to deepening of the thermocline and nutricline (Allen et al., 2002; Klein and Coste, 1984). The Eratosthenes region is classified as a no-bloom area by satellite-based chlorophyll analyses. The severe late spring-summer oligotrophy is followed by relatively higher chlorophyll values in winter (D'Ortenzio and Ribera d'Alcalà, 2009).

High- and low-latitude climate systems impact on the eastern Mediterranean Sea. In summer, subtropical high-pressure conditions cause stable dry and warm conditions throughout the Mediterranean area (Lionello, 2012). In winter, the North African subtropical high pressure is shifted southward, and cold and dry polar/continental air outbreaks occur into the eastern Mediterranean from the north (Lionello, 2012; Rohling et al., 2019, 2015). Expansion of the Siberian High is an important driver for advection of cold air toward the eastern Mediterranean. Intensification of the Siberian High during Holocene rapid climatic changes is thought to be an important driver of surface water cooling and atmospheric perturbations in the central-eastern Mediterranean Sea (Incarbona et al., 2008; Rohling et al., 2002b; Rohling et al., 2019). Prolonged and strengthened polar/continental air outbreaks promote sea surface heat loss and deep-water formation (Josey et al., 2011; Rohling et al., 2019; Velaoras et al., 2017).

3 – Material and Methods

3.1 - Sediment cores

ODP Site 967 (34°04.098'N, 32°43.523'E, 2,553 m water depth) is located at the base of the northern slope of the Eratosthenes Seamount, a structure that emerges from the Nile Delta Cone (Fig. 1). Sediments are dominated by horizontal and sub-horizontal brown and light gray, bioturbated nannofossil ooze and nannofossil clay, intercalated with sapropels and turbidites (Emeis et al., 1996). Specifically, there are five sapropel layers that show signs of moderate bioturbation (S13, S12, S11, b and S10) in the studied interval (Emeis et al., 1996), while no turbidites and/or other sedimentary disturbances were identified (Konijnendijk et al., 2014).

Sediment core LC21 (35°40'N, 26°35'E; 1,522 m water depth) was recovered in 1995 by *RV* Marion Dufresne in the southeastern Aegean Sea (Fig. 1). Lithology consists of hemipelagic sediments, with visible sapropels (S1, S3, S4, and S5) and tephra layers (Grant et al., 2016; Satow et al., 2015).

3.2 - Coccolith data

We carried out c~~C~~occolith ~~analysis~~ analyses at ODP Site 967 ~~was carried out~~ at 1 cm resolution between 14.80 and 21.49 m composite depth (mcd) (Emeis et al., 1996), for a total of 668 samples, which were analysed with a polarized microscope at ~ 1000× magnification. Rippled smear slides were prepared following standard procedures (Bown and Young, 1998). On average 350 specimens were identified following the taxonomic concepts ~~on~~ for living coccolithophores of Young et al. (2003) and Jordan et al. (2004). Taxa were grouped ~~in~~ as 'placoliths', 'miscellaneous group', 'upper photic zone (UPZ) group', 'lower photic zone (LPZ) group' and 'holococcoliths' (Di Stefano and Incarbona, 2004; Incarbona et al., 2010). Placoliths include small placoliths, small *Gephyrocapsa*, *Gephyrocapsa muellerae*, and *Gephyrocapsa oceanica*. The miscellaneous group includes *Helicosphaera* spp., *Coccolithus pelagicus*, *Syracosphaera histrica*, *Pontosphaera* spp., *Calcidiscus leptoporus*, *Coronosphaera* spp., *Braarudosphaera* spp., *Oolithotus fragilis*, *Calciosolenia* spp., and specimens of all the other species. UPZ group includes

Syracosphaera pulchra, *Umbellosphaera* spp., *Discosphaera tubifera*, *Rhabdosphaera* spp., *Umbilicosphaera* spp., and *Ceratolithus* spp.. LPZ group comprises *F. profunda*, which dominates the group, with negligible amounts of *Gladiolithus flabellatus* in a few samples. Holococcoliths include all the coccoliths produced during the haploid life-cycle stage (Incarbona et al., 2019).

The holococcolith analysis at Aegean Sea core LC21 was carried out by observation with a polarized microscope at about 1000× magnification, following the standard procedure for rippled smear slides (Bown and Young, 1998). Holococcolith percentage values were evaluated on 102 samples *versus* heterococcoliths specimens, examining about 500 coccoliths. *Florisphaera profunda* percentage values at LC21 Aegean Sea core were presented before (Grelaud et al., 2012), following the same procedure adopted in this study, and that earlier dataset is available at https://doi.pangaea.de/10.1594/PANGAEA.805357.

3.3 - Statistical analysis of the time series

~~A~~ We use a Monte Carlo approach based on MATLAB coding (Marino et al., 2015; Thirumalai et al., 2016) ~~has been used~~ to: (*i*) stack the $\delta^{18}O$ time series for ~~the~~ different stalagmites (SB11, SB23, and SB25) from Sanbao Cave, China, ~~(Cheng et al., 2009)~~ that cover T-II and the last interglacial period (Cheng et al., 2009); (*ii*) calculate rates of $\delta^{18}O$ change in the Sanbao Cave stalagmites; (*iii*) probabilistically evaluate the chronological (Bazin et al., 2013; Veres et al., 2013) and measurement uncertainties associated with the time series of atmospheric methane (CH_4) concentrations from EPICA Dome C (EDC) (Loulergue et al., 2008); and (*iv*) probabilistically evaluate chronological and counting uncertainties associated with the *F. profunda* (Grelaud et al., 2012) and new holococcolith records for core LC21.

Speleothem $\delta^{18}O$ time series from Sanbao Cave have been probabilistically evaluated and stacked across the 140-110 ka interval. Input data for the Monte Carlo routine are

sample ages with 1σ uncertainties, and speleothem $\delta^{18}O$ with 1σ uncertainties (Cheng et al., 2009). For each stalagmite (SB11, SB23, and SB25), individual data points are then separately and randomly sampled 10,000 times within their chronological and $\delta^{18}O$ uncertainties. The chronological uncertainties are evaluated using a random walk Monte Carlo routine that employs a Metropolis–Hastings approach to reject steps in the random walk that will result in age reversals (Rodríguez-Sanz et al., 2017). That is, we imposed a stratigraphic constraint (monotonic increase of age with depth, analogous to Rohling et al., 2014) to the data that are measured in a stratigraphically coherent manner along individual stalagmites. All realizations are then linearly interpolated on an equally spaced time scale and stacked to produce 10,000 speleothem $\delta^{18}O$ stacks with and without a correction that probabilistically quantifies the impacts of the global ^{18}O enrichment/depletion (Schrag et al., 2002) associated with ice-volume changes (Grant et al., 2012). Next, we calculated the 1st time derivative, to obtain rates of speleothem $\delta^{18}O$ change~~,~~ for each of the 10,000 ice-volume corrected 'stacks'. This is done by smoothing each realization using 0.75 kyr Gaussian window to remove sample-to-sample noise, which would result in spurious jumps in the estimated rates of change, and by then differentiating the smoothed realizations. Monte Carlo analysis of the EDC methane record and of the eastern Mediterranean coccolith time series are performed using the same approach. Finally, the 10,000 iterations of each of these time series are linearly interpolated and the probability distribution assessed at each time step, thereby determining the 68% (16th–84th percentile) and 95% (2.5th–97.5th percentile) probability intervals and the probability maximum (PMAX, modal value) of the data.

4 – Coccolith ~~taxa~~ taxon ecology

Placoliths are so-called 'r-strategist taxa' that rapidly exploit nutrients in the photic zone (Baumann et al., 2005; Young, 1994). In the eastern Mediterranean Sea, placoliths bloom in winter, after nutrient fertilization (Di Stefano et al., 2011; Knappertsbusch, 1993; Triantaphyllou et al., 2004; Ziveri et al., 2000).

Florisphaera profunda is a deep photic zone species that indicates the occurrence of a deep nutricline (McIntyre and Molfino, 1996; Molfino and McIntyre, 1990a). In low- and middle-latitude open ocean regions, the relative abundance of this species is anticorrelated with primary productivity (Beaufort et al., 2001, 1997; Hernández-Almeida et al., 2019).

In the Mediterranean Sea, except for a limited area in the central part of the basin, there is no apparent relationship between *F. profunda* abundance and satellite-observed (surface) primary productivity levels (Hernández-Almeida et al., 2019; Incarbona et al., 2008). However, *F. profunda* has been generally used to decipher water column stratification and development of a deep nutricline due to monsoon-fuelled freshwater discharge in the eastern Mediterranean and entrainment of nutrients into the lower photic zone from below (Castradori, 1993; Grelaud et al., 2012; Incarbona et al., 2019; Negri et al., 1999; Triantaphyllou et al., 2009b). This occurs through the develoment of a distinct DCM in the eastern Mediterranean during sapropel deposition~~, with~~. DCM development resulted from nutrient~~s entraining~~ entrainment into the photic zone from ~~below, injected by more buoyant~~ relatively buoyant intermediate waters~~. These were possibly~~ that likely ~~forming in~~originated from the Adriatic Sea, while the volume of MAW inflow ~~across~~ through the Sicily Strait was ~~plausibly~~ reduced (Myers et al., 1998; Rohling, 1991b; Rohling and Gieskes, 1989). Accordingly, relative abundances of placoliths and *F. profunda*, or their ratio, provide a robust indication of the depth of the nutricline in the eastern Mediterranean Sea. Specifically, presence (absence) of placoliths (*F. profunda*) in the coccolith assemblage reflects a shallow (deep) nutricline (Di Stefano et al., 2015; Flores et al., 2000; Molfino and McIntyre, 1990b).

The UPZ ~~are~~ group consistes of so-called ‘K-strategist taxa’, specialized to exploit a minimum uptake of nutrients in surface water (Bazzicalupo et al., 2020; Di Stefano and Incarbona, 2004; Young, 1994). Miscellaneous taxa reflect the lack of either an

apparent distinctive ecological preference or of an undertanding of their ecological preferences, with a potential weak K-strategy (Incarbona et al., 2010; Young, 1994). Holococcoliths prefer dwelling in warm, oligotrophic surface water and are abundant in the eastern Mediterranean Sea (D'Amario et al., 2017; Kleijne, 1991; Knappertsbusch, 1993; Dimiza et al., 2015; Oviedo et al., 2015; Skampa et al., 2019). Poor preservation of holococcoliths in sapropel S1 sediments was firstly recognised by Crudeli et al. (2006) and was later confirmed across the whole eastern Mediterranean, included the Eratosthenes Seamount (Incarbona et al., 2019; Incarbona and Di Stefano, 2019) and Pliocene sapropel layers in sedimentary sequencess on Cyprus ~~Island sediments~~ (Athanasiou et al., 2015). Importantly, potential preservation of tiny holococcolith crystals improves when dense water renewal ensures vigorous ventilation/oxygenation of the seafloor, even during short reventilation episodes that "interrupt" sapropel deposition (Incarbona et al., 2019).

5 –Chronology

The original shipboard age model by Sakamoto et al. (1998) at ODP Site 967 has since been ~~later~~ revised, because of some inconsistent tuning to orbital insolation (Konijnendijk et al., 2014; Lourens et al., 2001). More recently, Grant et al. (2017) developed a monsoon runoff (sapropel) proxy from the principal component analysis of sedimentary elemental data in ODP Site 967 that they tuned to precession minima. They use a zero phase lag, which relies upon the assumption that little or no lag exists when monsoon maxima did not immediately follow a high-amplitude glacial termination (Grant et al., 2016; Lourens et al., 2001). In this study, we adopt the chronology by Grant et al. (2017) for the coccolith data. Sedimentation rates~~,~~ between MIS 14 and MIS 9~~,~~ range from 1.4 cm kyr^{-1} to 3.9 cm kyr^{-1}, implying that the mean sampling resolution of our coccolith time series is about 340 years.

The LC21 chronology follows Grant et al. (2012) (see ~~also~~ section 6.1). The mean sedimentation rate is about 4.4 cm kyr^{-1}, with a mean sampling resolution of about 225 years.

6 – Results and Discussion

6.1 – Coccolith assemblages in Aegean Sea core LC21

Florisphaera profunda (Grelaud et al., 2012) and holococcoliths across T-II and the last interglacial in south-eastern Aegean core LC21 are used to evaluate their relationship with water column stratification and deep-sea ventilation, respectively. Several features make this core and the timespan that we target ideal to provide a 'proof of concept' for the interpretation of the new records from ODP Site 967 that spans multiple glacial-interglacial cycles. First, core LC21 has a radiometrically constrained chronology across T-II and the last interglacial period (Grant et al., 2012). This has been corroborated through comparison with western Mediterranean sediment cores and speleothem records, and it is consistent with the latest ice core chronology across the study interval (Marino et al., 2015). Second, prominent episodes of climate change punctuated T-II, including a multi-millennial Heinrich stadial associated with major freshwater discharge into the North Atlantic and AMOC slowdown (Deaney et al., 2017; Marino et al., 2015). Third, during the last interglacial period, an organic rich layer (sapropel S5) was deposited in the eastern Mediterranean under persistently anoxic or even euxinic conditions (Marino et al., 2007; Rohling et al., 2015, 2006). Sapropel S5 conditions developed in response to extensive monsoon-fuelled freshwater discharge along the North African Margin (Amies et al., 2019; Osborne et al., 2008; Rohling et al., 2002a; Rohling et al., 2004) that reduced surface salinity (van der Meer et al., 2007) and produced strong water column stratification (Amies et al., 2019; Grelaud et al., 2012; Marino et al., 2007; Rohling et al., 2006).

In Figure 2a-c we show *F. profunda* relative abundances from core LC21 (Grelaud et al., 2012) with upper mixed layer depth fluctuations reconstructed for the same core (Amies et al., 2019), and with the contemporaneous EDC time series of atmospheric CH_4 concentrations and the Sanbao Cave $\delta^{18}O$ stack, ~~both~~ which are ~~expected~~ thought

to reflect fluctuations in ~~the~~ boreal monsoon intensity ~~of the boreal monsoon~~ and attendant changes in the ~~wetland~~ spatial coverage of tropical wetlands (Cheng et al., 2016, 2009, 2006; Möller et al., 2013; Petrenko et al., 2009). We present t~~T~~he *F. profunda* time series (Grelaud et al., 2012) ~~is here presented~~ on the radiometrically constrained chronology of Grant et al. (2012), as natural logarithm of the original data. Within uncertainties of the various records, we note a strong similarity between the LC21 *F. profunda* record and variations of both Sanbao Cave $\delta^{18}O$ (Fig. 2a) and EDC CH_4 (Fig. 2b). Notably, a distinct *F. profunda* peak at ~129 ka appears contemporaneous with upper mixed layer thinning, with a maximum in the rates of Sanbao Cave $\delta^{18}O$ change and with the CH_4 overshoot in EDC. This suggests: (*i*) synchronous intensification of the African and Asian monsoons at the onset of the last interglacial period, in line with what has been documented for the early Holocene (Fleitmann et al., 2003; Marino et al., 2009; Nicholson et al., 2020; Tierney et al., 2008); and (*ii*) a rapid increase in freshwater discharge into the eastern Mediterranean at the onset of the last interglacial monsoon maximum, quantified as up to ~8.8 times the modern pre- Aswan Nile discharge and responsible for the most intense thinning of the upper summer mixed layer (Amies et al., 2019). Observation (*ii*) is particularly relevant because it alludes to the influence of the rates of monsoon intensification on stratification in the eastern Mediterranean. When large amounts of monsoon-fuelled freshwater are rapidly added to the basin, the strong evaporative climate of the Levant cannot keep up with sea--surface dilution (Rohling et al., 1991b) and the water column becomes strongly stratified (Rohling and Gieskes, 1989; Rohling et al., 2006; Marino et al., 2007; Athanasiou et al., 2015, 2017; Amies et al., 2019), causing shoaling of the pycnocline, the nutricline to be positioned at the base of the photic layer and the attendant development of a pronounced DCM.

In Figure 2d-f, LC21 holococcolith data are compared with North Atlantic and western Mediterranean Sea records. It is evident that there is no or poor preservation of holococcoliths during sapropel S5 (Fig. 2e). Peaks of holococcoliths below S5

correlate with low alkenone-derived SSTs in the Alboran Sea (Martrat et al., 2014) (Fig. 2d) and with variations in AMOC strength proxies (Figs. 2e,f) from the Iberian Margin. Specifically, log (Ca/Ti), benthic foraminiferal $\delta^{13}C$, and $C_{26}OH$ ratios (Hodell et al., 2015; Martrat et al., 2007) unequivocally indicate that AMOC ~~was severely~~had collapsed during Heinrich event HS11 (Böhm et al., 2015); we find that, at the same time, holococcolith preservation was enhanced. A similar relationship is evident above sapropel S5, especially with $C_{26}OH$ ratio data (Fig. 2f), and may be correlated with ~~the~~ North Atlantic cold event C26 (Oppo et al., 2006, 2001; Tzedakis et al., 2018). Coupled ocean-atmosphere hindcasts suggest that the AMOC slowdown/shutdown may have propagated through the Mediterranean Sea ~~as~~ in the form of major cooling and intense atmospheric perturbations (Manabe and Stouffer, 1997; Vellinga and Wood, 2002). Both cooling and atmospheric perturbations are major prerequisites for surface water buoyancy loss and deep-water formation, explaining enhanced Mediterranean bottom water ventilation during Heinrich and ~~stadial~~ Stadial events in the last glacial, based on benthic foraminifera $\delta^{13}C$ and alcohol index records (Cacho et al., 2000; Sprovieri et al., 2012; Toucanne et al., 2012). Our new results from the Aegean Sea explicitly link holococcolith preservation to Heinrich and Stadial events in response to deep-water formation and seafloor ventilation increases in the Mediterranean Sea during those events.

6.2 – Coccolith assemblages at ODP Site 967

At ODP Site 967, coccolith distribution patterns are compared (Figure 3) with: (*i*) June 21st insolation at 65°N (Laskar et al., 2004); (*ii*) the benthic $\delta^{18}O$ composite record from ODP Sites 967 and 968 ~~(Konijnendijk et al., 2015),~~ (Konijnendijk et al., 2015); and (*iii*) the LR04 benthic $\delta^{18}O$ stack (Lisiecki and Raymo, 2005). Overall, coccolith assemblages are dominated by placoliths, with percentages between 25 and 98% (average = 70%, Fig. 3D). The deep photic zone species *F. profunda* features high-amplitude fluctuations between intervals in which it is barely occurring (1%) and intervals in which it becomes the dominant (up to 74%)~~, and an average of 26%~~

(Fig. 3E). Placoliths' peak (low) abundances occur when *F. profunda* percentages are at a minimum (maximum), as highlighted by the pronounced anticorrelation (R^2= 0.95, n = 668) displayed in Figure 4.

The observed alternating dominance of the placoliths and *F. profunda* (see above) at ODP Site 967 suggests that between MIS 14 and MIS 9 the upper water column in the easternmost Mediterranean Sea repeatedly switched between ~~a~~ dominant winter-induced fertilization (placoliths' peaks, shallow nutricline), similar to today's winter conditions (Knappertsbusch, 1993), and a predominantly DCM-focused productivity ~~mostly occurring within the DCM~~ (*F. profunda*'s peaks, deep nutricline) during both glacial and interglacial periods. Shoaling of the pycnocline, which promoted a deep nutricline (DCM), in association with intensifications of the North African monsoon and sea-level lowering (Rohling and Gieskes, 1989; Rohling, 1991a, 1991b) is the most plausible explanation for the peak abundance of *F. profunda* at ODP Site 967 during sapropels and glacial periods, respectively. Accordingly, *F. profunda* would be particularly sensitive to ~~the~~ nutrient (re)distribution within the photic zone, with intervals of positive shifts in the basins freshwater budget (monsoon maxima, Rohling, 1991b) and reduced water exchange at straits (glacial lowstands, Rohling, 1991a)~~,~~ both leading to enhanced stratification in the upper water column, shoaling of the pycnocline, and development of a ~~deep~~ nutricline at the based of the photic layer. This conceptual framework indicated by box-model calculations (Rohling, 1991a,b) provides an explanation for the *F. profunda* peaks both in sapropel layers (e.g., S12, S11, b, S10) and during MIS 12 and MIS 10 glacial periods (see also Section 6.3).

The remaining three coccolith groups at Site 967 are largely subordinate. Low abundance of UPZ taxa (0.0-5.4%, 1.4% on average, Fig. 3F) and Miscellaneous taxa (0.0-11.1%, 1.2% on average, Fig. 3G) is unexpected in the severe oligotrophy of the eastern Mediterranean Sea, especially for UPZ taxa that include dominant coccolithophore species in summer/autumn (Knappertsbusch, 1993; Malinverno et

al., 2009; Oviedo et al., 2015). However, living coccolithophore surveys show that winter production (placolith blooming) is ~~even~~ about ~~one~~ an order of magnitude higher than summer production, thereby explaining the apparent ecological contradiction in taxa proportions (Knappertsbusch, 1993).

Holococcolith percentage values range between 0.0 and 20.8%, 1.9% on average (Fig. 3H). As was the case in~~for~~ late Quaternary sapropels, tiny holococcoliths are again not preserved ~~during~~ in sapropel layers, but ~~it is evident~~we also note that that poor preservation extends far beyond sapropel layers.

6.3 – Comparison between coccoliths, ~~and~~ element ratios and climatic indices at ODP Site 967

Florisphaera profunda and holococcolith distribution patterns at ODP Site 967 (Figs. 5A-B) are compared with sedimentary elemental ratios and climatic indices from the same sedimentary sequence (Grant et al., 2017). A principal component analysis carried out on elemental proxies by these authors highlighted that principal components PC1 (not shown) and PC2 (Fig. 5D) account for 79% of variance and reflect terrigenous input and sapropel deposition (enhanced monsoon runoff), respectively. Moreover, aeolian dust fluxes (Fig. 5E) and a North Africa humidity/aridity index (Fig. 5F) were calculated and are also compared with coccolith abundance fluctuations.

Intensification of East African monsoon precipitation coincided with northward displacement of the Intertropical Convergence Zone (ITCZ) and subsequent intensification of precipitation over the catchment basins of the Nile and other rivers, which fuelled enhanced freshwater discharge along the wider North African margin into the eastern Mediterranean (Ehrmann et al., 2016; Rohling et al., 2002a; Rohling et al., 2015). *Florisphaera profunda* proliferates because it benefits from the nutricline positioned in deep photic zone and the establishment of a DCM (Castradori, 1993; Girone et al., 2013; Grelaud et al., 2012; Incarbona et al., 2011;

Negri et al., 1999), following the rationale outlined above (Myers et al., 1998; Rohling, 1991a; Rohling and Gieskes, 1989). This scenario has been described for eastern Mediterranean sapropels and is further supported by the coupling of the *F. profunda* signal and enhanced humidity in North Africa that leads to enhanced monsoon runoff into the eastern Mediterranean, especially during S12, S11, b and S10 (Fig. 5). Also evident is decoupling between *F. profunda* and the humidity/aridity index, for instance during glacial sapropel S13 and during sapropel layer b. This ~~can be explained by the meaning of~~indicatessuggests that the climatic indices at ODP Site 967 ~~that~~ reflect increased rainfall over North Africa and Sahara, without ~~a clear indication of the~~sufficient northward monsoon penetration that determines the intensity of monsoon-related runoff into the eastern Mediterranean Sea (Grant et al., 2017). Also, different nutrient dynamics may have developed during the glacial sapropel S13, with surface fertilization that supports placolith-bearing species competition.

However, the coccolith record at Site 967 suggests that *F. profunda* increases are a recurring feature of the record that is not necessarily associated with the deposition of organic-rich layers deposition on the eastern Mediterranean seafloor, especially in glacial episodes~~s~~ (Fig. 5A). The Ba/Al signal indicates that many sapropel layers ~~likely were~~have been partially oxidized (Fig. 5G)~~ and~~, so that their currently visible extents do not represent the ~~real~~ original thickness of anoxic sediments. Yet, we argue that *F. profunda* peaks are not exclusively linked to the environmental changes ~~driven by these hydrographic perturbations~~associated with sapropel formation. Positive *Florisphaera profunda* ~~positive~~ peaks~~,~~ without a corresponding sapropel layer~~,~~ (be it visible, or oxidized) are evident in all eastern Mediterranean records that span sufficiently long time intervals (Castradori, 1993; Giunta et al., 2003; Maiorano et al., 2013; Negri et al., 1999; Triantaphyllou et al., 2010). The occurrence of *F. profunda* during glacial periods identifies a second mode of DCM development in the eastern Mediterranean, as proposed on the basis of planktonic foraminiferal assemblages

(Rohling and Gieskes, 1989) and modeling (Myers et al., 1998; Rohling, 1991a). Again, the DCM development would be driven by the pycnocline and nutricline shoaling within the lower part of the photic zone. But, for glacials, the eustatic sea-level drop (Fig. 5C) would have been the main trigger mechanism, after reducing water mass transport at both Gibraltar and Sicily Straits and ultimately shoaling the pycnocline and nutricline depth up to ~ 80 m (Myers et al., 1998; Rohling, 1991a). However, the scattered *F. profunda* abundance signal in MISs 12 and 10 suggests that other factors may operate in conjunction with sea-level fall, for reducing water transport across the Gibraltar and Sicily Straits. Among these, less frequent and intense northern outbreaks in deep water production sites and the inflow of low-density meltwater from the Atlantic Ocean may have weakened the Mediterranean thermohaline circulation and may have caused transient reductions in ~~reduced~~ the water transport at straits, like during last glacial cold spells (Sierro et al., 2005; Sprovieri et al., 2012; Toucanne et al., 2012; Azibeiro et al., 2021).

Holococcoliths are made of small calcite rhombohedra, arranged in different patterns. They are the most vulnerable coccoliths to selective dissolution (Roth and Coulbourn, 1982). Comparison between the new ODP 967 holococcolith record and the humidity/aridity index (Figs. 5B, F) shows strong similarities throughout the time span studied, which clearly point to the dissolution of ~~haploid~~ haploid-life calcite remains ~~in~~ at the Erathostenes seamount during humid phases. This agrees with the notion that surface buoyancy gain by freshwater river discharge negatively impacted deep-water formation in the eastern Mediterranean Sea, which enhanced organic carbon preservation (De Lange et al., 2008; Myers et al., 1998; Rohling et al., 2015) and, thus, worsened holococcolith preservation, like during sapropel S1 (Crudeli et al., 2006; Incarbona et al., 2019; Incarbona and Di Stefano, 2019) and sapropel S5 (Fig. 2, this study).

It is worth noting that the three major aeolian dust peaks ~~of dust~~ during MIS 13-12 (Fig. 5E) did not match with increasing holococcolith preservation but fall within 'no preservation' intervals. Aeolian dust peaks are associated ~~to~~ with ~~a~~ weakened monsoon activity and North Africa dry periods, as seen from the Ti/Al ratio (Konijnendijk et al., 2015; Lourens et al., 2001; Wehausen and Brumsack, 2000; Ziegler et al., 2010), and would imply a lower freshwater input into the eastern Mediterranean Sea. Ideally, these conditions would enhance deep water formation, ~~less~~ reduce organic matter preservation on the seafloor~~,~~ and increase~~d~~ preservation of holococcolith calcite. However, dust accumulation in marine cores depends on wind strength and direction (Moulin et al., 1997; Zabel et al., 1999). Thus, aeolian dust peaks are not necessarily tied to cooling and atmospheric perturbations that, for instance during the latest Quaternary, led to enhanced Mediterranean bottom water ventilation in coincidence of glacials and stadials (Cacho et al., 1999; 2000; Sprovieri et al., 2012; Toucanne et al., 2012).

6.4 – AMOC slowdown, holococcolith preservation and monsoon weakening

In Figure 6, North Atlantic geochemical records (Fig. 6A-B), Mediterranean holococcolith data (Fig. 6C), and oxygen isotopes of China speleothems (Fig. 6D) are plotted using their own original age models (Cheng et al., 2016; Grant et al., 2017; Hodell et al., 2015; Martrat et al., 2007). The grey boxes used for correlation are drawn and link correlative events in these various Northern Hemisphere records. Records shown in Figure 6 help with outlining a concept of atmosphere/ocean interactions that resulted in the correlation between Northern Hemisphere climate variability and surface water ecosystem modifications and seafloor diagenesis in the eastern Mediterranean.

The correlation boxes in Figure 6 are drawn assuming that AMOC slowdown/shutdown caused an atmospheric perturbation that impacted a vast area of the northern Hemisphere, including the eastern Mediterranean Sea, East African and

Asian monsoon sites (~~REFS for this assumption – from modelling would be best here?~~Vellinga and Wood, 2002). The log (Ca/Ti) record from the Iberian Margin (Fig. 6B) is a proxy for millennial-scale variability (Hodell et al., 2015): minima indicate stadial/Heinrich phases during which the AMOC was severely weakened or collapsed (McManus et al., 2004, 1999). Previous studies based on $\delta^{13}C$, alcohol index and sortable silt records support the hypothesis that Mediterranean bottom water ventilation at least in the western sub-basin was more intense during glacial periods and stadial events (Cacho et al., 2000, 1999; Frigola et al., 2008; Sprovieri et al., 2012; Toucanne et al., 2012) and strengthened Mediterranean outflow ~~water~~ into the Gulf of Cadiz and in the Iberian Margin (Sierro et al., 2020). ~~The~~ Simultaneous enhancement of EMDW ~~renewal~~ ventilation ~~on the seafloor~~ would have enhanced holococcolith preservation, as ~~already~~ observed below and above sapropel S1 (Incarbona et al., 2019; Incarbona and Di Stefano, 2019) and during HS11 and C26 in the Aegean Sea (this study, Fig. 2). The physico-chemical processes in the seafloor microsystem by which tiny holococcolith calcite rhombohedra are preferentially preserved under oxic conditions is not clear yet. Incarbona et al. (2019b) hypothesized a possible detrimental action of organic acid produced by bacteria under a dysoxic/anoxic state on the water/sediment interface, in analogy with ~~today's~~ results from modern surveys in the Gulf of California (Ziveri and Thunell, 2000). However, specific studies are needed to better understand the processes involved.

The link between AMOC slowdown/shutdown and East African, Indian, and Asian monsoon weakening is well-established (Deplazes et al., 2014; Porter and Zhisheng, 1995; Rohling et al., 2002; Rohling et al., 2006; Schulz et al., 1998; Sirocko et al., 1993; Tjallingii et al., 2008), ~~possibly operating by the~~and may involve severe drought development due to southward ITCZ ~~southward shift and severe drought~~displacement (Krebs and Timmermann, 2007; Vellinga and Wood, 2002; Zhang and Delworth, 2006). Yet, ~~we acknowledge that the~~an ITCZ shift~~,~~ and ~~the~~ associated Hadley cell ~~activity,~~changes ~~may~~ likely explain only part of the impacts on

monsoon circulation, which also depends on regional and local processes (Donohoe et al., 2013; Geen et al., 2020). For example, ~~A~~ recent modeling shows that Northern Hemisphere glacial cooling, increased ice-sheet albedo, and sea-level ~~fall,~~lowering produce an anomalous thermal gradient between the Arabian Peninsula and the Arabian Sea~~,~~ that ~~producing~~ resulting~~s~~ in a weakened Walker circulation in the Indian Ocean and drought in the monsoon systems of the Indo-Pacific region (DiNezio et al., 2018). As ~~already~~ mentioned before for the HS 11 and C26 cold spells (section 6.1), AMOC slowdown/shutdown also produces cooling and intense atmospheric perturbations in the Mediterranean region (Manabe and Stouffer, 1997; Vellinga and Wood, 2002), facilitating deep-water formation and bottom water ventilation (Cacho et al., 2000; Sprovieri et al., 2012; Toucanne et al., 2012). Thus, AMOC slowdown/shutdown may have both strengthened cold and dry polar/continental air outbreaks and reduced Indian-African monsoon activity, with both processes conducive to enhanced EMDW production (the prerequisite for holococcolith preservation).

In Fig. 6, grey correlation boxes indicate a link between AMOC slowdown/shutdown phases (Fig. 6B) and both the heaviest oxygen isotopic values in Chinese Sanbao Cave speleothems (Fig. 6D) and enhanced holococcolith preservation in the Mediterranean (Fig. 6C).

The atmospheric CH_4 record from Antarctica ice cores (Fig. 6E) reflects emissions from boreal and monsoonal wetlands (Guo et al., 2012; Landais et al., 2010). The signal has been be separated into three principal components, a glacial-interglacial forced component, a bi-hemispheric insolation driven component, and a millennial-scale oscillatory component, ~~that~~ which respectively explain 80%, 15% and 5% of the variance (Guo et al., 2012). Glacial-interglacial cycles force ~~a~~ globally synchronous monsoonal variations in methane emission. The other two forcings are hemispheric in nature, because of the two hemispheres' anti-phasing for low-latitude summer insolation changes in ITCZ oscillations and for millennial-scale bipolar see-saw

(strengthening/weakening) AMOC circulation (Guo et al., 2012). The limited number of grey correlation boxes between the Antarctic CH_4 signal and of Asian monsoon activity (Fig. 6D-E) suggests that the activity of ~~southern~~ Southern Hemisphere monsoon systems (South America, South Africa, Australia) ~~has~~ have been a major driver of methane emission between 550 and 300 ka However, we note the occurrence of three different peaks of Antarctic CH_4 during MIS 13, a signal which is also visible in Mediterranean holococcoliths and the China speleothem record (Fig. 6). This feature supports reduced emission from southern hemisphere methane sources during MIS 13 and an increased and synchronous emission from northern monsoons and boreal wetlands (Guo et al., 2012).

7 – Conclusions

The chronology and age uncertainties of SE Aegean Sea core LC21 coccolith data, Iberian Margin geochemical records, $\delta^{18}O$ in the Sanbao Cave stalagmites, and atmospheric methane concentrations from EDC have been probabilistically assessed for the last interglacial and TII. The *F. profunda* peak at the base of sapropel S5 layer is contemporaneous with a maximum in the rates of $\delta^{18}O$ change in Sanbao Cave and with the CH_4 overshoot in EDC, which ~~suggesting~~ suggests ~~the~~ an ~~intensification of the~~ African and Asian monsoon intensification at the onset of the last interglacial and the raising of the summer upper mixed layer depth. Holococcolith preservation was enhanced during Heinrich event HS11 and the C26 cold spell ~~C26~~, ~~while~~ when AMOC was severely weakened or collapsed. Cooling and atmospheric perturbations promoted ~~surface~~ surface-water buoyancy loss and deep-water formation-, and thus increased ~~higher~~ Mediterranean bottom water ventilation rates. These results ~~from the Aegean Sea~~ for LC21 explicitly link holococcolith preservation to episodes of enhanced deep-water formation and seafloor ventilation in the eastern Mediterraenan Sea during Heinrich and Stadial events.

We also analysed ~~A total of~~ 668 samples ~~were analysed~~ from ODP Site 967 ~~Site~~ to reconstruct variations in coccolithophore ecolog~~ical variations of coccolithophoresy~~ in the region of the Eratosthenes Seamount (eastern Mediterranean Sea) between about 550 and 300 ka (Middle Pleistocene, MIS 14-9). Placoliths and *F. profunda* abundance fluctuations are strongly anticorrelated ($R^2 = 0.95$, $n = 668$) and together dominate the coccolith assemblages at Site 967, which ~~suggesting~~ suggests that the surface water environment repeatedly switched between predominant winter-induced fertilization (shallow nutricline) and predominant monsoon-induced deep nutricline ~~deepening~~conditions (and Deep Chlorophyll Maximum development) associated with ~~, through~~ a shoaling of the pycnocline to a position within the lower photic zone. In analogy with results for core LC21, Middle Pleistocene phases of enhanced monsoon runoff into the eastern Mediterranean ~~may have~~appear to have caused shoaling of the pycnocline into the ~~base of the~~ lower photic layer, which provides a deep nutricline that fosters *F. profunda* proliferation. A second mode of *F. profunda* proliferation and DCM development is seen in glacials, when the nutricline shoaled into the lower photic zone due to sea-level lowering that reduced water-mass transport through the main Mediterranean straits. Thus, our coccolithophore assemblage analyses corroborate earlier suggestions of such a phenomenon based on planktonic foraminiferal analyses (Rohling and Gieskes, 1989) and modeling (Myers et al., 1998; Rohling, 1991a).

Scattered but statistically significant peaks of holococcoliths (up to ~ 20%) mark increased carbonate preservation on the seafloor ~~by~~ due to enhanced production of EMDW, ~~that~~ which match changes in recently proposed North Africa aridity indices ~~as recently proposed on the basis of elemental analysis~~ (Grant et al., 2017). Finally, holococcolith enhanced preservation during cold spells is linked to increased deep-water formation in the Mediterr~~r~~anean Sea, in response to Atlantic Meridional Overturning Circulation slowdown and weakened monsoon activity during Northern Hemisphere cold events.

Acknowledgments

We are grateful to an anonymous reviewer and to Fabienne Marret-Davies for their comments and suggestions. FFR2021 grant to A.I. is aAcknowledged. G.M. acknowledges support from the Universidade de Vigo's programme to attract excellent research talent (RR04092017), a Beatriz Galindo Fellowship (2020), and a generous start-up package. M.G. acknowledges support from the CALMED project (CTM2016-79547-R) and the Generalitat de Catalunya (MERS, 2014 SGR – 1356).

Bibliographic references

Allen, J.I., Somerfield, P.J., Siddorn, J., 2002. Primary and bacterial production in the Mediterranean Sea: A modelling study. J. Mar. Syst. 33–34, 473–495. doi:10.1016/S0924-7963(02)00072-6

Amies, J.D., Rohling, E.J., Grant, K.M., Rodríguez-Sanz, L., Marino, G., 2019. Quantification of African Monsoon Runoff During Last Interglacial Sapropel S5. Paleoceanogr. Paleoclimatology 34, 1487–1516. doi:10.1029/2019PA003652

Athanasiou, M., Boloubassi, I., Gogou, A., Klein, V., Dimiza, M.D., Parinos, C., Skampa, E., Triantaphyllou, M.V., 2017. Sea surface temperatures and environmental conditions during the 'warm Pliocene' interval (4.1-3.2 Ma) in the Eastern Mediterranean (Cyprus). Global Planetary Change 150, 46-57.

Athanasiou, M., Triantaphyllou, M.V., Dimiza, M.D., Gogou, A., Theodorou, G., 2015. Zanclean/Piacenzian transition on Cyprus (SE Mediterranean): calcareous nannofossil evidence of sapropel formation. Geo-Marine Letters 35, 367-385.

Azibeiro, L. A., Sierro, F. J., Capotondi, L., Lirer, F., Andersen, N., González-Lanchas, A., Alonso-Garcia, M., Flores, J.-A., Cortina, A., Grimalt, J. O., Martrat, B., Cacho, I., 2021. Meltwater flux from northern ice-sheets to the mediterranean during MIS 12. Quaternary Science Reviews, 268, 107108. https://doi.org/https://doi.org/10.1016/j.quascirev.2021.107108

694 Baumann, K.-H., Andruleit, H., Böckel, B., Geisen, M., Kinkel, H., 2005. The
695 significance of extant coccolithophores as indicators of ocean water masses,
696 surface water temperature, and paleoproductivity: a review. Pal{ä}ontologische
697 Zeitschrift 79, 93–112. doi:10.1007/bf03021756
698 Bazin, L., Landais, A., Lemieux-Dudon, B., Toyé Mahamadou Kele, H., Veres, D.,
699 Parrenin, F., Martinerie, P., Ritz, C., Capron, E., Lipenkov, V., Loutre, M.-F.,
700 Raynaud, D., Vinther, B., Svensson, A., Rasmussen, S.O., Severi, M., Blunier,
701 T., Leuenberger, M., Fischer, H., Masson-Delmotte, V., Chappellaz, J., Wolff,
702 E., 2013. An optimized multi-proxy, multi-site Antarctic ice and gas orbital
703 chronology (AICC2012): 120–800 ka. Clim. Past 9, 1715–1731.
704 doi:10.5194/cp-9-1715-2013
705 Bazzicalupo, P., Maiorano, P., Girone, A., Marino, M., Combourieu-Nebout, N.,
706 Pelosi, N., Salgueiro, E., Incarbona, A., 2020. Holocene climate variability of the
707 Western Mediterranean: Surface water dynamics inferred from calcareous
708 plankton assemblages. The Holocene. doi:10.1177/0959683619895580
709 Beaufort, L., de Garidel-Thoron, T., Mix, A.C., Pisias, N.G., 2001. ENSO-like
710 forcing on oceanic primary production during the Late Pleistocene. Science 293,
711 2440–2444. doi:10.1126/science.293.5539.2440
712 Beaufort, L., Lancelot, Y., Camberlin, P., Cayre, O., Vincent, E., Bassinot, F.,
713 Labeyrie, L., 1997. Insolation Cycles as a Major Control of Equatorial Indian
714 Ocean Primary Production. Science 278, 1451–1454.
715 Böhm, E., Lippold, J., Gutjahr, M., Frank, M., Blaser, P., Antz, B., Fohlmeister, J.,
716 Frank, N., Andersen, M.B., Deininger, M., 2015. Strong and deep Atlantic
717 meridional overturning circulation during the last glacial cycle. Nature 517, 73–
718 76. doi:10.1038/nature14059
719 Bonomo, S., Grelaud, M., Incarbona, A., Malinverno, E., Placenti, F., Bonanno, A.,
720 Stefano, E.D., Patti, B., Sprovieri, M., Genovese, S., Rumolo, P., Mazzola, S.,
721 Zgozi, S., Ziveri, P., 2012. Living Coccolithophores from the Gulf of Sirte
722 (Southern Mediterranean Sea) during the summer of 2008. Micropaleontology

723 58, 487–503.
724 Bown, Paul R., Young, J.R., 1998. Techniques, in: Bown, P.R. (Ed.), Calcareous
725 Nannofossil Biostratigraphy. Chapman and Kluwer Academic, London, pp. 16–
726 28.
727 Cacho, I., Grimalt, J.O., Pelejero, C., Canals, M., Sierro, F.J., Flores, J.A.,
728 Shackleton, N., 1999. Dansgaard-Oeschger and Heinrich event imprints in
729 Alboran Sea paleotemperatures. Paleoceanography 14, 698–705.
730 doi:10.1029/1999PA900044
731 Cacho, I., Grimalt, J.O., Sierro, F.J., Shackleton, N., Canals, M., 2000. Evidence for
732 enhanced Mediterranean thermohaline circulation during rapid climatic coolings.
733 Earth Planet. Sci. Lett. 183, 417–429. doi:10.1016/S0012-821X(00)00296-X
734 Castradori, D., 1993. Calcareous nannofossils and the origin of Eastern
735 Mediterranean sapropel. Paleoceanography 8, 459–471.
736 Cheng, H., Edwards, R.L., Broecker, W.S., Denton, G.H., Kong, X., Wang, Y.,
737 Zhang, R., Wang, X., 2009. Ice Age Terminations. Science (80-.). 326, 248–252.
738 doi:10.1126/science.1177840
739 Cheng, H., Edwards, R.L., Sinha, A., Spötl, C., Yi, L., Chen, S., Kelly, M., Kathayat,
740 G., Wang, X., Li, X., Kong, X., Wang, Y., Ning, Y., Zhang, H., 2016. The Asian
741 monsoon over the past 640,000 years and ice age terminations. Nature 534, 640–
742 646. doi:10.1038/nature18591
743 Cheng, H., Edwards, R.L., Wang, Y., Kong, X., Ming, Y., Kelly, M.J., Wang, X.,
744 Gallup, C.D., Liu, W., 2006. A penultimate glacial monsoon record from Hulu
745 Cave and two-phase glacial terminations. Geology 34, 217–220.
746 doi:10.1130/G22289.1
747 Crudeli, D., Young, J.R., Erba, E., Geisen, M., Ziveri, P., de Lange, G.J., Slomp,
748 C.P., 2006. Fossil record of holococcoliths and selected hetero-holococcolith
749 associations from the Mediterranean (Holocene-late Pleistocene): Evaluation of
750 carbonate diagenesis and palaeoecological-palaeocenographic implications.
751 Palaeogeogr. Palaeoclimatol. Palaeoecol. 237, 191–212.

752 doi:10.1016/j.palaeo.2005.11.022
753 D'Amario, B., Ziveri, P., Grelaud, M., Oviedo, A., Kralj, M., 2017. Coccolithophore
754 haploid and diploid distribution patterns in the Mediterranean Sea: Can a haplo-
755 diploid life cycle be advantageous under climate change? J. Plankton Res. 39,
756 781–794. doi:10.1093/plankt/fbx044
757 Dimiza, M.D., Triantaphyllou, M.V., Malinverno, E., Psarra, S., Karatsolis, B., Mara,
758 P., lagaria, A., Gogou, A., 2015. The composition and distribution of living
759 coccolithophores in the Aegean sea (NE Mediterranean). Micropaleontology 61,
760 521-540.
761 D'Ortenzio, F., Ribera d'Alcalà, M., 2009. On the trophic regimes of the
762 Mediterranean Sea: a satellite analysis. Biogeosciences 6, 139–148.
763 doi:10.5194/bg-6-139-2009
764 De Lange, G.J., Thomson, J., Reitz, A., Slomp, C.P., Principato, M.S., Erba, E.,
765 Corselli, C., 2008. Synchronous basin-wide formation and redox-controlled
766 preservation of a Mediterranean sapropel. Nat. Geosci. 1, 606–610.
767 doi:10.1038/ngeo283
768 Deaney, E.L., Barker, S., van de Flierdt, T., 2017. Timing and nature of AMOC
769 recovery across Termination 2 and magnitude of deglacial CO2 change. Nat.
770 Commun. 8, 14595. doi:10.1038/ncomms14595
771 Deplazes, G., Lückge, A., Stuut, J.-B.W., Pätzold, J., Kuhlmann, H., Husson, D.,
772 Fant, M., Haug, G.H., 2014. Weakening and strengthening of the Indian
773 monsoon during Heinrich events and Dansgaard-Oeschger oscillations.
774 Paleoceanography 29, 99–114. doi:10.1002/2013PA002509
775 Di Stefano, A., Foresi, L.M., Incarbona, A., Sprovieri, M., Vallefuoco, M., Iorio, M.,
776 Pelosi, N., Di Stefano, E., Sangiorgi, P., Budillon, F., 2015. Mediterranean
777 coccolith ecobiostratigraphy since the penultimate Glacial (the last 145,000years)
778 and ecobioevent traceability. Mar. Micropaleontol. 115.
779 doi:10.1016/j.marmicro.2014.12.002
780 Di Stefano, E., Incarbona, A., 2004. High-resolution palaeoenvironmental

781 reconstruction of ODP Hole 963D (Sicily Channel) during the last deglaciation
782 based on calcareous nannofossils. Mar. Micropaleontol. 52.
783 doi:10.1016/j.marmicro.2004.04.009
784 Di Stefano, E., Incarbona, A., Bonomo, S., Pelosi, N., 2011. Coccolithophores in
785 water samplesand fossil assemblages in sedimentary archives of the
786 Mediterranean Sea: A review, New Oceanography Research Developments:
787 Marine Chemistry, Ocean Floor Analyses and Marine Phytoplankton.
788 DiNezio, P.N., Tierney, J.E., Otto-Bliesner, B.L., Timmermann, A., Bhattacharya, T.,
789 Rosenbloom, N., Brady, E., 2018. Glacial changes in tropical climate amplified
790 by the Indian Ocean. Sci. Adv. 4, eaat9658. doi:10.1126/sciadv.aat9658
791 Donohoe, A., Marshall, J., Ferreira, D., Mcgee, D., 2013. The Relationship between
792 ITCZ Location and Cross-Equatorial Atmospheric Heat Transport: From the
793 Seasonal Cycle to the Last Glacial Maximum. J. Clim. 26, 3597–3618.
794 doi:10.1175/JCLI-D-12-00467.1
795 Ehrmann, W., Schmiedl, G., Seidel, M., Krüger, S., Schulz, H., 2016. A distal
796 140\,kyr sediment record of Nile discharge\hack{\newline} and East African
797 monsoon variability. Clim. Past 12, 713–727. doi:10.5194/cp-12-713-2016
798 Emeis, K.-C., Robertson, A.H.F., Richter, C., Party, S., 1996. Site 967. In:
799 Proceedings of the Ocean Drilling Program, Initial Reports, Leg 160 (Emeis, K.-
800 C., Robertson, A.H.F. and Richter, C. Eds). pp. 215–287.
801 Emeis, K.C., Sakamoto, T., Wehausen, R., Brumsack, H.J., 2000a. The sapropel
802 record of the eastern Mediterranean Sea - Results of Ocean Drilling Program Leg
803 160. Palaeogeogr. Palaeoclimatol. Palaeoecol. 158, 371–395. doi:10.1016/S0031-
804 0182(00)00059-6
805 Emeis, K.C., Struck, U., Schulz, H.M., Rosenberg, R., Bernasconi, S., Erlenkeuser,
806 H., Sakamoto, T., Martinez-Ruiz, F., 2000b. Temperature and salinity variations
807 of Mediterranean Sea surface waters over the last 16,000 years from records of
808 planktonic stable oxygen isotopes and alkenone unsaturation ratios. Palaeogeogr.
809 Palaeoclimatol. Palaeoecol. 158, 259–280. doi:10.1016/S0031-0182(00)00053-5

Fleitmann, D., Burns, S.J., Mudelsee, M., Neff, U., Kramers, J., Mangini, A., Matter, A., 2003. Holocene Forcing of the Indian Monsoon Recorded in a Stalagmite from Southern Oman. Science (80-.). 300, 1737–1739. doi:10.1126/science.1083130

Flores, J.A., Bárcena, M.A., Sierro, F.J., 2000. Ocean-surface and wind dynamics in the Atlantic Ocean off Northwest Africa during the last 140 000 years. Palaeogeogr. Palaeoclimatol. Palaeoecol. 161, 459–478. doi:10.1016/S0031-0182(00)00099-7

Flores, J.A., Sierro, F.J., Francés, G., Vazquez, A., Zamarreno, I., 1997. The last 100,000 years in the western Mediterranean: sea surface water and frontal dynamics as revealed by coccolithophores. Mar. Micropaleontol. 29, 351–366.

Frigola, J., Moreno, A., Cacho, I., Canals, M., Sierro, F.J., Flores, J.A., Grimalt, J.O., 2008. Evidence of abrupt changes in Western Mediterranean Deep Water circulation during the last 50 kyr: A high-resolution marine record from the Balearic Sea. Quat. Int. 181, 88–104. doi:10.1016/j.quaint.2007.06.016

Geen, R., Bordoni, S., Battisti, D.S., Hui, K., 2020. Monsoons, ITCZs, and the Concept of the Global Monsoon. Rev. Geophys. 58, e2020RG000700. doi:https://doi.org/10.1029/2020RG000700

Girone, A., Capotondi, L., Ciaranfi, N., Di Leo, P., Lirer, F., Maiorano, P., Marino, M., Pelosi, N., Pulice, I., 2013. Paleoenvironmental changes at the lower Pleistocene Montalbano Jonico section (southern Italy): Global versus regional signals. Palaeogeogr. Palaeoclimatol. Palaeoecol. 371, 62–79. doi:10.1016/j.palaeo.2012.12.017

Giunta, S., Negri, a., Morigi, C., Capotondi, L., Combourieu-Nebout, N., Emeis, K.C., Sangiorgi, F., Vigliotti, L., 2003. Coccolithophorid ecostratigraphy and multi-proxy paleoceanographic reconstruction in the Southern Adriatic Sea during the last deglacial time (Core AD91-17). Palaeogeogr. Palaeoclimatol. Palaeoecol. 190, 39–59. doi:10.1016/S0031-0182(02)00598-9

Grant, K.M., Grimm, R., Mikolajewicz, U., Marino, G., Ziegler, M., Rohling, E.J.,

2016. The timing of Mediterranean sapropel deposition relative to insolation, sea-level and African monsoon changes. Quat. Sci. Rev. 140, 125–141. doi:10.1016/j.quascirev.2016.03.026

Grant, K.M., Rohling, E.J., Bar-Matthews, M., Ayalon, A., Medina-Elizalde, M., Ramsey, C.B., Satow, C., Roberts, A.P., 2012. Rapid coupling between ice volume and polar temperature over the past 50,000 years. Nature 491, 744–747. doi:10.1038/nature11593

Grant, K.M., Rohling, E.J., Westerhold, T., Zabel, M., Heslop, D., Konijnendijk, T., Lourens, L., 2017. A 3 million year index for North African humidity/aridity and the implication of potential pan-African Humid periods. Quat. Sci. Rev. 171, 100–118. doi:https://doi.org/10.1016/j.quascirev.2017.07.005

Grelaud, M., Marino, G., Ziveri, P., Rohling, E.J., 2012. Abrupt shoaling of the nutricline in response to massive freshwater flooding at the onset of the last interglacial sapropel event. Paleoceanography 27. doi:10.1029/2012PA002288

Guo, Z., Zhou, X., Wu, H., 2012. Glacial-interglacial water cycle, global monsoon and atmospheric methane changes. Clim. Dyn. 39, 1073–1092. doi:10.1007/s00382-011-1147-5

Hernández-Almeida, I., Ausín, B., Saavedra-Pellitero, M., Baumann, K.-H., Stoll, H.M., 2019. Quantitative reconstruction of primary productivity in low latitudes during the last glacial maximum and the mid-to-late Holocene from a global Florisphaera profunda calibration dataset. Quat. Sci. Rev. 205, 166–181. doi:https://doi.org/10.1016/j.quascirev.2018.12.016

Hodell, D., Crowhurst, S., Skinner, L., Tzedakis, P.C., Margari, V., Channell, J.E.T., Kamenov, G., MacLachlan, S., Rothwell, G., 2013. Response of Iberian Margin sediments to orbital and suborbital forcing over the past 420 ka. Paleoceanography 28, 185–199. doi:10.1002/palo.20017

Hodell, D., Lourens, L., Crowhurst, S., Konijnendijk, T., Tjallingii, R., Jiménez-Espejo, F., Skinner, L., Tzedakis, P.C., Abrantes, F., Acton, G.D., Alvarez Zarikian, C.A., Bahr, A., Balestra, B., Barranco, E.L., Carrara, G., Ducassou, E.,

Flood, R.D., Flores, J.-A., Furota, S., Grimalt, J., Grunert, P., Hernández-Molina, J., Kim, J.K., Krissek, L.A., Kuroda, J., Li, B., Lofi, J., Margari, V., Martrat, B., Miller, M.D., Nanayama, F., Nishida, N., Richter, C., Rodrigues, T., Rodríguez-Tovar, F.J., Roque, A.C.F., Sanchez Goñi, M.F., Sierro Sánchez, F.J., Singh, A.D., Sloss, C.R., Stow, D.A.V., Takashimizu, Y., Tzanova, A., Voelker, A., Xuan, C., Williams, T., 2015. A reference time scale for Site U1385 (Shackleton Site) on the SW Iberian Margin. Glob. Planet. Change 133, 49–64. doi:10.1016/j.gloplacha.2015.07.002

Incarbona, A., Abu-Zied, R.H., Rohling, E.J., Ziveri, P., 2019. Reventilation Episodes During the Sapropel S1 Deposition in the Eastern Mediterranean Based on Holococcolith Preservation. Paleoceanogr. Paleoclimatology 34, 1597–1609. doi:10.1029/2019PA003626

Incarbona, A., Di Stefano, E., 2019. Calcareous nannofossil palaeoenvironmental reconstruction and preservation in sapropel S1 at the Eratosthenes Seamount (Eastern Mediterranean). Deep Sea Res. Part II Top. Stud. Oceanogr. 164, 206–215. doi:https://doi.org/10.1016/j.dsr2.2018.10.004

Incarbona, A., Di Stefano, E., Parti, B., Pelosi, N., Bonomo, S., Mazzola, S., Sprovieri, R., Tranchida, G., Zgozi, S., Bonanno, A., 2008. Holocene millennial-scale productivity variations in the Sicily Channel (Mediterranean Sea). Paleoceanography 23, 1–18. doi:10.1029/2007PA001581

Incarbona, A., Martrat, B., Di Stefano, E., Grimalt, J.O., Pelosi, N., Patti, B., Tranchida, G., 2010a. Primary productivity variability on the Atlantic Iberian Margin over the last 70,000 years: Evidence from coccolithophores and fossil organic compounds. Paleoceanography 25, 1–15. doi:10.1029/2008PA001709

Incarbona, A., Sprovieri, M., Di Stefano, A., Di Stefano, E., Salvagio Manta, D., Pelosi, N., Ribera d'Alcalà, M., Sprovieri, R., Ziveri, P., 2013. Productivity modes in the mediterranean sea during dansgaard-oeschger (20,000-70,000yr ago) oscillations. Palaeogeogr. Palaeoclimatol. Palaeoecol. 392. doi:10.1016/j.palaeo.2013.09.023

Incarbona, A., Ziveri, P., Di Stefano, E., Lirer, F., Mortyn, G., Patti, B., Pelosi, N., Sprovieri, M., Tranchida, G., Vallefuoco, M., Albertazzi, S., Bellucci, L.G., Bonanno, A., Bonomo, S., Censi, P., Ferraro, L., Giuliani, S., Mazzola, S., Sprovieri, R., 2010b. The Impact of the Little Ice Age on Coccolithophores in the Central Mediterranea Sea. Clim. Past 6, 795–805. doi:10.5194/cp-6-795-2010

Incarbona, A., Ziveri, P., Sabatino, N., Manta, D.S., Sprovieri, M., 2011. Conflicting coccolithophore and geochemical evidence for productivity levels in the Eastern Mediterranean sapropel S1. Mar. Micropaleontol. 81, 131–143. doi:10.1016/j.marmicro.2011.09.003

Jordan, R.W., Cros, L., Young, J.R., 2004. A revised classification scheme for living haptophytes. Micropaleontology 50, 55–79. doi:10.2113/50.Suppl_1.55

Josey, S.A., Somot, S., Tsimplis, M., 2011. Impacts of atmospheric modes of variability on Mediterranean Sea surface heat exchange. J. Geophys. Res. Ocean. 116, 1–15. doi:10.1029/2010JC006685

Kemp, A.E.S., Pearce, R.B., Koizumi, I., Pike, J., Rance, S.J., 1999. The role of mat-forming diatoms in the formation of Mediterranean sapropels. Nature 398, 57.

Kleijne, A., 1991. Holococcolithophorids from the Indian-Ocean, Red-Sea, Mediterranean-Sea and North-Atlantic Ocean. Mar. Micropaleontol. 17, 1–76. doi:Doi 10.1016/0377-8398(91)90023-Y

Klein, P., Coste, B., 1984. Effects of wind-stress variability on nutrient transport into the mixed layer. Deep Sea Res. Part A. Oceanogr. Res. Pap. 31, 21–37. doi:10.1016/0198-0149(84)90070-0

Knappertsbusch, M., 1993. Geographic distribution of living and Holocene coccolithophores in the Mediterranean Sea. Mar. Micropaleontol. doi:10.1016/0377-8398(93)90016-Q

Konijnendijk, T.Y.M., Ziegler, M., Lourens, L., 2014. Chronological constraints on Pleistocene sapropel depositions from high-resolution geochemical records of ODP Sites 967 and 968, Newsletters on Stratigraphy. doi:10.1127/0078-0421/2014/0047

926 Konijnendijk, T.Y.M., Ziegler, M., Lourens, L.J., 2015. On the timing and forcing
927 mechanisms of late Pleistocene glacial terminations: Insights from a new high-
928 resolution benthic stable oxygen isotope record of the eastern Mediterranean.
929 Quat. Sci. Rev. 129, 308–320. doi:10.1016/j.quascirev.2015.10.005
930 Krebs, U., Timmermann, A., 2007. Tropical Air–Sea Interactions Accelerate the
931 Recovery of the Atlantic Meridional Overturning Circulation after a Major
932 Shutdown. J. Clim. 20, 4940–4956. doi:10.1175/JCLI4296.1
933 Krom, M.D., Emeis, K.C., Van Cappellen, P., 2010. Why is the Eastern
934 Mediterranean phosphorus limited? Prog. Oceanogr. 85, 236–244.
935 doi:10.1016/j.pocean.2010.03.003
936 Krom, M.D., Kress, N., Brenner, S., Gordon, L.I., 1991. Phosphorus Limitation of
937 Primary Productivity in the Eastern Mediterranean-Sea. Limnol. Oceanogr. 36,
938 424–432.
939 Landais, A., Dreyfus, G., Capron, E., Masson-Delmotte, V., Sanchez-Goñi, M.F.,
940 Desprat, S., Hoffmann, G., Jouzel, J., Leuenberger, M., Johnsen, S., 2010. What
941 drives the millennial and orbital variations of δ18Oatm? Quat. Sci. Rev. 29, 235–
942 246. doi:https://doi.org/10.1016/j.quascirev.2009.07.005
943 Larrasoaña, J.C., Roberts, A.P., Rohling, E.J., Winklhofer, M., Wehausen, R., 2003.
944 Three million years of monsoon variability over the northern Sahara. Clim. Dyn.
945 21, 689–698. doi:10.1007/s00382-003-0355-z
946 Laskar, J., Robutel, P., Joutel, F., Gastineau, M., Correia, a C.M., Levrard, B., 2004.
947 Astrophysics A long-term numerical solution for the insolation. Astronomy 285,
948 261–285. doi:10.1051/0004-6361
949 Lionello, P., 2012. The Climate of the Mediterranean Region: From the Past to the
950 Future, 1st ed. Elsevier Inc. doi:10.1016/B978-0-12-416042-2.00009-4
951 Lisiecki, L.E., Raymo, M.E., 2005. A Pliocene-Pleistocene stack of 57 globally
952 distributed benthic ?? 18O records. Paleoceanography 20, 1–17.
953 doi:10.1029/2004PA001071
954 Loulergue, L., Schilt, A., Spahni, R., Masson-Delmotte, V., Blunier, T., Lemieux, B.,

955 Barnola, J.-M., Raynaud, D., Stocker, T.F., Chappellaz, J., 2008. Orbital and
956 millennial-scale features of atmospheric CH4 over the past 800,000 years. Nature
957 453, 383–386. doi:10.1038/nature06950
958 Lourens, L.J., 2004. Revised tuning of Ocean Drilling Program Site 964 and KC01B
959 (Mediterranean) and implications for the $δ$18O, tephra, calcareous nannofossil,
960 and geomagnetic reversal chronologies of the past 1.1 Myr. Paleoceanography
961 19, 1–20. doi:10.1029/2003PA000997
962 Lourens, L.J., Wehausen, R., Brumsack, H.J., 2001. Geological constraints on tidal
963 dissipation and dynamical ellipticity of the Earth over the past three million
964 years. Nature 409, 1029.
965 Maiorano, P., Tarantino, F., Marino, M., De Lange, G.J., 2013. Paleoenvironmental
966 conditions at Core KC01B (Ionian Sea) through MIS 13-9: Evidence from
967 calcareous nannofossil assemblages. Quat. Int. 288, 97–111.
968 doi:10.1016/j.quaint.2011.12.007
969 Malanotte-Rizzoli, P., Artale, V., Borzelli-Eusebi, G.L., Brenner, S., Crise, A., Gacic,
970 M., Kress, N., Marullo, S., Ribera D'Alcalà, M., Sofianos, S., Tanhua, T.,
971 Theocharis, A., Alvarez, M., Ashkenazy, Y., Bergamasco, A., Cardin, V.,
972 Carniel, S., Civitarese, G., D'Ortenzio, F., Font, J., Garcia-Ladona, E., Garcia-
973 Lafuente, J.M., Gogou, A., Gregoire, M., Hainbucher, D., Kontoyannis, H.,
974 Kovacevic, V., Kraskapoulou, E., Kroskos, G., Incarbona, A., Mazzocchi, M.G.,
975 Orlic, M., Ozsoy, E., Pascual, A., Poulain, P.M., Roether, W., Rubino, A.,
976 Schroeder, K., Siokou-Frangou, J., Souvermezoglou, E., Sprovieri, M., Tintoré,
977 J., Triantafyllou, G., 2014. Physical forcing and physical/biochemical variability
978 of the Mediterranean Sea: A review of unresolved issues and directions for future
979 research. Ocean Sci. 10, 281–322. doi:10.5194/os-10-281-2014
980 Malinverno, E., Triantaphyllou, M. V, Stavrakakis, S., Ziveri, P., Lykousis, V., 2009.
981 Seasonal and spatial variability of coccolithophore export production at the
982 South-Western margin of Crete (Eastern Mediterranean). Mar. Micropaleontol.
983 71, 131–147. doi:10.1016/j.marmicro.2009.02.002

984 Manabe, S., Stouffer, R.J., 1997. Coupled ocean-atmosphere model response to
985 freshwater input: Comparison to Younger Dryas Event. Paleoceanography 12,
986 321–336. doi:10.1029/96PA03932
987 Marino, G., Rohling, E.J., Rijpstra, W.I.C., Sangiorgi, F., Schouten, S., Sinninghe
988 Damsté, J.S., 2007. Aegean sea as driver of hydrographic and ecological changes
989 in the eastern Mediterranean. Geology 35, 675–678. doi:10.1130/G23831A.1
990 Marino, G., Rohling, E.J., Rodríguez-Sanz, L., Grant, K.M., Heslop, D., Roberts,
991 A.P., Stanford, J.D., Yu, J., 2015. Bipolar seesaw control on last interglacial sea
992 level. Nature 522, 197–201. doi:10.1038/nature14499
993 Marino, G., Rohling, E.J., Sangiorgi, F., Hayes, A., Casford, J.L., Lotter, A.F.,
994 Kucera, M., Brinkhuis, H., 2009. Early and middle Holocene in the Aegean Sea:
995 interplay between high and low latitude climate variability. Quat. Sci. Rev. 28,
996 3246–3262. doi:10.1016/j.quascirev.2009.08.011
997 Marino, M., Maiorano, P., Lirer, F., 2008. Changes in calcareous nannofossil
998 assemblages during the Mid-Pleistocene Revolution. Mar. Micropaleontol. 69,
999 70–90. doi:10.1016/j.marmicro.2007.11.010
1000 Martrat, B., Grimalt, J.O., Shackleton, N.J., de Abreu, L., Hutterli, M. a, Stocker,
1001 T.F., 2007. Four climate cycles of recurring deep and surface water
1002 destabilizations on the Iberian margin. Science 317, 502–507.
1003 doi:10.1126/science.1139994
1004 Martrat, B., Jimenez-Amat, P., Zahn, R., Grimalt, J.O., 2014. Similarities and
1005 dissimilarities between the last two deglaciations and interglaciations in the
1006 North Atlantic region. Quat. Sci. Rev. 99, 122–134.
1007 doi:10.1016/j.quascirev.2014.06.016
1008 McIntyre, A., Molfino, B., 1996. Forcing of Atlantic Equatorial and Subpolar
1009 Millennial Cycles by Precession. Science. doi:10.1126/science.274.5294.1867
1010 McManus, J.F., Francois, R., Gherardi, J.-M., Keigwin, L.D., Brown-Leger, S., 2004.
1011 Collapse and rapid resumption of Atlantic meridional circulation linked to
1012 deglacial climate changes. Nature 428, 834–837. doi:10.1038/nature02494

McManus, J.F., Oppo, D.W., Cullen, J.L., 1999. A 0.5-Million-Year Record of Millennial-Scale Climate Variability in the North Atlantic. Science 283.

Meier, K.J.S., Zonneveld, K.A.F., Kasten, S., Willems, H., 2004. Different nutrient sources forcing increased productivity during eastern Mediterranean S1 sapropel formation as reflected by calcareous dinoflagellate cysts. Paleoceanography 19, 1–12. doi:10.1029/2003PA000895

Millot, C., 1999. Circulation in the Western Mediterranean Sea. J. Mar. Syst. 20, 423–442. doi:10.1016/S0924-7963(98)00078-5

Molfino, B., McIntyre, A., 1990a. Precessional forcing of nutricline dynamics in the equatorial atlantic. Science 249, 766–769. doi:10.1126/science.249.4970.766

Molfino, B., McIntyre, A., 1990b. Nutricline variation in the equatorial Atlantic coincident with the Younger Dryas. Paleoceanography. doi:10.1029/PA005i006p00997

Möller, L., Sowers, T., Bock, M., Spahni, R., Behrens, M., Schmitt, J., Miller, H., Fischer, H., 2013. Independent variations of CH4 emissions and isotopic composition over the past 160,000 years. Nat. Geosci. 6, 885–890. doi:10.1038/ngeo1922

Myers, P.G., Haines, K., Rohling, E.J., 1998. Modeling the paleocirculation of the Mediterranean: The last glacial maximum and the Holocene with emphasis on the formation of sapropel S1. Paleoceanography 13, 586–606.

Negri, a., Capotondi, L., Keller, J., 1999. Calcareous nannofossils, planktonic foraminifera and oxygen isotopes in the late Quaternary sapropels of the Ionian Sea. Mar. Geol. 157, 89–103. doi:10.1016/S0025-3227(98)00135-2

Nicholson, S.L., Pike, A.W.G., Hosfield, R., Roberts, N., Sahy, D., Woodhead, J., Cheng, H., Edwards, R.L., Affolter, S., Leuenberger, M., Burns, S.J., Matter, A., Fleitmann, D., 2020. Pluvial periods in Southern Arabia over the last 1.1 million-years. Quat. Sci. Rev. 229, 106112. doi:https://doi.org/10.1016/j.quascirev.2019.106112

Oppo, D.W., Keigwin, L.D., McManus, J.F., 2001. Persistent suborbital climate

variability in marine isotope stage 5 and Termination II. Paleoceanography 16, 280–292.

Oppo, D.W., McManus, J.F., Cullen, J.L., 2006. Evolution and demise of the Last Interglacial warmth in the subpolar North Atlantic. Quat. Sci. Rev. 25, 3268–3277. doi:10.1016/j.quascirev.2006.07.006

Osborne, A.H., Vance, D., Rohling, E.J., Barton, N., Rogerson, M., Fello, N., 2008. A humid corridor across the Sahara for the migration of early modern humans out of Africa 120,000 years ago. Proc. Natl. Acad. Sci. U. S. A. 105, 16444–16447. doi:10.1073/pnas.0804472105

Ovchinnikov I.M., 1984. The formation of Intermediate Water in the Mediterranean. Oceanology 24, 168–173.

Oviedo, A., Ziveri, P., Álvarez, M., Tanhua, T., 2015. Is coccolithophore distribution in the Mediterranean Sea related to seawater carbonate chemistry? Ocean Sci 11, 13–32. doi:10.5194/os-11-13-2015

Petrenko, V. V, Smith, A.M., Brook, E.J., Lowe, D., Riedel, K., Brailsford, G., Hua, Q., Schaefer, H., Reeh, N., Weiss, R.F., Etheridge, D., Severinghaus, J.P., 2009. ¹⁴CH₄ Measurements in Greenland Ice: Investigating Last Glacial Termination CH₄ Sources. Science (80-.). 324, 506 LP – 508. doi:10.1126/science.1168909

Pinardi, N., Masetti, E., 2000. Variability of the large scale general circulation of the Mediterranean Sea from observations and modelling: A review. Palaeogeogr. Palaeoclimatol. Palaeoecol. 158, 153–174. doi:10.1016/S0031-0182(00)00048-1

POEM group, 1992. General-Circulation of the Eastern Mediterranean. Earth-Science Rev. 32, 285–309.

Porter, S.C., Zhisheng, A., 1995. Correlation between climate events in the North Atlantic and China during the last glaciation. Nature 375, 305–308. doi:10.1038/375305a0

Principato, M.S., Crudeli, D., Ziveri, P., Slomp, C.P., Corselli, C., Erba, E., de Lange,

1071 G.J., 2006. Phyto- and zooplankton paleofluxes during the deposition of sapropel
1072 S1 (eastern Mediterranean): Biogenic carbonate preservation and paleoecological
1073 implications. Palaeogeogr. Palaeoclimatol. Palaeoecol. 235, 8–27.
1074 doi:10.1016/j.palaeo.2005.09.021
1075 Robinson, A.R., Golnaraghi, M., 1994. The physical and dynamical oceanography of
1076 the Mediterranean Sea, in: Ocean Processes in Climate Dynamics: Global and
1077 Mediterranean Examples. pp. 255–306. doi:10.1007/978-94-011-0870-6_12
1078 Rodríguez-Sanz, L., Bernasconi, S.M., Marino, G., Heslop, D., Müller, I.A.,
1079 Fernandez, A., Grant, K.M., Rohling, E.J., 2017. Penultimate deglacial warming
1080 across the Mediterranean Sea revealed by clumped isotopes in foraminifera. Sci.
1081 Rep. 7, 16572. doi:10.1038/s41598-017-16528-6
1082 Rogalla, U., Andruleit, H., 2005. Precessional forcing of coccolithophore
1083 assemblages in the northern Arabian Sea: Implications for monsoonal dynamics
1084 during the last 200,000 years. Mar. Geol. 217, 31–48.
1085 doi:10.1016/j.margeo.2005.02.028
1086 Rohling, E.J., 1991a. Shoaling of the Eastern Mediterranean Pycnocline due to
1087 reduction of excess evaporation: Implications for sapropel formation.
1088 Paleoceanography 6, 747–753. doi:https://doi.org/10.1029/91PA02455
1089 Rohling, E.J., 1991b. A Simple Two-Layered Model for Shoaling of the Eastern
1090 Mediterranean Pycnocline Due to Glacio-Eustatic Sea Level Lowering.
1091 Paleoceanography 6, 537–541. doi:https://doi.org/10.1029/91PA01328
1092 Rohling, E J, Cane, T.R., Cooke, S., Sprovieri, M., Bouloubassi, I., Emeis, K.C.,
1093 Schiebel, R., Kroon, D., Jorissen, F.J., Lorre, A., Kemp, A.E.S., 2002a. African
1094 monsoon variability during the previous interglacial maximum. Earth Planet. Sci.
1095 Lett. 202, 61–75. doi:https://doi.org/10.1016/S0012-821X(02)00775-6
1096 Rohling, E.J., Foster, G.L., Grant, K.M., Marino, G., Roberts, A.P., Tamisiea, M.E.,
1097 Williams, F., 2014. Sea-level and deep-sea-temperature variability over the past
1098 5.3 million years. Nature 508, 477–482. doi:10.1038/nature13230
1099 Rohling, E.J., Gieskes, W.W., 1989. Late Quaternary changes in Mediterranean

1100 intermediate water density and formaton rate. Paleoceanography 4, 531–545.
1101 Rohling, E.J., Hopmans, E.C., Damsté, J.S.S., 2006. Water column dynamics during
1102 the last interglacial anoxic event in the Mediterranean (sapropel S5).
1103 Paleoceanography 21, 1–8. doi:10.1029/2005PA001237
1104 Rohling, Eelco J., Kemp, A.E.S., Cooke, S., Pearce, R.B., 2002. High-resolution
1105 stratigraphic framework for Mediterranean sapropel S5: Defining temporal
1106 relationships between records of Eemian climate variability. Palaeogeogr.
1107 Palaeoclimatol. Palaeoecol. 183, 87–101. doi:10.1016/S0031-0182(01)00461-8
1108 Rohling, E.J., Marino, G., Grant, K.M., 2015. Mediterranean climate and
1109 oceanography, and the periodic development of anoxic events (sapropels). Earth-
1110 Science Rev. 143, 62–97. doi:10.1016/j.earscirev.2015.01.008
1111 Rohling, E.J., Marino, G., Grant, K.M., Mayewski, P.A., Weninger, B., 2019. A
1112 model for archaeologically relevant Holocene climate impacts in the Aegean-
1113 Levantine region (easternmost Mediterranean). Quat. Sci. Rev. 208, 38–53.
1114 doi:https://doi.org/10.1016/j.quascirev.2019.02.009
1115 Rohling, E J, Mayewski, P., Abu-Zied, R., Casford, J., Hayes, A., 2002b. Holocene
1116 atmosphere-ocean interactions: Records from Greenland and the Aegean sea.
1117 Clim. Dyn. 18, 587–594. doi:10.1007/s00382-001-0194-8
1118 Rohling, E.J., Sprovieri, M., Cane, T., Casford, J.S.L., Cooke, S., Bouloubassi, I.,
1119 Emeis, K.C., Schiebel, R., Rogerson, M., Hayes, a., Jorissen, F.J., Kroon, D.,
1120 2004. Reconstructing past planktic foraminiferal habitats using stable isotope
1121 data: A case history for Mediterranean sapropel S5. Mar. Micropaleontol. 50, 89–
1122 123. doi:10.1016/S0377-8398(03)00068-9
1123 Rossignol-Strick, M., Nesteroff, W., Olive, P., Vergnaud-Grazzini, C., 1982. After
1124 the deluge: Mediterranean stagnation and sapropel formation. Nature 295, 105.
1125 Roth, P.H., Coulbourn, W.T., 1982. Floral and solution patterns of coccoliths in
1126 surface sediments of the North Pacific. Mar. Micropaleontol. 7, 1–52.
1127 doi:10.1016/0377-8398(82)90014-7
1128 Sakamoto, T., Janecek, T., Emeis, K., 1998. 4 . Continuous Sedimentary Sequences

From the Eastern Mediterranean Sea : Composite Depth Sections 1 160, 37–59.

Satow, C., Tomlinson, E.L., Grant, K.M., Albert, P.G., Smith, V.C., Manning, C.J., Ottolini, L., Wulf, S., Rohling, E.J., Lowe, J.J., Blockley, S.P.E., Menzies, M.A., 2015. A new contribution to the Late Quaternary tephrostratigraphy of the Mediterranean: Aegean Sea core LC21. Quat. Sci. Rev. 117, 96–112. doi:https://doi.org/10.1016/j.quascirev.2015.04.005

Schrag, D.P., Adkins, J.F., McIntyre, K., Alexander, J.L., Hodell, D.A., Charles, C.D., McManus, J.F., 2002. The oxygen isotopic composition of seawater during the Last Glacial Maximum. Quat. Sci. Rev. 21, 331–342.

Schulz, H., Rad, U., Erlenkeuser, H., 1998. Correlations between Arabian Sea and Greenland climate oscillations of the past 110,00 years. Nature 393, 54–57.

Sierro, F.J., Hodell, D. a., Curtis, J.H., Flores, J. a., Reguera, I., Colmenero-Hidalgo, E., Bárcena, M. a., Grimalt, J.O., Cacho, I., Frigola, J., Canals, M., 2005. Impact of iceberg melting on Mediterranean thermohaline circulation during Heinrich events. Paleoceanography 20, 1–13. doi:10.1029/2004PA001051

Sierro, F.J., Hodell, D.A., Andersen, N., Azibeiro, L.A., Jimenez-Espejo, F.J., Bahr, A., Flores, J.A., Ausin, B., Rogerson, M., Lozano-Luz, R., Lebreiro, S.M., Hernandez-Molina, F.J., 2020. Mediterranean Overflow Over the Last 250 kyr: Freshwater Forcing From the Tropics to the Ice Sheets. Paleoceanogr. Paleoclimatology 35, e2020PA003931. doi:https://doi.org/10.1029/2020PA003931

Sirocko, F., Sarnthein, M., Erlenkeuser, H., Lange, H., Arnold, M., Duplessy, J.C., 1993. Century-scale events in monsoonal climate over the past 24,000 years. Nature 364, 322–324. doi:10.1038/364322a0

Skampa, E., Triantaphyllou, M.V., Dimiza, M.D., Gogou, A., Malinverno, E., Stavrakakis, S., Panagiotopoulos, I.P., Parinos, C., Baumann, K.-H., 2019. Coupling plankton - sediment trap - surface sediment coccolithophore regime in the North Aegean Sea (NE Mediterranean). Marine Micropaleontology 152, 101729.

1158 Spratt, R.M., Lisiecki, L.E., 2016. A Late Pleistocene sea level stack. Clim. Past 12,
1159 1079–1092. doi:10.5194/cp-12-1079-2016
1160 Sprovieri, M., Di Stefano, E., Incarbona, A., Salvagio Manta, D., Pelosi, N., Ribera
1161 d'Alcalà, M., Sprovieri, R., 2012. Centennial- to millennial-scale climate
1162 oscillations in the Central-Eastern Mediterranean Sea between 20,000 and 70,000
1163 years ago: evidence from a high-resolution geochemical and
1164 micropaleontological record. Quat. Sci. Rev. 46, 126–135.
1165 doi:https://doi.org/10.1016/j.quascirev.2012.05.005
1166 Stockhecke, M., Timmermann, A., Kipfer, R., Haug, G.H., Kwiecien, O., Friedrich,
1167 T., Menviel, L., Litt, T., Pickarski, N., Anselmetti, F.S., 2016. Millennial to
1168 orbital-scale variations of drought intensity in the Eastern Mediterranean. Quat.
1169 Sci. Rev. 133, 77–95. doi:10.1016/j.quascirev.2015.12.016
1170 Thirumalai, K., Quinn, T.M., Marino, G., 2016. Constraining past seawater δ18O and
1171 temperature records developed from foraminiferal geochemistry.
1172 Paleoceanography 31, 1409–1422. doi:10.1002/2016PA002970
1173 Tierney, J.E., Russell, J.M., Huang, Y., Damsté, J.S.S., Hopmans, E.C., Cohen, A.S.,
1174 2008. Northern Hemisphere Controls on Tropical Southeast African Climate
1175 During the Past 60,000 Years. Science (80-.). 322, 252 LP – 255.
1176 doi:10.1126/science.1160485
1177 Tjallingii, R., Claussen, M., Stuut, J.B.W., Fohlmeister, J., Jahn, A., Bickert, T.,
1178 Lamy, F., Röhl, U., 2008. Coherent high- and low-latitude control of the
1179 northwest African hydrological balance. Nat. Geosci. 1, 670–675.
1180 doi:10.1038/ngeo289
1181 Toucanne, S., Jouet, G., Ducassou, E., Bassetti, M.A., Dennielou, B., Angue Minto'o,
1182 C.M., Lahmi, M., Touyet, N., Charlier, K., Lericolais, G., Mulder, T., 2012. A
1183 130,000-year record of Levantine Intermediate Water flow variability in the
1184 Corsica Trough, western Mediterranean Sea. Quat. Sci. Rev. 33, 55–73.
1185 doi:10.1016/j.quascirev.2011.11.020
1186 Triantaphyllou, M. V, Antonarakou, A., Dimiza, M.D., Anagnostou, C., 2010.

1187 Calcareous nannofossil and planktonic foraminiferal distributional patterns
1188 during deposition of sapropels S6, S5 and S1 in the Libyan Sea (Eastern
1189 Mediterranean). Geo-Marine Lett. 30, 1–13. doi:10.1007/s00367-009-0145-7
1190 Triantaphyllou, M. V, Antonarakou, A., Kouli, K., Dimiza, M.D., Kontakiotis, G.,
1191 Papanikolaou, M.D., Ziveri, P., Mortyn, P.G., Lianou, V., Lykousis, V.,
1192 Dermitzakis, M.D., 2009a. Late Glacial-Holocene ecostratigraphy of the south-
1193 eastern Aegean Sea, based on plankton and pollen assemblages. Geo-Marine
1194 Lett. 29, 249–267. doi:10.1007/s00367-009-0139-5
1195 Triantaphyllou, M. V, Ziveri, P., Gogou, A., Marino, G., Lykousis, V., Bouloubassi,
1196 I., Emeis, K.C., Kouli, K., Dimiza, M.D., Rosell-Melé, A., Papanikolaou, M.,
1197 Katsouras, G., Nunez, N., 2009b. Late Glacial-Holocene climate variability at the
1198 south-eastern margin of the Aegean Sea. Mar. Geol. 266, 182–197.
1199 doi:10.1016/j.margeo.2009.08.005
1200 Triantaphyllou, M. V, Ziveri, P., Tselepides, A., 2004. Coccolithophore export
1201 production and response to seasonal surface water variability in the oligotrophic
1202 Cretan Sea (NE Mediterranean). Micropaleontology 50, 127–144.
1203 Tzedakis, P.C., Drysdale, R.N., Margari, V., Skinner, L.C., Menviel, L., Rhodes,
1204 R.H., Taschetto, A.S., Hodell, D.A., Crowhurst, S.J., Hellstrom, J.C., Fallick,
1205 A.E., Grimalt, J.O., McManus, J.F., Martrat, B., Mokeddem, Z., Parrenin, F.,
1206 Regattieri, E., Roe, K., Zanchetta, G., 2018. Enhanced climate instability in the
1207 North Atlantic and southern Europe during the Last Interglacial. Nat. Commun.
1208 9, 4235. doi:10.1038/s41467-018-06683-3
1209 van der Meer, M.T.J., Baas, M., Rijpstra, W.I.C., Marino, G., Rohling, E.J.,
1210 Sinninghe Damsté, J.S., Schouten, S., 2007. Hydrogen isotopic compositions of
1211 long-chain alkenones record freshwater flooding of the Eastern Mediterranean at
1212 the onset of sapropel deposition. Earth Planet. Sci. Lett. 262, 594–600.
1213 doi:10.1016/j.epsl.2007.08.014
1214 Velaoras, D., Papadopoulos, V.P., Kontoyiannis, H., Papageorgiou, D.K., Pavlidou,
1215 A., 2017. The Response of the Aegean Sea (Eastern Mediterranean) to the

1216 Extreme 2016–2017 Winter. Geophys. Res. Lett. 44, 9416–9423.
1217 doi:10.1002/2017GL074761
1218 Vellinga, M., Wood, R.A., 2002. Global Climatic Impacts of a Collapse of the
1219 Atlantic Thermohaline Circulation. Clim. Change 54, 251–267.
1220 doi:10.1023/A:1016168827653
1221 Veres, D., Bazin, L., Landais, A., Toyé Mahamadou Kele, H., Lemieux-Dudon, B.,
1222 Parrenin, F., Martinerie, P., Blayo, E., Blunier, T., Capron, E., Chappellaz, J.,
1223 Rasmussen, S.O., Severi, M., Svensson, A., Vinther, B., Wolff, E.W., 2013. The
1224 Antarctic ice core chronology (AICC2012): an optimized multi-parameter and
1225 multi-site dating approach for the last 120 thousand years. Clim. Past 9, 1733–
1226 1748. doi:10.5194/cp-9-1733-2013
1227 Wehausen, R., Brumsack, H., 2000. Chemical cycles in Pliocene sapropel-bearing
1228 and sapropel-barren eastern Mediterranean sediments. Palaeogeogr.
1229 Palaeoclimatol. Palaeoecol. 158, 325–352.
1230 Young, J.R., 1994. Functions of coccoliths, in: Winter, A., Siesser, W.G. (Eds.),
1231 Coccolithophores. Cambridge Univ. Press, Cambridge, pp. 63–82.
1232 Young, J.R., Geisen, M., Cros, L., Kleijne, A., Sprengel, C., Probert, I., Østergaard,
1233 J., 2003. A guide to extant coccolithophore taxonomy. J. Nannoplankt. Res. 125.
1234 Zhang, R., Delworth, T.L., 2006. Impact of Atlantic multidecadal oscillations on
1235 India/Sahel rainfall and Atlantic hurricanes. Geophys. Res. Lett. 33.
1236 doi:10.1029/2006GL026267
1237 Ziegler, M., Lourens, L.J., Tuenter, E., Hilgen, F., Reichart, G.-J., Weber, N., 2010.
1238 Precession phasing offset between Indian summer monsoon and Arabian Sea
1239 productivity linked to changes in Atlantic overturning circulation.
1240 Paleoceanography 25, 1–16. doi:10.1029/2009PA001884
1241 Ziveri, P., Broerse, A.T.C., van Hinte, J.E., Westbroek, P., Honjo, S., 2000. The fate
1242 of coccoliths at 48°N 21°W, Northeastern Atlantic. Deep Sea Res. Part II Top.
1243 Stud. Oceanogr. 47, 1853–1875. doi:10.1016/S0967-0645(00)00009-6
1244 Ziveri, P., Thunell, R. C., 2000. Coccolithophore export production in Guaymas

Basin, Gulf of California: response to climate forcing. Deep-Sea Research Part II, 47, 2073–2100. https://doi.org/http://dx.doi.org/10.1016/S0967-0645(00)00017-5

Captions

Fig. 1: location of ODP Site 967 and of records used for correlation. A) Red arrows indicate the location of International Ocean Discovery program (IODP) Site U1385 in the Iberian Margin, ODP Site 967 in the eastern Mediterranean, Core LC21 in the Aegean Sea, Sanbao Cave in China and EPICA Dome C in Antarctica. B) Inset map of the red box in A). The blue and red circles respectively indicate the location of core LC21 and ODP Site 967. The dashed line shows the Nile cone province. Black arrows point out the path of Eastern Mediterranean Deep-water from Adriatic and Aegean Sea.

Fig. 2: plot of coccolith data in the Aegean Sea core LC21 and comparison with selected records. a) *Florisphaera profunda* percentage values (blue circles), expressed as natural logarithm (Grelaud et al., 2012). The 1st derivative of Sanbao Cave speleothem $\delta^{18}O$ (orange line) for each of the 10,000 ice-volume corrected 'stacks', following the chronology by Cheng et al. (2009) and after ice-volume correction. b) *Florisphaera profunda* percentage values (blue line), expressed as natural logarithm (Grelaud et al., 2012). Epica Dome C CH_4 (grey circles and grey line), following the Antarctic Ice Core chronology AICC2012 (Bazin et al., 2013) c) *Florisphaera profunda* percentage values (blue line), expressed as natural logarithm (Grelaud et al., 2012). Upper Summer Mixed Layer depth in the three different experiments by Amies et al. (2019) (respectively pink, orange and red lines for experiments A, B and C). d) Alkenone-derived SST (red circles) from the Alboran Sea (Martrat et al., 2014). e) Holococcoliths percentage values (blue circles, this study) and superimposed $\delta^{13}C$ values of the benthic foraminifera species *Cibicidoides*

wuellestorfi from the Iberian Margin (green circles) (Martrat et al., 2007). f) Ca/Ti ratio, expressed as logarithm (green line), in sediments from the Iberian Margin (Hodell et al., 2015), superimposed to the C_{26}OH ratio from the same area (red circles) (Martrat et al., 2007). Thick lines represent the 3-pt running average and coloured shadows indicate the 95% confidence level. The sapropel S5 and HS11 extent is also shown.

Fig. 3: plot of coccolith data at ODP Site 967 and comparison with selected records. A) June 21st insolation curve at 65°N (Laskar et al., 2004). B) Benthic δ^{18}O composite record from ODP Sites 967 and 968 (Konijnendijk et al., 2015). C) LR04 benthic δ^{18}O stack (Lisiecki and Raymo, 2005). D) Downcore percentage variations of Placoliths. E) Downcore percentage variations of *F. profunda*. F) Downcore percentage variations of UPZ taxa. G) Downcore percentage variations of Miscellaneous taxa. H) Downcore percentage variations of holococcoliths. Black horizontal bars show the error associated to countings for a 95% confidence level. Red filling indicates values higher than the total average percentage. Horizontal thick black lines indicate MIS boundaries from Lisiecki and Raymo (2005). Horizontal yellow boxes show visible sapropel layers in the ODP 967 composite section (Emeis et al., 2000a).

Fig. 4: scatter plot of placoliths and *F. profunda* percentage values at ODP Site 967. The black line shows the linear fit. The equation of the linear fit, R^2 correlation index and number of samples are also reported.

Fig. 5: coccolith, element ratios, indices and principal component scores at ODP Site 967. A) *Florisphaera profunda* percentage values (black circles, the black line is the 3-pt running average, this study). B) Holococcolith percentage values (blue circles, the blue line is the 3-pt running average, this study). C) Relative sea-level (Spratt and Lisiecki, 2016). D) PC2 of elemental proxies that reflects sapropel/monsoon runoff

layers (Grant et al., 2017). E) The Aeolian residual by Larrasoaña et al. (2003) plotted by the Grant et al. (2017) chronology. F) The North Africa humidity/aridity index (Grant et al., 2017). G) The Ba/Al ratio (Grant et al., 2017). Horizontal thick black lines indicate MIS boundaries from Lisiecki and Raymo (2005). Horizontal yellow boxes show visible sapropel layers in the ODP 967 composite section (Emeis et al., 2000a).

Fig. 6: correlation among Mediterranean, North Atlantic, Asian and Antarctica records. A) Alkenone-based SSTs (°C) at Site MD01-2444, Iberian Margin (Martrat et al., 2007). B) Log (Ca/Ti) at IODP Site U1385, Iberian Margin (Hodell et al., 2015). Note the reversed axis. C) 3-pt running average of holococcolith percentage values at ODP Site 967, eastern Mediterranean Sea (present study). Note the reversed axis. D) $\delta^{18}O$ speleothem data at Sanbao Cave, China (Cheng et al., 2016). Note the reversed axis. E) Epica Dome C CH_4, Antarctica (Bazin et al., 2013).
Grey boxes indicate correlations among different records: cooling and AMOC weakening/shutdown in the Iberian Margin (A, B), holococcolith preservation in the eastern Mediterranean seafloor (C), monsoon activity weakening in China (D) and EDC methane concentration decrease in Antarctica (see Section 6 for further explanation).

Figure

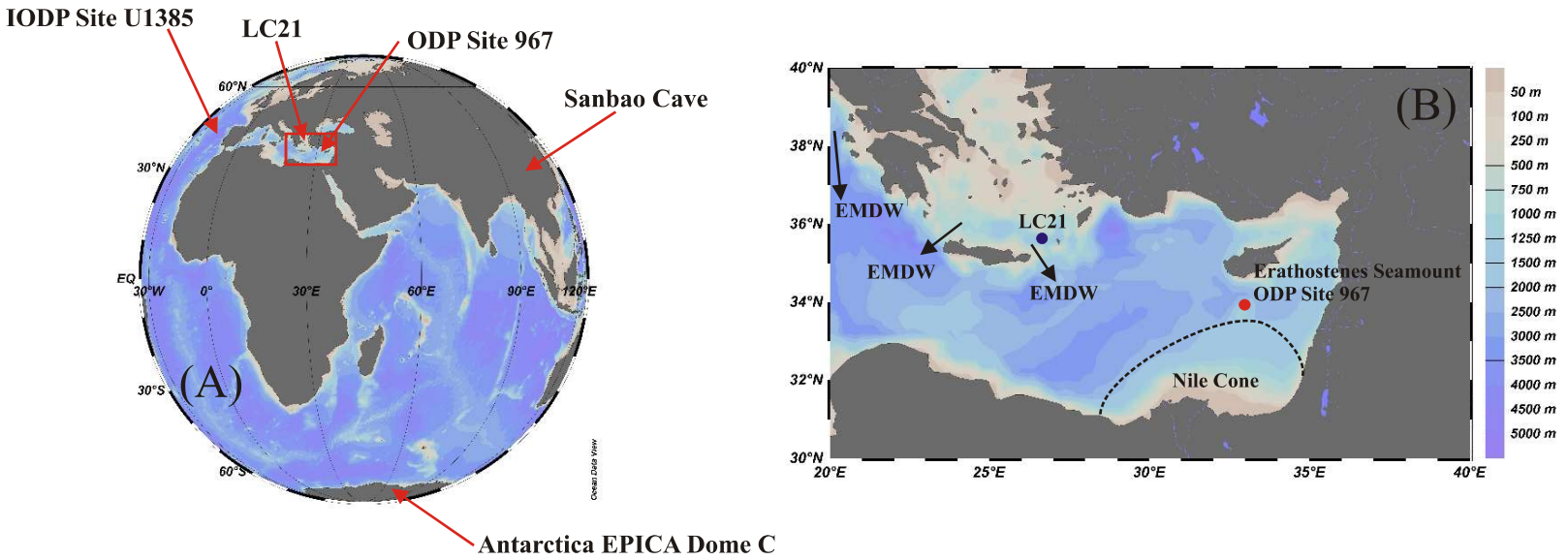

Figure

Click here to access/download;Figure;Fig. 2(967).png

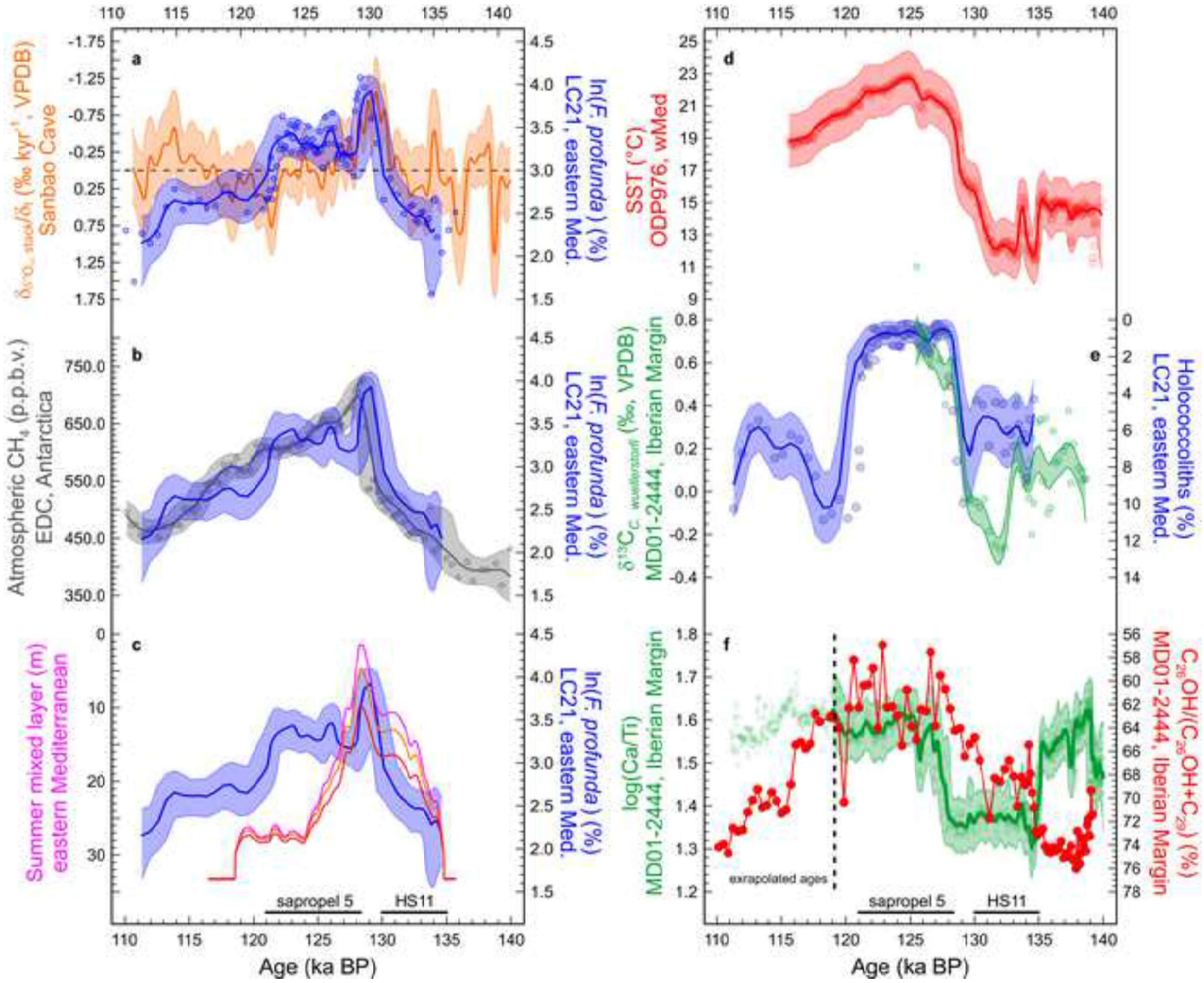

Figure

Click here to access/download;Figure;Fig. 3(967).jpg

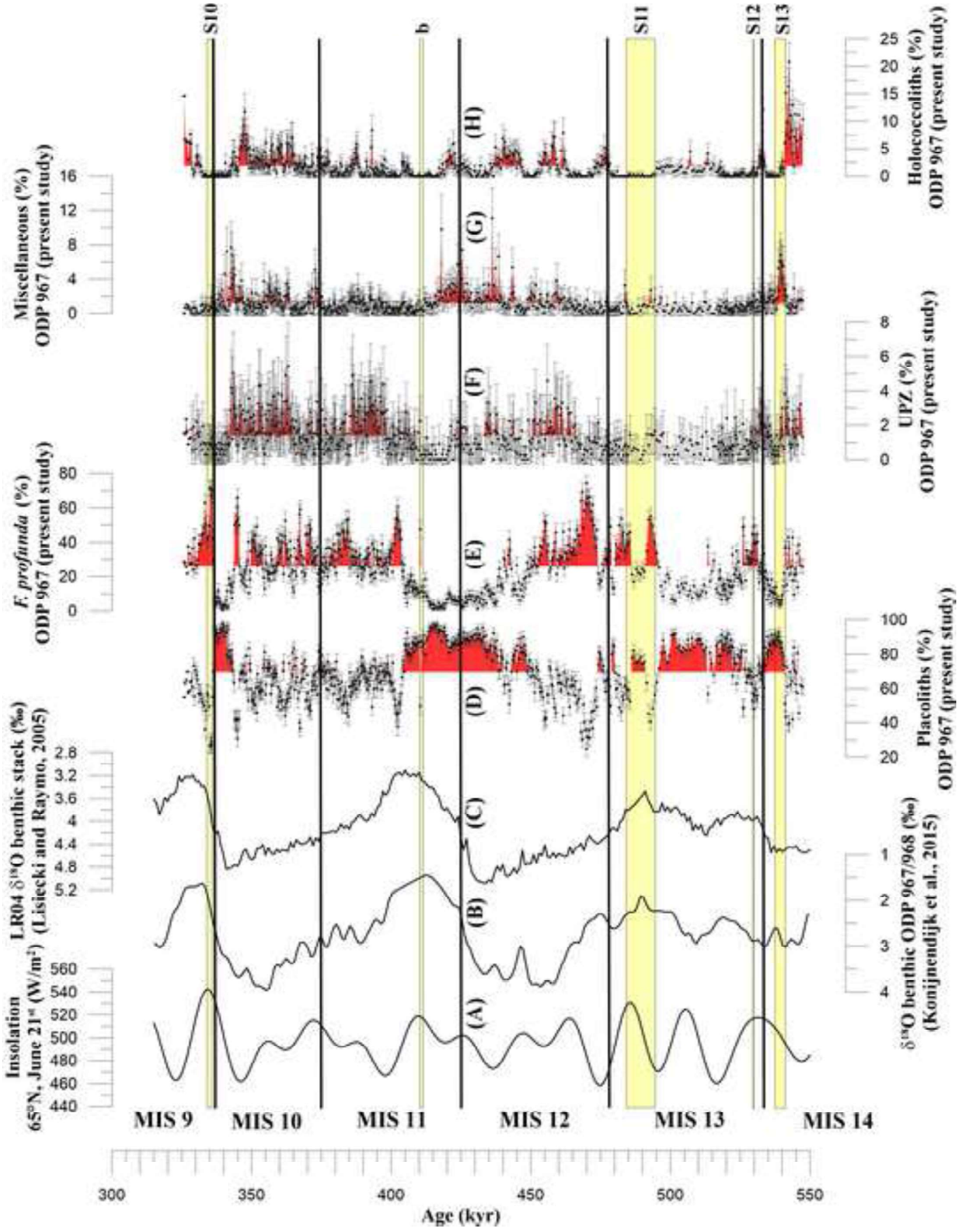

Figure

Click here to access/download;Figure;Fig. 4(967).pdf

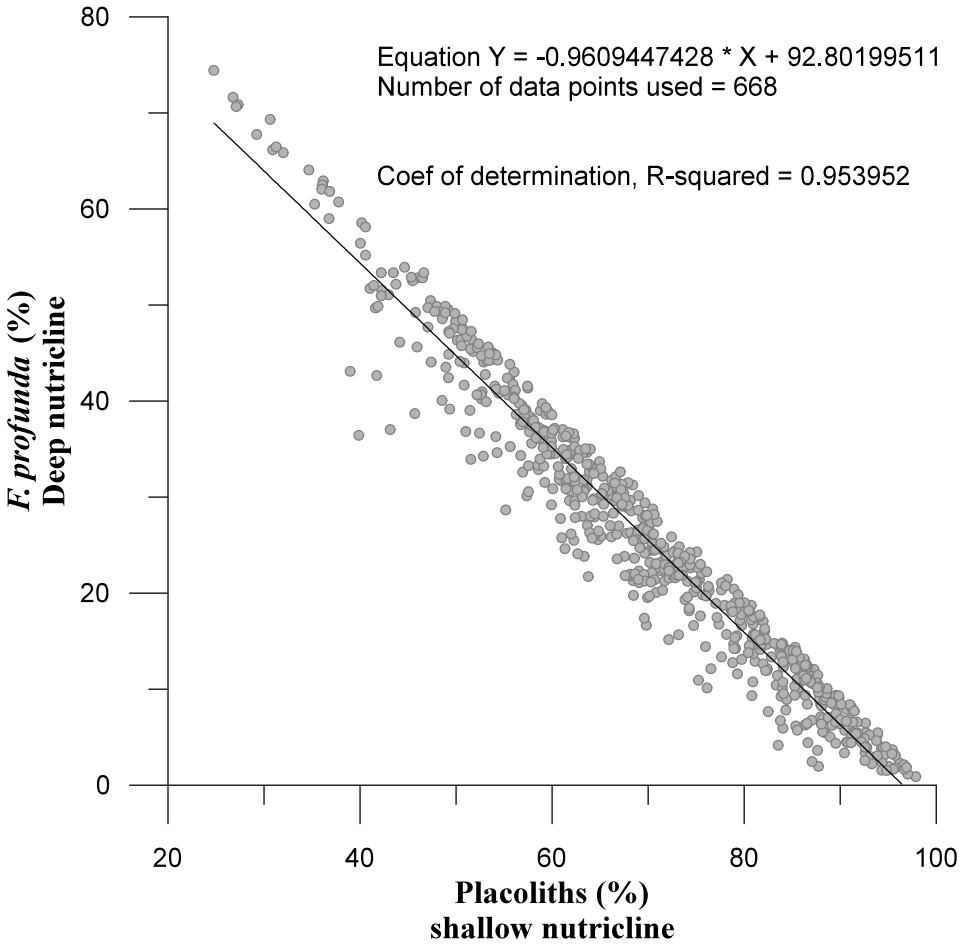

Figure

Click here to access/download;Figure;Fig. 5(967).pdf

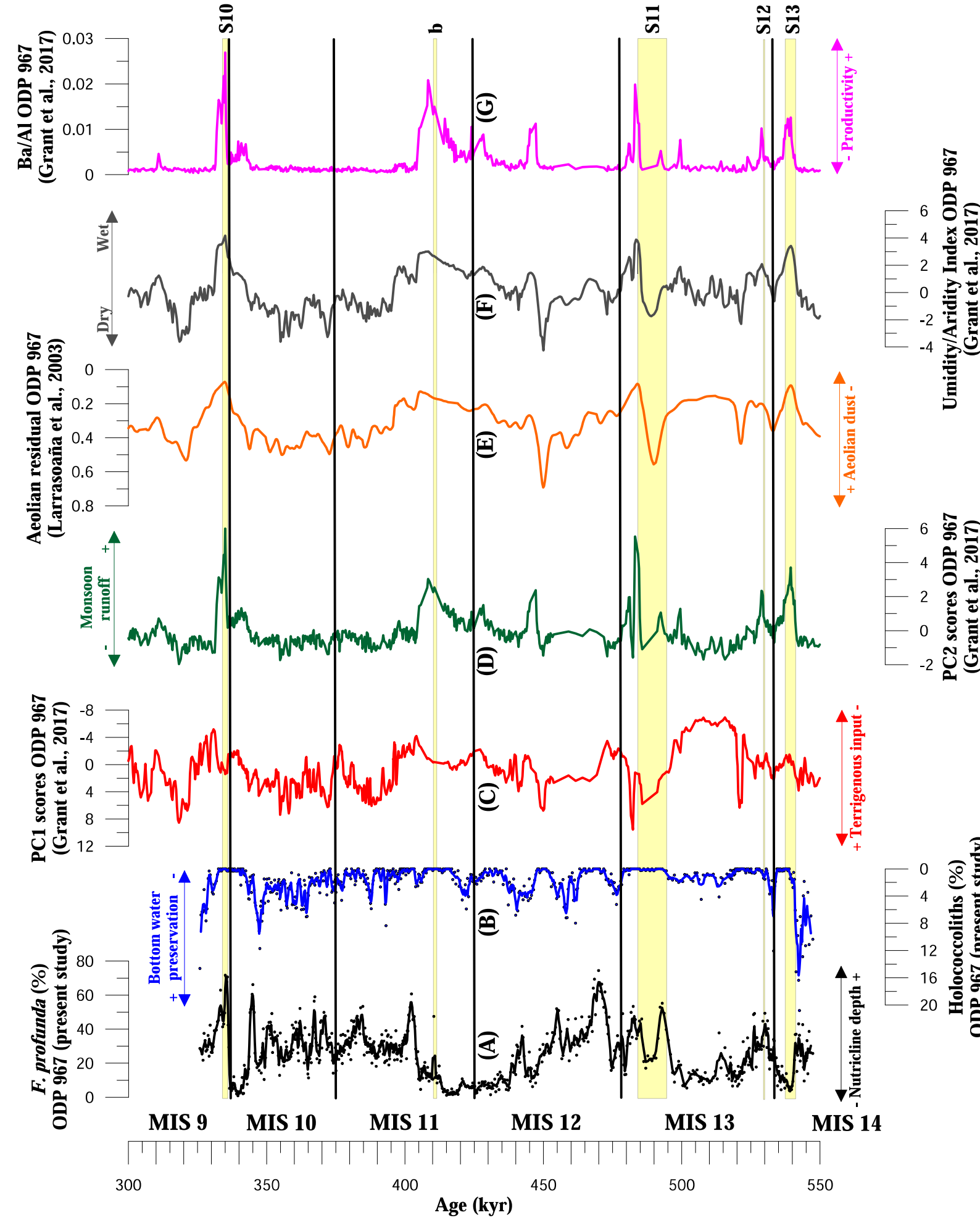

Figure

Click here to access/download;Figure;Fig. 6(967).pdf